# AN INVESTIGATION OF THE PROCTODEAL REGION WITH RESPECT TO DEVELOPMENT AND BREAKDOWN OF THE CLOACAL MEMBRANE IN *XENOPUS LAEVIS*

Deborah Marie Jones

A dissertation submitted to the Faculty of Science, University of the Witwatersrand, Johannesburg, in fulfillment of the requirements for the degree of Master of Science

Johannesburg, 2009

# CONTENTS

I declare that this dissertation is my own, unaided work. It is being submitted for the Degree of Master of Science in the University of the Witwatersrand, Johannesburg. It has not been submitted before for any degree or examination in any other University.

Deborah Marie Jones

4th day of February 2009

# ABSTRACT

Anorectal malformations are common congenital anomalies which disable the newborn. In order to gain insight into the development and causes of these anomalies, the normal development of the hindgut requires elucidation at the structural and molecular level. During normal embryonic development of the alimentary canal, the proctodeum develops at the posterior end of the embryo and together with the stomodeum, is the only region where the ectoderm and endoderm are directly juxtaposed. The juxtaposed ectoderm and endoderm go on to form the cloacal membrane, which eventually perforates to allow continuity to the exterior. This study investigated morphological features and mechanisms involved in proctodeal development and cloacal membrane dissolution in *Xenopus laevis* embryos. Embryos were collected, staged and processed for various techniques. Analysis using time course, confocal, scanning electron microscopy and histology revealed the presence of a proctodeal depression by stage 21. This is earlier in development than the initial appearance of the stomodeum. Prominent morphological features found in the proctodeal region included cilia and vacuolated cells. Immunolocalization of the basement membrane between the proctodeal ectoderm and hindgut endoderm, and apoptosis detection proved inconclusive, but the results suggest that they may play a role in hindgut development. BMP-4 expression, often associated with apoptosis and thought to be involved in anorectal malformations, decreased in the proctodeal region as the embryos developed. The combination of morphological and molecular evidence as found in *Xenopus laevis* provides a greater understanding of hindgut development. These results may stimulate further research into anorectal malformations in an attempt to provide a more comprehensive understanding of the mechanisms involved in the occurrence of these anomalies.

# ACKNOWLEDGEMENTS

With thanks to:

The Faculty of Health Sciences, for a Medical Research Endowment Fund Grant
Sigma Xi, for a Grant in Aid-of-Research
*Development*, for a Travelling Fellowship to go to Boston
The University of the Witwatersrand, for a Travel Grant to travel to Budapest

The Embryonic Development and Differentiation Research Programme
The School of Anatomical Sciences
Central Animal Services

Caroline Lalkhan and Abe Seema from the Electron Microscope Unit, for all their assistance

Dr Margot Hosie and Therésè Dix-Peek, for the protocols and reagents used in Bax and Bcl-2 immunolocalization

Professor Barry Fabian, for all his advice

Hazel Sive and Amanda J.G. Dickinson from the Whitehead Institute, Massachusetts Institute of Technology, for the ongoing collaboration, wonderful experiences in Boston and use of their laboratories and reagents

Tanya Augustine for all her support

Judy, David and Christopher Jones for all their encouragement

Professor Beverly Kramer

# LIST OF FIGURES

# INTRODUCTION

During early development, the hindgut region of the human embryo forms a common cavity, known as the cloaca. This cavity forms at the posterior region of the embryo, caudal to the primitive streak (Florian, 1933). It is lined by endoderm and is separated from the ectodermal exterior by a membrane referred to as the cloacal membrane (Allan and Kramer, 2002). The cloacal membrane perforates to form the cloacal opening, during the seventh week of intrauterine life in human development (Moore, 1988; Allan and Kramer, 2002; Dravis *et al.*, 2004). The cloaca then becomes divided into two compartments by the downgrowth of the median, sagittally placed, mesodermal urorectal septum, until it reaches the cloacal membrane. The ventral compartment of the divided cloaca forms the urogenital sinus while dorsally, it will form the rectum (van der Putte, 1986; Hendren, 1998; Paidas *et al.*, 1999; Qi *et al.*, 2000a). This septation thus divides and separates the urinary and faecal excretion pathways (Dravis *et al.*, 2004). Septation by the urorectal septum of the cloaca is however, controversial and is still under debate as to the exact mechanisms involved (Kluth and Lambrecht, 1997; Qi *et al.*, 2000a; Nebot-Cegarra *et al.*, 2005). It is not known whether the septation of the cloaca is a passive process, whether it occurs via the active downgrowth of the urorectal septum or if the septation is a combination of both passive and active processes (Qi *et al.*, 2000b; Mo *et al.*, 2001). As the normal development of the cloaca and the proctodeal region is still being disputed, this has lead to difficulties in understanding the underlying factors that result in malformations of the anorectal region.

Malformations of the hindgut region can be classed as anorectal malformations and are one of the most common groups of congenital abnormalities (Bitoh *et al.*, 2001; Sasaki *et al.*, 2004) affecting approximately 1:5 000 new born infants, with a slight male predominance (Touloukin, 1979; Dravis *et al.*, 2004). A wide range of such

anomalies exist, ranging from mild to extremely severe and include urorectal septal defects, high anorectal malformations and low anorectal malformations (abnormalities involving the proctodeum, anal pit and the region that forms the distal one third of the anal canal and anus) (Kluth *et al.*, 1995). Many infants with anorectal anomalies die shortly after birth and most of those that survive have to undergo extensive surgery (Peña, 1997).

One of the most severe anorectal malformations in humans is cloacal exstrophy, which occurs in 1: 250 000 births (Hendren, 1998). These infants present with a cloacal membrane that is enlarged and which ruptures before the urorectal septum descends, which is before the eighth week of gestation in humans (Bruch *et al.*, 1996; Hendren, 1998). The colon ends blindly or a fistula is created between the urinary bladder and the colon (Siebert *et al.*, 2005). It is thought that this abnormality is due to an interference of ectodermal and endodermal cell migration, which causes a weakness in the cloacal membrane and makes it unstable. Due to the instability, of the membrane it is thought to rupture too early on in development (Bruch *et al.*, 1996; Siebert *et al.*, 2005). This early rupture is thought to lead to a decrease in mesoderm, a major component of the urorectal septum, thus preventing the development of this septum and septation of the cloaca (Siebert *et al.*, 2005).

"Cloaca" is another anomaly of the cloacal region and occurs in approximately 1: 50 000 births (Hendren, 1998). It is the most complicated type of imperforate anus in females (Hendren, 1998) and results in variations of malformations in the convergence of the rectum, vagina and bladder in a urogenital sinus (Hendren, 1998).

As anorectal malformations are often very complex and diverse, the underlying mechanisms responsible for these malformations are not completely understood (Bitoh *et al.*, 2001). A number of factors are however thought be involved in influencing the formation of such anomalies (Moore, 1988). These include the misexpression of genes (Shapira *et al.*, 1999), such as BMP-4 (Jain and Weaver,

2004); defects in signalling pathways, such as the apoptotic pathway; incorrect septation of the cloaca (de Vries and Friedland, 1974; Qi *et al.*, 2000a; Dravis *et al.*, 2004) and the inadvertent presence of mesoderm between the ectoderm and endoderm in the proctodeal region. Exogenous factors that have been strongly implicated in birth defects of the anorectal region include changes in androgen production and exposure to toxic environmental agents (Shapira *et al.*, 1999; Dravis *et al.*, 2004). However, information regarding normal development of the cloacal region is lacking and needs to be fully understood in order to try and explain malformations of this region more fully (Qi *et al.* 2000a).

A number of animal models have been used to create a better understanding of the development of these malformations, as the sequence of events and mechanisms involved in gut development is similar in all vertebrates (Horb and Slack, 2001; Mandhan *et al.*, 2006). One model organism that is commonly used in gastrointestinal tract studies and in general developmental biology is the South African clawed toad, *Xenopus laevis* (Callery, 2006). The use of *Xenopus laevis* has provided extensive knowledge in many areas of developmental biology and contributed to the understanding of diverse factors and mechanisms involved in such processes as differentiation, development and growth (Collart *et al.*, 2005).

*Xenopus* embryos have many benefits that make them useful in experimentation. They are relatively large, easily accessible at different stages of development, they develop externally so that their development can be easily assessed and they heal well after surgical applications (Chalmers and Slack, 1998; Khokha *et al.*, 2002).

In the development of *Xenopus laevis*, the cells of the fertilized ovum undergo cleavage and the resulting blastula consists of a ball of cells with a fluid filled space, known as the blastocoel (Alberts *et al.* 2002). Re-organization of these cells occurs and a process of highly integrated cell movements, known as gastrulation (Gilbert, 2003) gives rise to a multilayered structure. Thereafter, the body axes become

established and the gut tube develops (Alberts *et al.*, 2002). At the beginning of gastrulation, cells involute into the interior and extend to form the blastopore (Wacker *et al.*, 1998; Alberts *et al.*, 2002). Gastrulation produces the three primary germ layers (Heasman, 1997; Zhang *et al.*, 1998; Wacker *et al.*, 2000; Tam *et al.*, 2003; Tortora, 2005). This cellular rearrangement forms a distinct pattern in *Xenopus* as the three domains of the blastula, the animal cap, the equatorial zone and the vegetal mass form the ectoderm, the mesoderm and the endoderm respectively (Balinsky, 1965; Zhang *et al.*, 1998). As development continues, the endoderm contributes to the lining of the alimentary canal (Chalmers and Slack, 1998; Chalmers and Slack, 2000; Tam *et al.*, 2003). The mesoderm is fated to form muscles and connective tissue and other components, whilst the ectoderm is the precursor of the epidermis (Balinsky, 1975) and nervous tissue (Alberts *et al.*, 2002). As growth of the embryo progresses, the body plan of the adult is developed and organogenesis, including the formation of the alimentary canal, takes place (Alberts *et al.,* 2002).

During morphogenesis of the alimentary canal, once the primary germ layers have been established, regional specification occurs whereby each germ layer is positioned along the body axes and becomes committed to a specific region and presumptive tissue type. Through the use of transplantation experiments, Horb and Slack (2001) found that this specification of the endoderm only occurs at the late tailbud stages, between stage 28 and stage 30 in *Xenopus laevis*, after the mesoderm has become correctly specified. It is interesting to note that this specification occurs later in development than the initial appearance of the proctodeal depression and dissolution of the cloacal membrane. The specification of these germ layers is thought to rely on maternally expressed genes in the egg as well as intercellular signalling (Haffen *et al.*, 1987; Hardin and Armstrong, 1997; Zhang *et al.*, 1998). Finally, differentiation occurs, whereby the specific proteins and mRNAs for each region of the gastrointestinal tract are translated and transcribed (Horb and Slack, 2001).

The alimentary canal of the frog develops into three regions: the stomodeum, mesenteron and proctodeum (Marshall, 1893). The mesenteron initially communicates with the exterior through the blastopore and gives rise to most of the gastrointestinal tract, from the pharynx to the rectum, as well as accessory organs, such as the bladder and thyroid gland. During the early stages of development, the foregut and hindgut end as blind diverticulae (Balinsky, 1965). As development progresses, ectodermal invaginations are formed at the anterior and posterior regions of the embryo. Here the outer ectoderm and inner endoderm are directly juxtaposed without any intervening mesoderm (Rugh, 1951). The anterior invagination forms the stomodeum, whilst at the posterior end of the embryo the proctodeum is formed (Balinsky, 1965).

In the stomodeal region of the *Xenopus laevis* embryo at the end of gastrulation or tailbud stage of development, the basement membrane between the juxtaposed outer stomodeal ectoderm and inner foregut endoderm disintegrates (Dickinson and Sive, 2006). The outer ectodermal layer can be said to consist of two fairly distinct layers, namely the outer ectoderm and the inner ectoderm (Wardle *et al*., 2002). The inner layer of ectoderm forms the primordium for the presumptive mouth whilst the outer layer of ectoderm forms the secretory cement gland (Wardle *et al.*, 2002). In the presumptive mouth region, the ectoderm invaginates to form the stomodeum (Takahama *et al.*, 1988), which deepens due to flexure of the head. The stomodeum then becomes much more prominent as development continues (Torrey, 1963). The stomodeal ectoderm and foregut endoderm fuse and thinning of the ectodermal and endodermal cell layers occurs in this region (Fig. 1). Localized cell death in the ectoderm is thought to be responsible for the ectodermal thinning. Subsequently, the cells of the ectoderm and endoderm intercalate to form a bilaminar layer known as the buccopharyngeal membrane (Takahama *et al.*, 1988; Dickinson and Sive, 2006). Small perforations appear in this membrane which merge and eventually lead to the disintegration of the whole membrane. This produces a pharyngeal opening in the depths of the stomodeal cavity, which is connected to the foregut by a channel, the

pharynx (Balinsky, 1965; Dickinson and Sive, 2006) and has been termed the "primary mouth" by Dickinson and Sive (2006) (Fig. 1).

Similar development appears to occur at the posterior region of the X*enopus laevis* embryo (Dickinson and Sive, 2006), although the literature does not elucidate the exact mechanisms involved in the development of this region. In the proctodeal region however, no neural crest cells are present. This is in contrast to the stomodeal region where neural crest cells are found around the "primary mouth." These cells participate in the formation of the facial features and the "secondary mouth," which is the opening of the oral cavity to the exterior and includes the facial features directly surrounding this region (Dickinson and Sive, 2006).

In the posterior region of the *Xenopus laevis* embryo, near to the position of the blastopore opening (Tahara and Nakamura, 1961; Chalmers and Slack, 1998), the ectoderm invaginates to form the proctodeum (Balinsky, 1965). The blastopore does not persist as the cloacal opening in *Xenopus laevis*, as in some other amphibians. Instead it becomes the neurenteric canal, linking the archenteron to the neural tube. It persists for only a short time and then disappears (Balinsky, 1965).

The invaginated ectoderm of the proctodeum is directly juxtaposed to the hindgut (cloacal) endoderm. As development of the proctodeum progresses, these cell layers thin, leading to the formation of the anal or proctodeal plate or cloacal membrane (Torrey, 1963; Balinsky, 1965). The cloacal membrane eventually perforates and the hindgut persists as a dilated cloacal cavity, with the dorsal wall forming the postanal gut, by extending into the tail rudiment (Balinsky, 1965). This creates a free passage of communication between the hindgut and the exterior (Torrey, 1963). The postanal gut is not maintained for a lengthy period of time and disappears soon after formation. Unlike in humans and other mammals however, the cloaca in *Xenopus laevis* does not divide and form separate urinary and genital tracts but persists as a

cloacal cavity (Balinsky, 1965). The cloaca thus serves as a means of excretion for faeces, urine and gametes (Balinsky, 1975).

For normal development of the stomodeum and proctodeum to occur, in many organisms it appears important that there is fusion between the developing outer ectoderm and inner endoderm in the respective regions and that there is disintegration of the corresponding membranes (Dickinson and Sive, 2006). The persistence of a basement membrane in these regions may thus inhibit the development of the stomodeum and proctodeum. As the basement membrane between the stomodeal ectoderm and foregut endoderm has been found to disappear many hours prior to perforation of the buccopharyngeal membrane in the chick (Waterman and Schoenwolf, 1980) and *Xenopus laevis* (Dickinson and Sive, 2006) it is thought to have an indirect role in the dissolution of the buccopharyngeal membrane. The role of the basement membrane between the stomodeal ectoderm and foregut endoderm is thus thought to be important in the early formation of the "primary mouth," but is not thought to be involved in later events such as intercalation of the ectoderm and endoderm and cell death (Dickinson and Sive, 2006).

Both laminin and fibronectin are glycoproteins and are structural components of basement membranes (Waterman and Balian, 1980; Hormia *et al.* 1998; Alberts *et al.*, 2002). A decrease in concentration of these proteins in the stomodeal region indicated the early disappearance of the basement membrane between the ectoderm and endoderm in *Xenopus laevis* (Dickinson and Sive, 2006). The basement membrane in this region was also found to disappear in stages and not as a whole entity (Dickinson and Sive, 2006). Small perforations in the basement membrane between the stomodeal ectoderm and foregut endoderm, creating a fenestrated appearance, are thought to initiate the dissolution of the basement membrane (Waterman, 1977; Dickinson and Sive, 2006). The dissolution of the basement membrane is also thought to enable the fusion of the stomodeal ectoderm and foregut endoderm in *Xenopus laevis* and has been found in conjunction with increased cell

death or decreased cell proliferation in other developing regions of the embryo (Murray and Edgar, 2000). Thus, not only may basement membrane dissolution play a role in cloacal membrane disintegration, but apoptosis may be a contributing factor as well (Dickinson and Sive, 2006).

As mentioned, apoptosis plays an important role in the breakdown of the buccopharyngeal membrane in *Xenopus laevis*. Dickinson and Sive (2006) found that apoptosis is involved in a process leading to thinning of the stomodeal ectoderm and rupture of the buccopharyngeal membrane. This is in accordance with studies done on the buccopharyngeal membrane of rats (Qi *et al.*, 2000a) and mice (Dickinson and Sive, 2006), although no bursts of cell death were observed in other vertebrate studies. Apoptosis has also been found to play a role in the disintegration of the cloacal membrane in humans (Paidas *et al.*, 1999) and it may be an important mechanism for dissolution of the cloacal membrane in this region in *Xenopus laevis*.

Apoptosis is an active mode of physiological cell death (Tilly, 1994; Darzynkiewicz *et al.*, 1997). It is often referred to as programmed cell death and plays an important role in normal embryonic development (Vaux, 1993; Darzynkiewicz *et al.*, 1997; Jacobson *et al.*, 1997; Bossy-Wetzel *et al.*, 1998; Pollard and Earnshaw, 2002). During apoptosis a complex cascade of events takes place, involving activation and maintenance of many different cellular pathways (Darzynkiewicz *et al.*, 1997). In order for apoptosis to occur, signals are required to trigger the process and allow for the continuation of the cascade of events involved in this process (Majno and Joris, 1995). Although apoptosis is intrinsically driven, the cells still need to rely on other cells and external signals, such as hormones and growth factors in order to undergo cell death (Boise *et al.*, 1993; Cohen, 1993; Schwartzman and Cidlowski, 1993; Baker *et al.*, 1994).

Apoptosis can be distinguished by certain morphological characteristics. However, cells undergoing apoptosis can be identified by biochemical methods before they

present with the morphological features of this process. During the initiation of apoptosis a specific endonuclease is activated to cleave the nuclear chromatin at internucleosomal sites (Arends *et al.*, 1990; Boise *et al.*, 1993; Brown *et al.*, 1993; Gorczyca *et al.*, 1993; Darzynkiewicz *et al.*, 1997; Bossy-Wetzel *et al.*, 1998). Oligonucleosomal DNA fragments are produced, in size multiples of approximately 185 base pairs (Gold *et al.*, 1993; Mundle *et al.*, 1994; Tilly, 1994; Migheli *et al.*, 1995). One method for detecting the DNA fragments cleaved during apoptosis is the terminal deoxynucleotidyl transferase mediated dUTP nick end-labelling (TUNEL) method that labels the 3'-end of extracted DNA (Tilly, 1994; Darzynkiewicz *et al.*, 1997).

During apoptosis the cells have to pass through at least two check points. One is controlled by the *Bcl-2/Bax* family of proteins (Schlaifer *et al.*, 1996) and another by cysteine and possibly the serine proteases (Darzynkiewicz *et al.*, 1997). *Bcl-2* is an oncogene that is primarily located in the outer mitochondrial membrane (Bossy-Wetzel *et al.*, 1998) although it can also be found in the cytosol, parts of the endoplasmic reticulum and nuclear envelope (Reed, 1994; Krajewska *et al.*, 1996a). Bcl-2 was first detected due to its role in B-cell malignancies (Boise *et al.*, 1993; Reed, 1994) and protects cell against apoptosis (Reed, 1994; Darzynkiewicz *et al.*, 1997). Bcl-2 is thought to prevent the loss of the mitochondrial transmembrane potential during apoptosis (Darzynkiewicz *et al.*, 1997) and/or influence calcium levels in apoptosis (Reed, 1994). However, from previous studies Bcl-2 overexpression fails to prevent apoptosis under all circumstances (Cohen, 1993; Reed, 1994) thereby illustrating that Bcl-2 is alone insufficient to prevent apoptosis or that there are independent pathways that regulate apoptosis (Reed, 1994; Krajewski *et al.*, 1995).

Bcl-2 can inhibit the activity of one of its homologues, Bax, which is a pro-apoptotic protein and is responsible for the acceleration of apoptosis (Reed, 1994; Bossy-Wetzel *et al.*, 1998). It has been suggested that Bax either serves as a negative

regulator of Bcl-2 or it directly or indirectly influences signalling, thereby inducing apoptosis (Ohta *et al.*, 1995).

One gene that has been associated with cell death (Goltzené *et al.*, 2000) and localized to the proctodeum, in separate instances is the *bone morphogenetic protein-4 (BMP-4)*. The BMPs are secreted growth factors (Yao *et al.*, 2006) and act as morphogens (Schohl and Fagotto, 2002). They have been found to be responsible for a number of mechanisms in the development of embryos, including ventral signalling (Dale *et al.*, 1992; Graff *et al.*, 1994; Sagerström *et al.*, 1996; Graff, 1997; Heasman, 1997; Dale and Jones, 1999; Angerer *et al.*, 2000; Giudice, 2001; Lee *et al.*, 2001), mesoderm development (Miyanaga *et al.*, 2002; Perriton *et al.*, 2002; Haworth *et al.*, 2004), ectoderm patterning (Dale and Jones, 1999) including epidermis specification (Wilson *et al.*, 1997; Shapira *et al.*, 1999) and patterning of the left-right axis (Branford *et al.*, 2000). BMPs are thought to interact with the extracellular domain of cell surface receptors including serine/threonine kinases (Dale and Jones, 1999) and can activate a MAP kinase pathway to induce apoptosis in *Xenopus* embryos (Dale and Jones, 1999; Kurata *et al.*, 2001; Karaulanov *et al.*, 2004). BMP-4 is a member of the transforming growth factor-β (TGF-β) superfamily (Dale *et al.*, 1992). The zygotic expression of BMP-4 in *Xenopus* begins at the midblastula stage, induces ventralization after the onset of gastrulation and continues until about stage 34 of development (Dale *et al.*, 1992; Goldman *et al.*, 2006). The amino acid sequence of *Xenopus* BMP-4 shows 80% similarity with the human protein (Dale *et al.*, 1992) and studies using zebrafish suggest evolutionary conserved mechanisms of BMP-4 between lower and higher vertebrates (Martínez-Barberá *et al.*, 1997).

BMP-4 is expressed in the gut (Mandhan *et al.*, 2006) and more specifically in the proctodeal region as well as the anterior region of various embryos, including zebrafish and *Xenopus* (Martínez-Barberá *et al.*, 1997). Downregulation of BMPs has been linked to abnormal excretion of waste materials in malformations of the cloaca (Pyati *et al.*, 2006). This was demonstrated in zebrafish larvae with reduced

BMP signalling (Pyati *et al.*, 2006). Alterations in BMPs thus appear to be involved in the abnormal development of the cloacal region. Misexpression of this gene, in conjunction with other genes and factors, may account in part for anomalies observed in development of this region (Angerer *et al.*, 2000; Qi *et al.*, 2002). Thus, it is of interest to determine the expression of BMP in the "normal" development of the cloacal region, including dissolution of the cloacal membrane.

Few studies have been conducted in relation to the morphological development of the hindgut in *Xenopus laevis*. Such information is needed to substantiate and expand on the results obtained from the genetic and molecular studies more prevalent in the literature to provide a comprehensive background of hindgut development.

The aims of this study were to therefore investigate the embryonic development and elucidate on the mechanisms involved in the development of the proctodeum with respect to development and breakdown of the cloacal membrane in *Xenopus laevis*. More specifically, this study aimed to:

1. Describe the normal development of the cloacal region in *Xenopus laevis.*
2. Describe the dissolution of the cloacal membrane if possible.
3. Determine whether apoptosis plays a role in the dissolution of the cloacal membrane.
4. Identify factors such as BMP-4 which may be responsible for the dissolution of the cloacal membrane.

Figure 1. A diagram illustrating "primary mouth" development in *Xenopus laevis*. At stage 22 of development, in the region where the primary mouth will develop there is direct apposition of the outer ectoderm and inner endoderm. Dissolution of the basement membrane between ectoderm and endoderm occurs at stage 24 and by stage 32 the ectoderm has started to invaginate to form the stomodeum. Programmed cell death occurs in the ectoderm at stage 34, leading to thinning of this layer. By stage 37 a bilaminar layer has been created and at stage 39 the ectoderm and endoderm intercalate to form the pharyngeal membrane. By stage 40 this membrane has ruptured giving rise to the primary mouth and creating a free passage of communication between the exterior and foregut. (Taken from Dickinson and Sive, 2006).

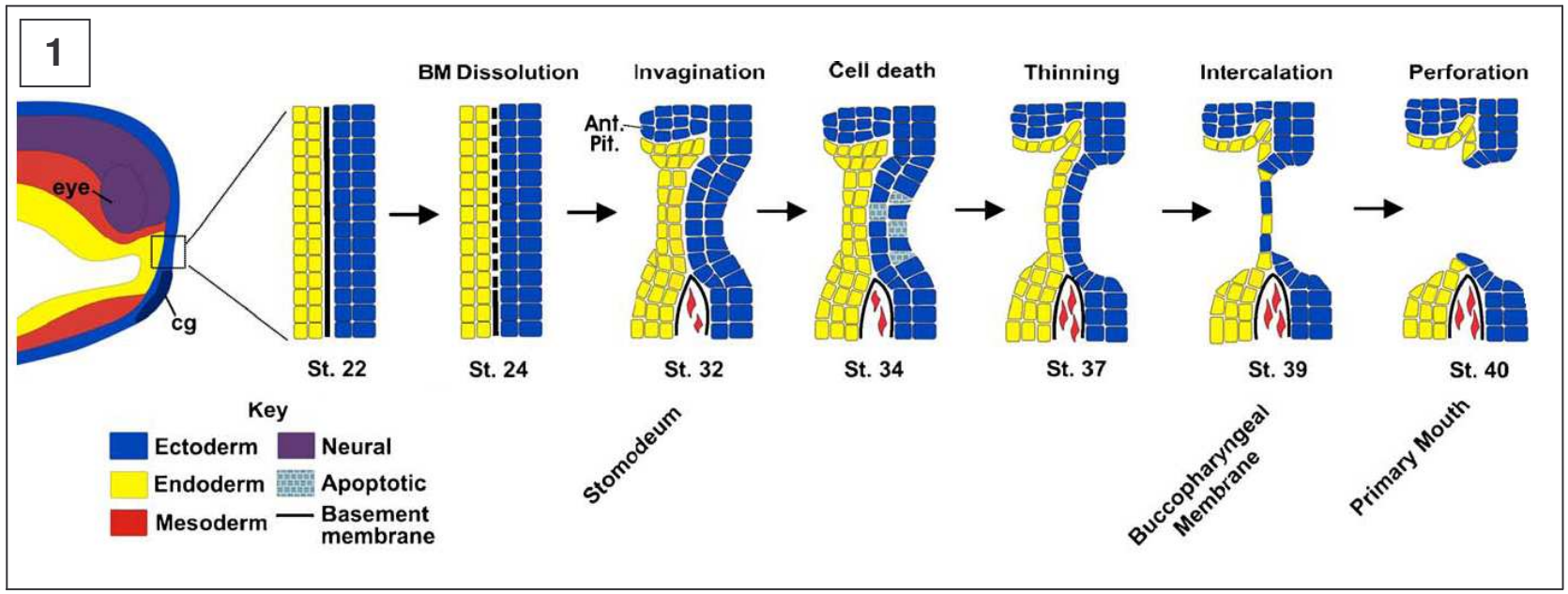
1
BM Dissolution
Invagination
Cell death
Thinning
Intercalation
Perforation
eye
cg
Ant. Pit.
St. 22
St. 24
St. 32
St. 34
St. 37
St. 39
St. 40
Key
Ectoderm
Endoderm
Mesoderm
Neural
Apoptotic
Basement membrane
Stomodeum
Buccopharyngeal Membrane
Primary Mouth

2

# MATERIALS AND METHODS

Six female and two male *Xenopus laevis* frogs (Fig. 2) were obtained for use in this experiment. They were housed in the Central Animal Unit, University of the Witwatersrand. Animal ethics clearance was obtained (animal ethics clearance number: 2006/15/02A).

## 2.1 FROG PREPARATION

### 2.1.1 Stimulation of Frogs to Lay

*Xenopus laevis* embryos were collected for use in this experiment after initiating the natural mating of the male and female frogs in amplexus. Prior to mating, the male frogs were primed with subcutaneous injections of 100 IU of human chorionic gonadotropin (hCG) (Sigma, CG10) into the dorsal lymph sac (Fig. 3), every three days until black nuptial pads were well developed on the medial aspect of the forelimbs. The female frogs were initially primed with subcutaneous injections of 50 IU of hCG into the dorsal lymph sac, at least five days before ovulation was induced.

Immediately prior to mating, a female frog was induced to ovulate with a subcutaneous injection of 300-600 IU of hCG and a male frog was stimulated with a subcutaneous injection of 50 IU of hCG. The female and male frogs were then placed in a darkened tank in the late afternoon in order to encourage mating. The female frogs began laying eggs about 9-10 hours after the induction of ovulation by the injection of hCG. The eggs were fertilized by the male as they emerged from the cloaca of the female.

The eggs were collected the following day in 1X Modified Barth's saline solution (MBS) with a high salt concentration (Appendix I). They were dejellied and placed

in an incubator at 15ºC-22ºC depending on the stages required. The eggs were then allowed to develop in a controlled environment.

2.1.2 Dejelling Embryos

Once collected, the jelly membranes surrounding the eggs were removed in a process known as dejelling. The eggs were placed in a 1X Modified Marc's ringer (Appendix I) with 2% cysteine at pH 8.0. The eggs were swirled gently for 2-4 minutes in the cysteine solution until the jelly membranes were visible in the solution and the eggs had started to pack closely together. The cysteine solution was then decanted and the fertilized eggs were repeatedly rinsed 2-10 times in 0.1X MBS (Appendix I), for approximately ten minutes. Following the removal of the jelly membranes, the embryos were placed in clean petri dishes in 0.1X MBS and allowed to develop to the appropriate stages.

2.1.3 Staging of the Embryos

Embryos used in this experiment were staged according to Nieuwkoop and Faber, 1967 (Fig. 4). Initially, investigations were undertaken to determine the most appropriate developmental stages of the embryos for suitable analysis of the proctodeal region. From the literature, a range of embryonic stages appropriate for analysis was ascertained. A number of embryos at each of these stages were fixed in 10% neutral buffered formalin (Appendix II), dehydrated in a graded series of alcohols, embedded in resin, serially sectioned at 6-8 μm and stained with Gill's haematoxylin (Appendix III) and eosin. The sections were then viewed under a light microscope and assessed to determine the appropriate stages for analysis. At stage 21 a small depression was apparent which deepened during development and by stage 24 the cloacal membrane had broken down. It was thus concluded that embryos between stage 21 to stage 26 would be evaluated. This range of embryonic stages would illustrate some of the morphological features and some of the processes involved from the initiation of proctodeal depression development through the thinning of the cloacal membrane to perforation of the cloacal membrane. For *in situ* hybridization,

embryos at stages 22, 24 and 26 only were used for analysis. For each technique, at least six embryos per stage were used for analysis, except for the immunohistochemical technique for the immunolocalization of the pro-apoptotic protein Bax and the anti-apoptotic protein Bcl-2, where only one embryo per stage was used for analysis. This latter technique came about solely to determine the efficacy of the TUNEL method.

## 2.2 TIME COURSE

Initially the development of the proctodeum was to be observed using a time lapse facility. Embryos ranging from stage 17 to stage 24 were placed individually in depressions made in 1% agar coated small petri dishes in 0.1X MBS, with the ventral surface facing downwards. The petri dishes were then placed on a Zeiss Axiovert inverted phase contrast light microscope with sterile incubation facilities or on a confocal microscope (Zeiss Confocal Laser Scan Microscope). The intact embryos were very dense and the proctodeal depression was not seen under either of these microscopes. A compromise was reached and the petri dishes, with the ventral surfaces of the embryos facing upwards were then positioned on a stereomicroscope (Olympus) with transmitted light and images were captured manually with an Olympus digital camera every hour over a time period of four hours. The microscope was situated in a sterile environment and the temperature of the room was 23ºC. This temperature was monitored closely with a thermometer.

## 2.3 CONFOCAL MICROSCOPY

The confocal microscope was used to view the interior structures of the embryo, focusing on the proctodeal region and the cloacal membrane.

The embryos were prepared for optical fluorescent sectioning by fixation in Bouin's solution (Appendix II) at 4ºC, for 2-12 weeks. The embryos were then washed in

0.1% ammonium hydroxide in 70% ethanol overnight at 4ºC. The following day, the embryos were bleached in a hydrogen peroxide solution (0.5% hydrogen peroxide, 1% formamide in 0.5% SSC (sodium chloride/sodium citrate buffer solution). They were left in this solution overnight at 4ºC, after which they were cleared in a 3:1 benzyl benzoate/benzyl alcohol solution for at least 24 hours. The combination of the fixative and the benzyl benzoate/benzyl alcohol treatment produced autofluoresence of the embryonic cells. The embryos were placed in depression petri dishes and viewed with a confocal microscope (Zeiss Confocal Laser Scan Microscope), using a wavelength of 488 nm. Sagittal z-sectioning was performed to produce slices through the embryo.

## 2.4 SCANNING ELECTRON MICROSCOPY

Three dimensional images of the developing proctodeum and the surface features of the proctodeal region were defined using a scanning electron microscope.

Embryos were fixed in 2.5% glutaraldehyde in phosphate buffered saline (PBS) (Appendix I) at 4ºC, for 2-12 weeks. The embryos were washed for 3 x 5 minutes in PBS and post-fixed in 1% osmium tetroxide in PBS for 1 hour. The embryos were then washed for 3 x 5 minutes in PBS and dehydrated through a graded series of alcohols. The embryos were taken through 50% alcohol for 15 minutes, 70% alcohol for 2 x 15 minutes, 95% alcohol for 15 minutes and finally 100% alcohol for 15 minutes. They were then placed in another change of 100% alcohol and left at 4ºC overnight. The following day, embryos were taken for critical point drying to the Electron Microscope Unit. The specimens were mounted on to scanning electron microscope stubs and coated with gold palladium. The embryos were kept in a dessicator and viewed with an electron microscope (JEOL 840 SEM) at 15 kV.

## 2.5 HISTOLOGY

Embryos were prepared for histology by fixing in 10% neutral buffered formalin at 4ºC, for 2-12 weeks. Fixed embryos were washed in PBS and then dehydrated in a series of alcohols. Once dehydrated, the embryos were processed and embedded in plastic resin, using a JB-4 Embedding Kit (Agar Scientific, R1130). The embryos were initially placed in the infiltration solution, on a slow rotator at 4ºC, for approximately 20 minutes. The embryos were then placed in another change of infiltration solution and left at 4ºC overnight. The following day, the infiltration solution was removed and the embryos were placed in plastic moulds, to which the resin embedding solution was added. The embryos were orientated and left overnight at room temperature to allow for polymerization of the resin.

Once the resin had polymerized, the embryos were removed from the moulds and serially, sagittally sectioned at 6-8 μm. The resin sections were floated in a water bath containing 0.2% ammonium hydroxide, picked up on glass slides and left overnight at room temperature to dry.

Once dry, the sections were stained with Gill's haematoxylin and eosin. The sections were placed in Gill's haematoxylin for 30 minutes, washed in running tap water for 10 minutes, placed in eosin for 5 minutes and rinsed for 30 seconds in tap water. After this, the sections were dehydrated in a series of alcohols, mounted with entellen and viewed under a light microscope.

## 2.6 IMMUNOLOCALIZATION OF THE BASEMENT MEMBRANE MARKERS FIBRONECTIN AND LAMININ

The role of the basement membrane between the proctodeal ectoderm and hindgut endoderm in the development of the proctodeal region was analysed using assays for the expression of the basement membrane components fibronectin and laminin.

2.6.1 Embryo Preparation and Immunolocalization

*Xenopus laevis* embryos and the rat kidney were fixed in 4% paraformaldehyde (Appendix II). The embryos were fixed for 1-2 hours and the rat kidney was left in fixative overnight. The embryos and rat kidney were then washed in PBS for 3 x 15 minutes. The rat kidney was embedded in paraffin wax. The embryos were dehydrated in a graded alcohol series, placed in a final change of 100% alcohol and stored at -20ºC for 1-3 days. Specimens were then brought to room temperature, rehydrated in a graded series of alcohols and embedded in paraffin wax. The embryos and rat kidney were serially sectioned at 10 µm and placed on silane-coated slides (Appendix V).

The sections were dewaxed in xylene, hydrated through a graded series of alcohols to distilled water and placed in tris/saline. The sections were then placed in 3% hydrogen peroxide in distilled water for 10 minutes and washed for 3 x 15 minute in tris/saline. The sections were placed in a damp chamber and the non-specific staining blocked with 10% swine serum diluted in tris/saline, for 10 minutes. They were then drained and serial sections were incubated with either polyclonal fibronectin antibody (DakoCytomation, A0245) diluted in tris/saline at a concentration of 1:400 or polyclonal laminin antibody (Sigma, L9393) diluted in tris/saline at a concentration of 1:25. The sections were left overnight at 4ºC in a well-sealed, damp chamber.

The following day, the sections were drained and washed for 3 x 5 minutes in tris/saline containing 1% horse serum. They were then incubated with the swine anti-rabbit secondary antibody (DakoCytomation, P0217), diluted in tris/saline at a concentration of 1:50, for 1 hour in a damp chamber. The sections were drained and washed for 3 x 5 minutes in tris/saline. Following this, they were incubated in the 3.3'-diaminobenzidine (DAB) solution (Appendix IV) for 5 minutes, washed in tris/saline and placed in distilled water. The sections were washed in gently running water for 5 minutes, after which they were dehydrated through a graded series of alcohols, cleared in xylene and mounted in entellen.

The above protocol was followed for the localization of both fibronectin and laminin. However, various minor adjustments had to be made to this protocol to ensure greater specificity of the localization of these proteins.

For the localization of fibronectin a step to permeabilize the cell membranes was included. Once the sections were dewaxed and hydrated, they were placed in a 1% Triton-x-100, 1% dimethyl sulfoxide solution made up in PBS for 3 hours, to permeabilize the cell membranes. The sections were then washed briefly in tris/saline. The sections were then placed in 3% hydrogen peroxide in distilled water and the original protocol followed.

No adjustments were initially made to the immunohistochemistry protocol for laminin localization. However, no results were obtained and a protein assay and dot blot were thus performed to investigate the viability of the laminin antibody.

The protein assay and dot blot indicated that the antibody was still viable although the dot blot only produced a faint result, indicating that the anti-laminin may have been degrading although laminin was present in the samples. A new antibody was ordered and antigen retrieval was performed. This involved placing the sections in 1 mM ethylenediaminetetraacetic acid (EDTA) (pH 8.0), following the dewaxing and hydration of the sections. The sections were then heated in a microwave oven on a medium heat (360 W) for 2 x 5 minutes and then allowed to cool for 20 minutes. The sections were then placed in 3% hydrogen peroxide in distilled water and the original protocol was continued.

### 2.6.2 Controls for Immunohistochemistry of Fibronectin and Laminin

Both positive and negative controls were included for the immunohistochemical technique. Positive controls were used to ensure the efficacy of the technique, whilst negative controls were used to ensure the specificity of the antibodies.

Kidney dissected from an adult male Sprague-Dawley rat (animal ethics clearance number: 2007/33/4), killed with an overdose of euthanase, acted as a positive control for both the laminin and the fibronectin antibodies.

Kidney sections and sections of the embryos were used as negative controls. In the kidney sections the primary and secondary antibodies were omitted and replaced with tris/saline (Appendix I) respectively. A further negative control involving the omission of the primary antibody and replacement with 10% swine serum was included. The serial sections adjacent to the embryo sections, on which immunolocalization was performed for either laminin or fibronectin, were used as negative controls. In these sections the relevant primary antibody was omitted and replaced with tris/saline.

The serial sectioning allowed for an accurate interpretation of data as the immunolocalization technique for fibronectin and laminin was performed in the same specific region of each embryo. As the embryos were sectioned relatively thickly (to ensure that the thin basement membranes could be easily identified and visualized) and the area of interest is fairly small, only a few sections per embryo were available. Therefore, there were not enough sections on which to perform negative controls directly on the embryos involving the omission of the secondary antibodies and replacement with buffer and omission of the primary antibodies and replacement with 10% swine serum. These negative controls were however performed on the kidney control tissue, which was also used as a positive control. Due to the thickness of sectioning it was also not always possible to perform negative controls directly on the embryos for both fibronectin and laminin, per embryo.

### 2.6.3 Protein Assay and Dot Blot

A protein assay was initially performed to determine if protein was present in the experimental samples and a dot blot was performed to investigate the viability of the polyclonal laminin antibody.

*2.6.3.1 Sample Extraction*

In order to obtain a sample for the protein assay and dot blot, fertilised *Xenopus laevis* eggs at various stages of development were collected and placed in a homogeniser with five times the volume of homogenizing buffer (Appendix I). The eggs were homogenized slowly and this homogenate was placed into eppendorfs on ice until all samples were ready for use. The homogenate was centrifuged at 12 000 rpm for 20 minutes at 4ºC to remove the large particulate matter. The supernatant was then removed, aliquoted and stored in eppendorfs at -80ºC.

*2.6.3.2 Protein Assay*

Thick filter paper was used on to which 3 µl of the undiluted sample and 3 µl of the sample at a concentration of 1:10 was pipetted. This was left to dry for approximately 15 minutes, after which 10% trichloroacetic acid was poured on to the filter paper, covering it completely. This was left on for 30 seconds. The filter paper was then washed briefly in water and placed in Coomassie blue for 30 seconds. It was then washed again briefly in water and placed in a "destaining" solution until background staining was limited.

*2.6.3.3 Dot Blot*

The dot blot membrane was divided into sections and 10 µl of sample was pipetted on to each section. The sample was used undiluted and at a concentration of 1:10. The membrane was blocked in Bloto (Appendix IV) on a shaker for 1 hour at room temperature. The Bloto was then poured off and polyclonal laminin antibody (Sigma, L9393) was applied to the samples at a concentration of 1:500 and 1:1000. The samples were incubated in the primary antibody for 2 hours at room temperature. This was followed by 3 x 5 minute washes in tris with Tween-20 (Appendix I), on the shaker. Swine anti-rabbit (DakoCytomation, P0217) secondary antibody (1:20) was applied to the samples for 45 minutes at room temperature. This was followed by 3 x 5 minute washes in tris with Tween-20, on the shaker. The membrane was then washed for 5 minutes in tris buffered saline (Appendix I). The tris buffered saline

was poured off and POD (BM Blue POD substrate, precipitating) (Roche, 1 484 281) was added. When a blue reaction colour was apparent with minimal background staining, this was considered a satisfactory reaction and the reaction was stopped with distilled water.

## 2.7 TERMINAL DEOXYNUCLEOTIDYL TRANSFERASE MEDIATED dUTP NICK END-LABELLING (TUNEL) FOR DETECTION OF APOPTOTIC CELLS

The Apoptag kit (Chemicon, S7100) was used to detect apoptosis in the proctodeal region of the *Xenopus laevis* embryos.

### 2.7.1 Embryo Preparation and Staining

*Xenopus laevis* embryos were staged and the posterior regions sectioned free from the rest of the embryos, exposing the hindgut cavity. These posterior regions of the embryos were then fixed in 4% paraformaldehyde for 1-2 hours and washed in phosphate buffered saline with Tween-20 (PBT) (Appendix I) for 3 x 15 minutes. These samples were then dehydrated in a graded series of alcohols and placed in a final change of 100% alcohol and stored at -20ºC for up to 1 week.

The posterior regions of the embryos were processed with all washing steps taking place on a shaker. The posterior regions of the embryos were rehydrated in a graded series of alcohols and washed for 3 x 10 minutes in PBT. They were bleached in a hydrogen peroxide solution (Appendix IV) on a light box for 1-2 hours or until the embryos became white. This was followed by 3 x 10 minute washes in PBS. The posterior regions of the embryos were then treated with proteinase K (Roche, 03 115 887 001) diluted in PBS at a concentration of 1-2 µg/ml for 5-10 minutes. This was followed by 2 x 10 minute washes in PBT, after which the posterior regions of the embryos were refixed in 4% paraformaldehyde for 15-20 minutes. The samples were then taken through 5 x 10 minute washes in PBT and incubated in the equilibration buffer, provided in the kit, for 1-5 hours. As much buffer as possible was then

removed and the samples were incubated overnight at room temperature in a solution of reaction buffer (77 µl) and TdT enzyme (33 µl) provided in the kit.

The following day, the posterior regions of the embryos were incubated at 37ºC for 1 hour. The reaction buffer and TdT enzyme solution was removed and replaced by stop solution. The samples were incubated in this solution for 1 hour, after which they were washed for 3 x 10 minutes in maleic acid buffer (MAB) (Appendix I). The samples were then placed in blocking solution (Appendix IV) for 2 hours after which they were placed in anti- digoxigenin-peroxidase (anti-DIG-peroxidase) diluted with the blocking solution for 2 days at 4ºC.

Following incubation, the posterior regions of the embryos were washed for 5 x 30 minutes in MAB. They were then incubated in the peroxidase substrate (0.05% DAB in tris/HCl) for approximately 15 minutes until a brown staining reaction was produced, with minimal background staining. The samples were then washed in distilled water for 3 x 10 minutes and fixed in 4% paraformaldehyde overnight at 4ºC. The following day, the background staining was reduced using 100% alcohol and the posterior regions of the embryos were viewed.

Once the posterior regions of the embryos had been viewed, they were taken through two changes of xylene and embedded in paraffin wax. They were then serially sectioned at 10 µm, mounted in entellen and viewed.

The protocol used for the labelling of the whole embryos was modified and adapted for apoptosis detection in the control testis sections.

The sections were dewaxed in xylene, hydrated in a graded series of alcohols and placed in running for 5 minutes. The sections were treated with proteinase K (20 µg/ml) (Roche, 03 115 887 001) diluted in PBS for 15 minutes and then washed for 2 x 2 minutes in distilled water. The sections were quenched in 3% hydrogen

peroxidase in PBS for 5 minutes and rinsed with PBS for 2 x 5 minutes. The excess liquid was removed and the equilibration buffer, provided in the kit, was applied to the sections for approximately 30 minutes. The working strength TdT enzyme was prepared prior to use (77 µl reaction buffer and 33 µl TdT enzyme) and applied to the sections, which were then incubated at 37ºC for 1 hour. The sections were then placed in the working strength stop/wash buffer (1 ml stop/wash buffer, provided in the kit and 34 ml distilled water) for 10 minutes. The sections were washed for 3 x 1 minute in PBS. The anti-DIG-peroxidase was applied to the sections and incubated in a damp chamber for 30 minutes at room temperature. The sections were washed for 4 x 2 minutes in PBS and covered with 0.05% DAB in PBS for 5 minutes. The sections were washed in distilled water for 3 x 1 minute and left in distilled water for 5 minutes. The sections were then dehydrated in a graded series of alcohols, cleared in xylene and mounted with entellen.

2.7.2 Controls for the TUNEL Technique

A positive control, namely testis was included to ensure the effectiveness of the technique. Testes were obtained from a Sprague-Dawley rat (animal ethics clearance number: 2007/33/4), killed by an overdose of euthanase. The testes were fixed in 4% paraformaldehyde overnight, routinely processed and embedded in paraffin wax. Sections of 10 µm were cut and placed on glass slides, to which the experimental protocol was applied.

Negative controls were also included in this technique. This involved omitting the reaction buffer and terminal deoxynucleotidyl transferase enzyme (TdT) and replacing it with PBS.

## 2.8 IMMUNOLOCALIZATION OF BAX AND BCL-2 FOR DETECTION OF APOPTOTIC CELLS

The TUNEL method proved to be quite erratic and results in detecting apoptotic cells, especially in the later stages of this study, were inconclusive. Immunolocalization of the pro-apoptotic protein Bax and anti-apoptotic protein Bcl-2 was performed to determine the efficacy of the TUNEL technique and ascertain if this was a more appropriate method for apoptotic cell detection, than TUNEL. Sufficient antibody was also only available to perform immunolocalization on a few embryos. Therefore only one embryo per stage was used in analysis and the results aided in enhancing and confirming those obtained from the TUNEL method.

### 2.8.1 Embryo Preparation and Immunolocalization

*Xenopus laevis* embryos and mouse colon were fixed in Carnoy's fixative made up in absolute methanol (Appendix II). The embryos were fixed for 1-2 hours and the mouse colon was left in fixative overnight. The embryos and mouse colon were then washed in PBS for 3 x 15 minutes, dehydrated in a graded series of alcohols and embedded in paraffin wax. The embryos and mouse colon were then serially sectioned at 10 μm and placed on silane-coated slides.

The sections were dewaxed in xylene, hydrated through a graded series of alcohols to distilled water and placed in PBS. Antigen retrieval was then performed on the sections, by placing the sections in a container and covering them with tris-EDTA buffer (pH 9.0) (Appendix I). The sections were then heated in a microwave oven on medium heat (720 W) for 2 x 5 minutes and allowed to cool for 20 minutes. The sections were then washed for 3 x 2 minutes and the endogenous peroxidase activity was quenched by placing the sections in 1% hydrogen peroxide in PBS for 10 minutes. The sections were washed for 2 x 5 minutes in PBS, placed in a damp chamber and covered with 10% goat serum diluted in PBS for 20 minutes to block non-specific staining. The sections were then drained and serial sections were incubated with either polyclonal rabbit anti-human Bax (DakoCytomation, A3533)

diluted in diluent for the anti-serum at a concentration of 1:50 or monoclonal mouse anti-human Bcl-2 (DakoCytomation, M0887) diluted in diluent for the anti-serum at a concentration of 1:50. The sections were left overnight at 4ºC in a well-sealed, damp chamber.

The following day, the sections were drained and washed with PBS for 2 x 2 minutes. They were then incubated with the appropriate secondary antibody for 1 hour in a damp chamber. The secondary antibody used for localization of Bax was polyclonal goat anti-rabbit (DakoCytomation, P0448), diluted in PBS at a concentration of 1:200, whilst polyclonal goat anti-mouse (DakoCytomation, P0447) diluted in PBS was used at a concentration of 1:200 for the detection of Bcl-2. The sections were then washed in PBS for 2 x 2 minutes and treated with DAB (Roche, 1 718 096) (Appendix IV) for 5 minutes. The sections were rinsed in distilled water for 2 minutes, dehydrated in a graded series of alcohols, cleared in xylene and mounted in entellen.

2.8.2 Controls for Immunohistochemistry of Bax and Bcl-2

Both positive and negative controls were included in the immunohistochemical technique. Positive controls were used to ensure the efficacy of the technique, whilst negative controls were used to ensure the specificity of the primary antibodies.

Colon dissected from an adult female NMRI x NMRI mouse (animal ethics clearance number: 2007/19/2A), killed with an overdose of euthanase, acted as a positive control for both the Bax and the Bcl-2 antibodies.

Colon sections and sections of the embryos were used as negative controls. In the colon sections, the primary and secondary antibodies were omitted independently and replaced with diluent (Appendix IV) and PBS respectively. A further negative control involving the omission of the primary antibody and replacement with 10% goat serum was included. The serial sections adjacent to the embryonic sections

where both the primary and secondary antibodies were applied for Bax or Bcl-2 immunolocalization, were used as negative controls. In these sections the relevant primary antibody was omitted and replaced with diluent.

The serial sectioning allowed for an accurate interpretation of data as the immunolocalization technique for Bax and Bcl-2 was performed in the same specific region of each embryo. As the embryos were sectioned relatively thickly, at 10 µm and the proctodeal region is fairly small, only a few sections per embryo were cut. Therefore there were not enough sections on which to perform negative controls involving the omission of the secondary antibodies and replacement with buffer and omission of the primary antibodies and replacement with 10% swine serum. These negative controls were however performed on the colon control tissue, with the positive control, to ensure the specificity of the localization. In fact it was not always possible to include embryonic sections whereby both the primary antibodies had been omitted and replaced with diluent, per embryo.

## 2.9 *IN SITU* HYBRIDIZATION FOR *BONE MORPHOGENETIC PROTEIN-4*

Whole mount *in situ* hybridization was performed on stages 22, 24 and 26 *Xenopus laevis* embryos, to determine the regionalization of expression of *Bone Morphogenetic Protein-4 (BMP-4)*.

### 2.9.1 Controls for *In Situ* Hybridization

*BMP-4* expression occurs in the anterior region of *Xenopus laevis* embryos, at stage 14 (Karaulanov *et al.*, 2004). Therefore stage 14 embryos were used as controls for *BMP-4* expression.

To ensure the viability of the technique another specific probe that gave a distinctive pattern of hybridization was used as a standard control. The control probe used was *Xenopus Cement Gland-1* (*XCG-1*), which has specific expression and is a marker of

the secretory cement gland in the anterior region of *Xenopus laevis* embryos. *In situ* hybridization for this gene was performed on embryos at stages 14, 22, 24 and 26. Sense probes (the same sense as the mRNA) for both *BMP-4* and *XCG-1* were prepared and used as negative controls.

### 2.9.2 Probe Preparation

Antisense and sense probes were prepared from both BMP-4 and XCG-1 plasmids. The BMP-4 plasmid was constructed by Dr J. Gamse and the XCG-1 plasmid was constructed by Dr H. Sive. Both were kind gifts from the Sive Laboratory, Whitehead Institute, Massachusetts Institute of Technology, Boston, USA.

#### *2.9.2.1 Plasmid Linearization*

The New England Biolabs website: www.neb.com was consulted to determine the correct buffers, restriction enzymes and conditions needed for plasmid linearization.

In order to linearize the BMP-4 and XCG-1 plasmids, they were cut with restriction enzymes. The *BMP-4* antisense probe was made using the *ECORI* Buffer and by cutting with *ECORI*, whilst the sense probe was made using the New England Buffer 3 and by cutting with *BamHI*. Both *XCG-1* probes were made using the New England Buffer 3. The antisense probe was cut with *Not1*, whilst *BamHI* was used for cutting in the sense probe preparation. To linearize the plasmids, 10 µg of each DNA template was placed in a separate eppendorf tube. To each tube, 2 µl of the specific restriction enzyme was added with 10 µl of the specific buffer. For the *BMP-4* sense probe and both *XCG-1* probes, 10 µl of bovine serum albumin (BSA) was added to each eppendorf tube. Each tube was then made up to 100 µl with autoclaved distilled water. The tubes were then placed in a 37ºC water bath overnight.

#### *2.9.2.2 DNA Gels*

The following day the tubes were taken out of the water bath and a sample of each DNA was run on an agarose gel to check the linearized DNA.

To make the gel, 0.5 g agarose was added to 50 ml 1X tris/acetate/EDTA (TAE) buffer (Appendix I) and heated for 1-2 minutes in the microwave. Approximately 5 µl ethidium bromide was then added. The gel was poured and left for about 30 minutes to set. The samples (10 µg/ 100 µl) and a DNA ladder were prepared and loaded into the gel. The gel was placed in 1X TAE buffer and run at 70 V until the dye had approximately reached the half way mark of the gel. The samples were then viewed using ultraviolet light.

*2.9.2.3 Linear DNA Clean Up*

Once the DNA samples had been checked on the agarose gel, the DNA was purified using a QIAquick PCR (Polymerase Chain Reaction) Purification Kit (Qiagen, 28104). All the centrifuge steps were done at 13 000 rpm (~ 17 900 x g) in a conventional microcentrifuge. Each ~ 100 µl DNA sample was added to 500 µl of Buffer PB, provided in the kit. Each sample was placed in a QIAquick column, in a provided 2 ml collection tube, and centrifuged for 1 minute, in order to bind the DNA. The flow-through was discarded and the QIAquick column placed back into the same tube. To wash, 0.75 ml of Buffer PE, provided in the kit, was added to each QIAquick column and centrifuged for 1 minute. The flow-through was discarded and the QIAquick column placed back into the same tube. The column was centrifuged again for another minute, to completely remove any residual ethanol buffer. Each QIAquick column was then placed in a clean 1.5 ml eppendorf tube and the DNA was eluted by adding 40 µl of autoclaved, distilled water (pH 8.5) to each sample (to the centre of the QIAquick membrane) and centrifuging the columns for 1 minute.

The concentration of the purified DNA samples was then determined, using a nanodrop. The graph (absorbance vs. wavelength) and the 260/280 wavelength ratio (normal ratio: 1.75-2.00) generated by the software allowed for interpretation of contamination.

*2.9.2.4 Transcription*

Once the concentrations of the DNA samples were determined, the DNA was used to transcribe RNA. The *BMP-4* antisense and the *XCG-1* sense probes were transcribed with T7 RNA polymerase and the *BMP-4* sense and *XCG-1* antisense probes were transcribed with T3 RNA polymerase. For each transcription reaction, 2-3 µg of DNA template was added to 5 µl of transcription enzyme, 2 µl RNAsin (inhibitor of exogenous RNA), 10 µl of 5 x transcription buffer and 5 µl DIG RNA Labelling Mix (Roche, 11 277 073 910). Each sample was then made up to 50 µl with autoclaved distilled water. The eppendorf tubes containing each sample were placed in a 37ºC water bath for approximately five hours.

Once the RNA was transcribed, the solution appeared cloudy and 25 µl of lithium chloride solution was added to each eppendorf. The samples were then incubated overnight at -20ºC.

The following day the samples were centrifuged at 4ºC for 20 minutes, at 14 000 rpm. The supernatant was discarded and 1 ml 70% ethanol was added to each sample. The samples were then centrifuged again at 4ºC for 20 minutes, at 14 000 rpm. The supernatant was discarded and the pellets were left to air dry for approximately 10 minutes, after which 30 µl of autoclaved distilled water was added to each sample.

*2.9.2.5 RNA Gels*

The concentrations of the RNA probes were then determined with the nanodrop and the probes were checked on a formaldehyde gel.

The formaldehyde gel was made up with 0.5 g agarose, 5 ml 10X MOPS buffer (Appendix I) and 43.5 ml distilled water. This was heated in the microwave for 1-2 minutes, after which it was topped up to 48.5 ml with distilled water. To this, 2.55 ml 37% formaldehyde was added. The gel was then poured and left for at least 30 minutes to set.

The RNA samples were prepared by adding 1 µg of RNA solution to 7.5 µl of RNA loading buffer (premixed with EtBr and BPB) (Sigma, R4268) and made up to 15 µl with distilled water. The samples were then heated at 65ºC for 10 minutes.

When set, the gel was placed in 1X MOPS buffer (Appendix I). The samples and a RNA ladder were loaded and the gel was run at 65-70V. When the purple dye reached just below the halfway mark, the current was turned off and the gel was viewed using ultra violet light.

2.9.3 Embryo Preparation, Hybridization and Staining

*Xenopus laevis* embryos at stages 14, 22, 24 and 26 were fixed in 4% paraformaldehyde overnight at 4ºC and processed over a number of days.

The day following fixation, the embryos were rinsed for 3 x 15 minutes in PBT and dehydrated in a graded series of methanol. The embryos were then placed in a final change of 100% methanol and stored at -20ºC until needed.

The embryos were then brought back to room temperature and processed for *in situ* hybridization, with all washes occurring on a shaker. They were rehydrated in a series of methanols and washed for 3 x 15 minutes in PBT. The embryos were then rinsed in 0.1 M triethanolamine (Appendix IV) for 2 x 5 minutes. After this the embryos were washed in 4 ml triethanolamine containing 12.5 µl acetic anhydride for 5 minutes. Another 12.5 µl acetic anhydride was then added to the 4 ml triethanolamine containing 12.5 µl and the embryos were washed for 5 minutes. The embryos were then washed in PBT for 3 x 15 minutes and bleached in a hydrogen peroxide solution on a light box, for 1-2 hours or until they became white. The embryos were then washed in 2X SSC (Appendix I) for 15 minutes, followed by 2 x 15 minute washes in PBT. They were then placed in hybridization buffer (Appendix I) and incubated at 60ºC overnight.

The following day the probes were added at concentrations of 1 µg/ml to fresh aliquots of hybridization buffer, which had been warmed at 60ºC. The embryos were placed in the probe/hybridization solution and incubated overnight at 60ºC. Fresh aliquots of hybridization buffer and 2X SSC and 0.2X SSC (Appendix I) solutions were placed in the 60ºC incubator for use the next day.

The probes were then removed from the specimens, the next day and fresh, warmed hybridization buffer was added to the embryos. The embryos were then incubated for 30 minutes at 60ºC. The embryos were washed in warm 2X SSC at 60ºC for 3 x 30 minutes and then in warm 0.2X SSC at 60ºC for 3 x 30 minutes. This was followed by a wash in 0.2X SSC at room temperature and 3 x 15 minute washes in MAB. The embryos were then placed in blocking solution for 2-3 hours after which they were placed in the antibody solution consisting of 1 ml blocking solution and 0.63 µl Anti-DIG-AP (Roche, 11 093 274 910). The embryos were then incubated in this antibody solution at 4ºC overnight.

The next day, the embryos were taken through a series of washes. They were washed in MAB for 6 x 30 minutes, followed by 2 x 30 minute washes in alkaline phosphatase buffer (Appendix I). The embryos were then incubated in the dark in a solution of 36 µl 4-nitroblue-tetrazolium chloride (Roche, 1 383 213) and 28 µl 5-bromo-4-chloro-3-indolyl-phosphate (Roche, 1 383 221) in 10 ml AP buffer. The staining was checked periodically under the dissecting microscope. When the staining reaction was satisfactory the embryos were rinsed in MAB for 3 x 10 minutes. They were then fixed in 4% paraformaldehyde at 4ºC overnight.

The following day, the embryos were placed in 100% methanol to clear any background staining. They were then rehydrated quickly in a methanol series, fixed in 4% paraformaldehyde and viewed.

Figure 2. A male *Xenopus laevis* frog (left) and a female *Xenopus laevis* frog (right) used in this experiment.

Figure 3. A male *Xenopus laevis* frog being injected with 50 IU human chorionic gonadotropin into the right dorsal lymph sac, prior to mating.


2


3

3

# RESULTS

The *Xenopus laevis* embryos used in this experiment were staged according to Nieuwkoop and Faber, 1967. Initially, through histological analysis of sections of the embryos using Gill's haematoxylin and eosin, it was determined that embryos at stages 21-26 (Fig. 4) should be used for analysis, as these stages showed development of the proctodeum and dissolution of the cloacal membrane.

In embryos at stage 21 (Fig. 4a) closure of the neural tube had occurred and the secretory cement gland at the anterior region of the embryo had become a prominent feature in the whole embryos and in histological sections. At this stage, the proctodeal depression had become morphologically discernible (Fig. 5e). In embryos at stage 22 of development (Fig. 4b), the eyes were protruding and the lateral and ventral outlines of the embryo had a slightly concave appearance. As development continued, the embryos became more elongated and the concave ventral outline of the embryos was more pronounced at stage 23 (Fig. 4c). The jaw and gill areas of the embryos at this stage of development were distinctly separated by a groove. At stage 24 (Fig. 4d) the gill area was seen to be more prominent than the jaw area and the tailbud was easily discernible in the whole embryos (Fig. 5h). This was also the stage at which the embryos had a motor reaction in response to external stimuli. From histological analysis of sagittal sections it was determined that this was the stage at which the cloacal membrane had perforated (see Fig. 26). At stage 25 (Fig. 4e) the tailbud of the embryos was more extended and fin formation was apparent. The ear vesicles were invaginated at this stage and started to protrude at stage 26 (Fig. 4f) of development. The fin was seen to become broader at the dorso-caudal end of the body (Fig. 5l) and the myotomes were visible for the first time. At this stage, the cloacal membrane was no longer intact (see Fig. 28). However, various morphological features such as the presence of vacuolated cells (see Figs. 26b, 27c)

seen in the histological sections in the ectoderm of the cloacal region indicated that active processes are ongoing in cells around this region in embryos where perforation of the cloacal membrane has occurred.

## 3.1 TIME COURSE

As whole embryos were too dense for the changes related to the proctodeum to be captured on either the phase contrast time lapse facility or the confocal microscope, images of the developing embryos were captured manually. The images were captured every hour over a period of four hours and the embryos were staged accordingly. In order to capture the images, the embryos were placed on a stereomicroscope with transmitted light. Three embryos at different stages of development ranging from stage 17 to stage 24 at the start of the observation time, when the initial images were captured (Fig. 5) were observed. This showed the progression of growth and development of the external features of the embryos and the external development of the proctodeal region over time.

An embryo (stage 17) at the start of the observation time was very round in shape and the open blastopore was visible at the posterior region of the embryo (Fig. 5a). The rest of the ectodermal surface of the embryo had a smooth appearance and there was no sign of any additional ectodermal depression in the posterior region. Little change in the exterior morphological features was apparent in the image taken of the embryo one hour later (Fig. 5b). The embryo was at approximately stage 18 at this point in time. However, two hours after the initial observation, by which time the embryo had reached approximately stage 19, the embryo had elongated slightly and the blastopore was more ventrally positioned (Fig. 5c). Three hours after the initial observation, the embryo was at approximately stage 20 of development. The neural tube appeared narrower than earlier on in development (Fig. 5d), indicating that the neural tube was in the process of closing. However no ectodermal invagination was apparent on the posterior-ventral surface where the proctodeum is expected to develop.

An embryo at stage 21 of development at initiation of observation showed that the blastopore had closed. A small depression, the proctodeum, was visible on the posterior-ventral surface of the embryo (Fig. 5e). This depression was slit-like, but more rounded anteriorly. One hour after the initial observation (stage 22), the proctodeal depression appeared to have enlarged slightly (Fig. 5f). Two hours after initiation of observation, the embryo was at approximately stage 23 of development and had a more concave shape. The proctodeum was slightly more rounded in appearance and was ventrally placed (Fig. 5g). Four hours after initiation of observation, the embryo was in early stage 24 of development and the proctodeal depression appeared less distinct than earlier on in development (Fig. 5h).

The beginning of tailbud formation was seen in an embryo at stage 24 at the initiation of observation. The posterior end of the embryo was slightly wider than in embryos earlier on in development (Fig. 5i) but the proctodeal depression was barely visible in the embryo at stage 24. Little change in the depression was evident in this embryo one hour after the initial observation when the embryo had reached approximately stage 25 of development (Fig. 5j). However, the embryo had a substantially different appearance three hours after the initial observation, as the tailbud had extended and the midsection of the embryo was far narrower than the anterior and posterior ends (Fig. 5k). The embryo was in the early phase of stage 26 of development. The cloacal opening was more ventrally positioned than in earlier development. Four hours after the initial observation there was difficulty in positioning the embryo with the ventral surface facing upwards to capture an image. At this point in time, fin formation was evident and although the cloacal opening itself was not visible, the lateral image showed the position of this opening clearly (Fig. 5l). At this point in time, the embryo was between stages 26 and 27 of development.

Thus, no clear proctodeal depression was apparent on the posterior-ventral surface of the embryo until stage 21. From this stage onwards the depression enlarged slightly and became more rounded in appearance. As the embryo elongated and fin formation

occurred, the proctodeal depression became more ventrally placed and was less distinct than in previous stages by the time the embryo had reached stage 26.

## 3.2 CONFOCAL MICROSCOPY

The confocal microscope was used to view the interior features of the proctodeal region and in particular, the dissolution of the cloacal membrane. Images of single optical sections were obtained from sagittal z-sectioning and analysed.

Initially, at stage 21, at the posterior end of the embryo, the ectodermal surface appeared fairly smooth. There was slight curvature of the ectoderm on the ventral surface, however, no marked proctodeal depression was yet apparent (Fig. 6). At stage 22 a marked depression was apparent at the posterior end of the embryo on the ventral surface, indicating the proctodeum (Fig. 7). At stage 23 the proctodeal depression was similar in appearance to that at stage 22 and no pronounced deepening or change of this depression was apparent. There was also no clear evidence of the structure of the cloacal membrane (Fig. 8). The cloacal membrane, however, had perforated by stage 24 and there was now a free channel extending from the hindgut to the exterior, corresponding with the results of the histological study. This opening, where the hindgut opens to the exterior, will now be referred to as the cloacal opening (Fig. 9). This opening appeared to have increased in size during stages 25 (Fig. 10) and 26 (Fig. 11) of development of the embryos. By stage 26 the cloacal opening appeared more ventrally placed (as noted in whole embryos), corresponding with an increase in development and size of the tail bud and the beginning of fin formation. This was particularly apparent with the stereomicroscope in producing the time lapse series. The cells around the cloacal opening appeared to bulge at this stage (Fig. 11).

## 3.3 SCANNING ELECTRON MICROSCOPY

At stage 21, the blastopore was still evident but there was no marked ectodermal invagination at the posterior region indicating the proctodeal depression (Fig. 12). The surface ectodermal cells had a fairly smooth appearance with distinct cell borders. Short cilia were seen to occur in tufts and the tufts were evenly dispersed across the surface of the ectodermal cells (Fig. 13). At stage 22 a clear depression was seen on the ventral surface at the posterior region of the embryos (Fig. 14a). The depression was slit-like in appearance and although it was not possible to analyze the depth of the depression, it appeared quite shallow as some interior structures were visible (Fig. 14b). The ciliary tufts were still evenly dispersed across the ectodermal surface of the embryos and small clusters of cilia were apparent surrounding the proctodeum. In a number of stage 22 embryos, rod-like structures, approximately 1 µm in length, were found around the proctodeal depressions (Fig. 14c). These may possibly be bacteria as bacteria range in size but can be this small (Alberts *et al.*, 2002). As development of the embryos continued, the proctodeum increased in size and by stage 23, the proctodeum had an oval appearance (Fig. 15a). Although the depression was fairly small in size, it appeared to have deepened (Fig. 15b). A number of cilia were present around the proctodeal depression (Fig. 15c). By stage 24, the proctodeal depression was more pronounced (Fig. 16a) and from confocal microscopy (Fig. 9) and histological sections, the hindgut was seen to join to the exterior at the cloacal opening. This opening was still oval in shape but the cells in this cloacal region were arranged in a prominent circular protrusion around the opening (Fig. 16b). The opening was deeper than the proctodeal depression in earlier stages (Fig. 16c). One stage 24 embryo showed a deviation in the features of the cloacal region (Fig. 17). The location of the depression was in the expected area on the ventral surface at the posterior region of the embryo. However, the morphology of the depression differed from other stage 24 embryos analysed in that it was narrow and slit-like in appearance. The ectodermal cells around the depression appeared larger than the cells of more typical stage 24 embryos at the same magnification. Although there were cilia dispersed across the surface of the embryo, no cilia were

concentrated directly around the cloacal opening as was typical of other stage 24 embryos (Fig. 16b).

Another feature that was quite common to stage 25 (Fig. 18) and 26 embryos, was cellular looking "plugs" situated in the opening of the cloaca. These "plugs" were quite dense in appearance and took up the majority of the opening, which at stage 25 had increased in size and was more rounded in appearance (Figs. 19a, 19b). At stage 25 the protrusion of the cells surrounding the cloacal opening was also more pronounced (Fig. 19a) than that seen in stage 24 embryos (Fig. 16b). By stage 25 the cilia in the cloacal region were more clustered together and elongated than in earlier stages of development (Fig. 19b). Stage 26 embryos were morphologically very similar to stage 25 embryos with regard to the cloacal region. The opening was large and round in appearance at stage 26. The cells around the cloacal opening had a definite protruding appearance thus emphasising the cloacal opening (Figs. 20a, 20b). The ectodermal cells of the cloacal opening appeared to extend into the invagination, and the invagination appeared to be extremely deep as the interior structures were not discernible (Fig. 20c). The cilia at this stage were elongated and clumped together (Figs. 21, 22) and more numerous around the cloacal opening, than in earlier stages.

## 3.4 HISTOLOGY

The histology of proctodeal development and cloacal membrane dissolution was analysed on sections stained with Gill's haematoxylin and eosin.

The hindgut endodermal cells were relatively large and round and there were numerous yolk platelets scattered throughout the endoderm and the rest of the embryo. The ectodermal cells were found to be cuboidal to low columnar in shape. In the proctodeal region the cuboidal to low columnar ectodermal cells appeared to become slightly flatter as the cloacal membrane thinned over time.

At stage 21, when the neural tube had closed (Fig. 4a) a slight indentation of the ventral ectoderm was apparent in the posterior region of the embryos (Figs. 23a, 23b), which corresponded to the depression seen in the whole embryos with the stereomicroscope (Fig. 5e). This occurred close to the region where the hindgut, lined by endoderm, is developing. Development of the embryo to stage 22 showed little or no change in the size and depth of the ectodermal invagination (Figs. 24a, 24b), compared to that of stage 21 embryos (Figs. 23a, 23b). The proctodeal depression corresponded to that seen with the confocal (Fig. 7) and the scanning electron microscopes (Fig. 14a). Although numerous embryos were sectioned and stained for histological analysis there was difficulty in obtaining sections where direct apposition of the ectoderm and endoderm was clearly evident and thus the basement membrane separating the two was not always apparent. This may have been due to the plane of sectioning. Although at stage 22 (Figs. 24a, 24b) there may have been direct apposition of these cell layers, it was sometimes difficult to distinguish the mesoderm from the endoderm and to determine exactly where the hindgut terminated. At stage 23 direct apposition of the ectodermal and endodermal cell layers, which had thinned, was more apparent (Figs. 25a, 25b). At this stage there was also an increase in the number of cilia around the proctodeal region, which was in accordance with the results obtained using the scanning electron microscope (Fig. 15b). Dissolution of the cloacal membrane occurred at stage 24 and a free passage was formed between the hindgut and the exterior (Fig. 26a). At this stage there was some flocculated substance in the cloacal opening, which had a cellular appearance (Fig. 26b). There were also a few vacuolated or secretory looking cells scattered between the ectodermal cells in the proctodeal region (Fig. 26b). The number of cilia had also increased on the ectodermal surface around the cloacal opening, as seen in the scanning electron micrographs and were quite a prominent feature in this region (Fig. 26c). The histology of the cloacal region appeared similar in stage 25 (Fig. 27a) and stage 24 embryos (Figs. 26a, 26b). The cloacal openings appeared to be of a similar size at these two stages. No cloacal membrane was seen and the free passage between the hindgut and exterior was visible in stage 25 embryos, as in stage 24

embryos (Fig. 27a). At stage 25, there was an increase in vacuolated or secretory cells interspersed between the ectodermal cells at this stage, compared to stage 24 (Fig. 27b). A few cells were found to be prominently projecting from the ectodermal surface into the cloacal opening at stage 25 (Fig. 27c). The cloacal opening was clearly evident at stage 26 (Figs. 28a, 28b) and had increased in width, compared to earlier stages, corresponding to scanning electron micrographs (Fig. 20). A dense flocculation of cellular looking material was visible, forming "plugs" in the cloacal openings of numerous embryos (Fig. 28b). The cilia around the cloacal opening were more concentrated in this region and appeared more elongated and dense (Fig. 29). Numerous vacuolated or secretory looking cells scattered between the ectodermal cells were also visible in this region (Fig. 29).

## 3.5 IMMUNOLOCALIZATION OF THE BASEMENT MEMBRANE MARKERS FIBRONECTIN AND LAMININ

Immunolocalization of fibronectin and laminin was undertaken to determine the role of the basement membrane which lies between the proctodeal ectoderm and hindgut endoderm in proctodeal development and cloacal membrane dissolution.

### 3.5.1 Protein Assay and Dot Blot

Initially, there was difficulty in obtaining immunolocalization of laminin, even in the control tissue. A protein assay and dot blot were thus performed to investigate if there was protein in the samples and if the laminin antibody was viable and present in the embryonic tissue.

The results of the protein assay for laminin revealed a blue reaction when the sample was used undiluted (Fig. 30a), indicating the presence of protein in the *Xenopus laevis* embryonic sample. When the sample was used at a concentration of 1: 10 no reaction was evident (Fig. 30b) suggesting that at this dilution, the protein concentration in the sample was very weak and that if results were to be obtained

from the dot blot, it was likely that a reaction would be seen when the sample was used undiluted.

A blue/grey reaction was visible in the dot blot but only with the *Xenopus laevis* embryonic sample undiluted (Figs. 31a, 31c), but not at a concentration of 1:10 (Figs. 31b, 31d), as predicted. This reaction was visible with the anti-laminin used at both the recommended concentrations. However, at a concentration of 1:1000, a slightly paler blue/grey reaction was produced (Fig. 31c) than that with the anti-laminin at a concentration of 1:500 (Fig. 31a). Although the anti-laminin appeared to have bound to the laminin protein in these samples and would thus be viable, the reactions were both considered quite weak. This may have been due to degradation of the laminin antibody. A fresh laminin antibody was thus obtained and the immunohistochemical protocol altered slightly in order to ensure that the results acquired for basement membrane visualization were of sufficient quality.

### 3.5.2 Controls for Immunohistochemistry of Fibronectin and Laminin

A tissue sample, namely kidney, in which basement membranes of the tubules and glomeruli are prominent and have fibronectin and laminin components in their thick basement membranes was used as a positive control to determine the efficacy of the immunolocalization technique. The localization of fibronectin and laminin was visualized as a brown reaction with DAB.

Fibronectin was immunolocalized within the basement membranes of the kidney tubules and glomeruli (Fig. 32a), proving the efficacy of the technique. No immunolocalization was seen in the negative controls of the kidney where the primary antibody had been replaced with buffer (Fig. 32b), or where the secondary antibody was replaced with buffer (Fig. 32c) or where the primary antibody had been replaced with serum (Fig. 30d).

Localization of laminin was apparent in the basement membrane of the tubules of the kidney (Fig. 33a). The antibody was thus specific to the basement membrane. No immunolocalization was seen in the negative controls of the kidney where the primary antibody had been replaced with buffer (Fig. 33b), or where the secondary antibody had been replaced with buffer (Fig. 33c) or where the primary antibody had been replaced with serum (Fig. 33d).

3.5.3 Immunolocalization of Fibronectin and Laminin

There was no intense localization of either fibronectin or laminin in the proctodeal region of the embryos at any stage of development analysed. In addition the embryos immunolocalized for fibronectin exhibited high background staining. In the embryos at stages 21 and 22 of development, there was some dark labelling between the proctodeal ectoderm and hindgut endoderm, possibly indicating the presence of the basement membrane. However, these results are tentative and not conclusive and further investigations need to be undertaken in order to confirm them.

In embryos at stage 21 of development, a discontinuous dark brown reaction was apparent between the proctodeal ectoderm and the adjacent mesoderm as well as between the hindgut endoderm and the adjacent mesoderm, when immunolocalized for both fibronectin (Figs. 34a, 34e) and laminin (Figs. 34c, 34g). However, the immunolocalization of laminin was less distinct than that of fibronectin. This immunolocalization is possibly indicative of the presence of a discontinuous basement membrane between the respective two cell layers and the intervening mesoderm as the comparative serial section negative controls for fibronectin (Figs. 34b, 34f) and laminin (Figs. 3d, 34h) had no localized labelling and minimal background staining. Obviously this basement membrane does not correspond directly to the basement membrane between ectoderm and endoderm, as in these sections which were not exactly sagittally aligned, intervening mesoderm is still noted.

Embryos at stage 22 of development also presented with a dark brown discontinuous reaction between the proctodeal ectoderm and hindgut endoderm when immunolocalized for fibronectin (Figs. 35a, 35c, 35e) and laminin (Figs. 35g, 35i). The laminin localization was less distinct than that of the fibronectin, but in both instances the dark immunolocalization may be an indication of the basement membrane, as the negative controls for both fibronectin (Figs. 35b, 35d, 35f) and laminin (Figs. 35h, 35j) showed no localization and minimal background staining. As the reaction was discontinuous in both cases, it is possible that the basement membrane is breaking down at this point in development.

No immunolocalization of either fibronectin (Figs. 36d, 36d) or laminin (Figs. 36e, 36g) was seen between the proctodeal ectoderm and hindgut endoderm of embryos at stage 23 of development. The sections immunolocalized for fibronectin and laminin were similar in appearance to the negative controls in which there was no specific labelling in either the fibronectin (Figs. 36a, 36c) or the laminin (Figs. 36f, 36h) negative controls.

At stage 24 of embryonic development from the histological study it is clear that there has been complete dissolution of the cloacal membrane as there is a passage connecting the hindgut to the exterior. Therefore in embryos at this stage and in those at later stages no basement membrane and therefore no immunolocalization of fibronectin or laminin was expected in the region between the proctodeal ectoderm and hindgut endoderm.

Embryos at stage 24 of development showed no immunolocalization of fibronectin (Figs. 37a, 37b), which was similar to the negative control (Figs. 38a, 38b) which was clear, or laminin (Figs. 39a, 39c), which was also similar to the negative control (Figs. 39b, 39d) in the cloacal region.

There was also an absence of fibronectin (Figs. 40a, 40c) and laminin (Figs. 41a, 41c) immunolocalization in the cloacal region of embryos at stage 25 of development. The embryo sections immunolocalized for the respective proteins appeared similar to the negative controls for fibronectin (Figs. 40b, 40d) and laminin (41b, 41d). The same was found to be true of embryos at stage 26 of development where no specific labelling was seen in the sections of embryos immunolocalized for fibronectin (Figs. 42a, 42b). The sections appeared similar to the negative controls for fibronectin (Figs. 43a, 43b). No specific labelling was seen in the embryos sections immunolocalized for laminin either (Figs. 44a, 44c) and these appeared similar to the laminin negative controls (Figs. 44b, 44d).

## 3.6 TERMINAL DEOXYNUCLEOTIDYL TRANSFERASE MEDIATED dUTP NICK END-LABELLING (TUNEL)

The TUNEL technique was used to analyse the role of apoptosis in the formation of the proctodeum and in dissolution of the cloacal membrane. Apoptotic cells were visualized as brown with DAB. The data obtained from this technique is not entirely satisfactory and careful consideration must be given to these results.

The testes are known to contain a relatively large number of cells that undergo programmed cell death and this tissue was thus used as a positive control to ensure the efficacy of the technique. A number of labelled cells indicating apoptosis, visualized as brown were apparent in the positive control, with a low degree of background staining (Fig. 45a). The omission of the enzyme in the protocol on the testes tissue showed no labelling (Fig. 45b) and therefore showed that the labelling was specific to apoptotic cells.

Similarly, the embryonic negative controls, where the enzyme was omitted from the protocol showed no specific labelling, although some background staining was visible at all stages (Figs. 46a-j). At stage 21 (Figs. 46a, 46b) and stage 22 (Fig. 46c) the

embryonic negative controls showed background staining, particularly in the outer ectoderm. This may be attributed to the presence of pigment granules concentrated in the ectoderm, although the embryos were bleached to try and eradicate this hindrance. A few labelled cells, possibly apoptotic in nature were found to be scattered across the surface ectoderm and around the posterior region in embryos that had reached stage 21 of development (Fig. 47a). A fair number of these labelled cells were concentrated in the region of the blastopore, which at this stage was almost closed (Fig. 47a). There were no darkly labelled cells in the cloacal region of the embryos at this stage, but this was difficult to ascertain, as there was a high degree of background staining, particularly in the outer ectoderm (Figs. 47b, 47c).

At stage 22 of development, labelled cells were visible in the outer ectodermal layer of the embryos (Figs. 48a, 48b), with many of them concentrated to the ectoderm of the proctodeum (Fig. 48c). These labelled cells were also found scattered throughout the posterior region of embryos (Fig. 48b). Due to the high number of labelled cells, it was thought that they may not be specifically labelled. However, individual cells appeared to be distinctly brown compared to some surrounding lighter stained cells. A number of embryos at this stage, however, did not have labelled cells in the proctodeal region, although some background staining was evident (Figs. 49a, 49b).

At stage 23 of development, the majority of embryos showed a number of labelled cells scattered throughout the ectoderm (Figs. 50a, 50b) with a few of these labelled cells concentrated in the proctodeal region (Figs 50b, 50c). A few labelled cells were also localized to the hindgut endoderm, near the cloacal membrane and in the cloacal membrane itself in a couple of embryos (Figs 51a, 51b). Apoptotic cells were thought to be specifically labelled, although some of the labelled cells may have appeared darker due to background staining or pigment granules. A few of the embryos at this stage however, showed only background staining and no specific labelling in the proctodeal region (Figs. 52a, 52b).

Although the cloacal membrane was absent in embryos at stage 24 of development, possible apoptosis in the cloacal region of embryos at this stage and further along in development was analysed. At stage 24 of development, a few labelled cells were found to be scattered across the surface ectoderm (Figs. 53a, 53b). However no labelled cells were visible around the cloacal opening (Fig. 53c).

It was difficult to find consistency with regard to the localization of labelled cells in the cloacal region of the embryos at stages 25 and 26 of development. At stage 25, a few labelled cells were found to be dispersed throughout the surface ectoderm (Figs. 54a, 54b) with some concentrated to the outer ectoderm around the cloacal opening (Fig. 54c) in a number of embryos. In a similar number of embryos no labelled cells were visible around the cloacal opening. However, some background staining was apparent (Figs. 55a, 55b). A similar pattern was found to occur in embryos at stage 26 of development. A few surface ectodermal cells were darkly labelled (Figs. 56a, 56b) with a number concentrated in the ectoderm around the cloacal opening (Figs. 56b, 56c). Whilst a number of embryos showed this pattern of labelled cells in the cloacal region, a comparable number of embryos showed no labelling in cells around the cloacal opening (Figs. 57a, 57b).

## 3.7 IMMUNOLOCALIZATION OF BAX AND BCL-2 FOR DETECTION OF APOPTOTIC CELLS

As the results pertaining to the role of apoptosis in the dissolution of the cloacal membrane were unconvincing using the TUNEL method, immunohistochemistry for Bax and Bcl-2 was performed on a limited number of embryos. The immunohistochemical method was performed to determine whether the detection of the pro-apoptotic protein Bax and anti-apoptotic protein Bcl-2 produced clearer results with regard to apoptosis localization. Even though immunohistochemistry was only performed on one embryo per stage, interesting results were obtained, but

these too must be interpreted with care until a larger sample size is available for further analysis.

### 3.7.1 Controls for Immunohistochemistry of Bax and Bcl-2

The colon is known to have many cells undergoing programmed cell death and thus should contain the Bax protein. In addition, numerous colon cells are not undergoing apoptosis and so should have the Bcl-2 protein present. Mouse colon was therefore used as a positive control to determine the efficacy of the immunolocalization technique. The localization of Bax and Bcl-2 was visualized as brown cells with DAB. The whole cell did not always appear to be labelled and this may be because Bax and Bcl-2 are located in the mitochondrial membrane and cytosol as well as the nuclear envelope.

Bax-positive cells were seen concentrated in the glandular epithelium of the colon (Fig. 58a). No immunolocalization was seen in the negative controls of the colon where the primary antibody had been replaced with diluent (Fig. 58b), or where the secondary antibody had been replaced with buffer (Fig. 58c) or where the primary antibody had been replaced with serum (Fig. 58d).

Bcl-2-positive cells were also concentrated in the glandular epithelium and cells of the lamina propria of the colon (Fig. 59a). No immunolocalization was seen in the negative controls of the colon where the primary antibody had been replaced with diluent (Fig. 59b), or where the secondary antibody had been replaced with buffer (Fig. 59c) or where the primary antibody had been replaced with serum (Fig. 59d). In the control where the anti-Bcl-2 was replaced with serum there was some non-specific generalized background staining.

### 3.7.2 Immunolocalization of Bax and Bcl-2

The outermost ectodermal layer of the embryo at stage 21 of development was intensely dark in appearance (Figs. 60a, 60b, 60c). As the negative control (Figs. 60f,

60g) showed no immunolocalization, with minimal background staining, it was thought that most of this layer did in fact contain the protein Bax and was thus a highly apoptotic layer. A few cells in the ectoderm of the proctodeal region were also labelled brown and were thought to be apoptotic (Figs. 60b, 60c). As only a few sections for immunolocalization of Bax were carried out, it is difficult to determine the positioning of these cells. In contrast to the immunolocalization of Bax, the outermost ectodermal layers of the embryo at stage 21 showed no immunolocalization of Bcl-2 (Figs. 60d, 60e). A number of Bcl-2-positive cells were located in the ectoderm of the proctodeal region and were thus thought to be anti-apoptotic (Figs. 60d, 60e). There appeared to be a similar number of Bax-positive and Bcl-2-positive cells in the proctodeal region.

At stage 22 of development a few Bax-positive cells were dispersed within the ectoderm of the embryo (Fig. 61a). However, there were no Bax-positive cells localized in the proctodeal region (Figs. 61b). A few Bcl-2-positive cells were also visible in the ectoderm of the stage 22 embryo (Figs. 61c), but no Bcl-2-positive cells were localized to the proctodeal region (Fig. 61d) and this section was comparable to the negative control (Figs. 61e, 61f).

The outermost ectodermal layer of the embryo at stage 23 was labelled intensely brown, showing Bax-positive cells (Fig. 62a). There were also numerous labelled cells apparent in the hindgut endoderm and around the cloacal membrane (Fig. 62b). This was in contrast to the negative control where Bax immunolocalization was absent (Figs. 62e, 62f). At this stage, the ectodermal layer of the embryo was found to contain Bcl-2-positive cells (Fig. 62c). Bcl-2-positive cells, although few in number, were also visible in the endoderm of the hindgut (Fig. 62d). There were far more Bax-positive cells than Bcl-2 positive cells at this stage of development.

A few Bax-positive cells were visible in the ectoderm of the stage 24 embryo (Fig. 63a) with a few localized to the ectoderm in the region of the cloacal opening (Fig.

63b). The embryo was not well sectioned and what is thought to be the cloacal opening may in fact have been a tear, although it is in the region of the cloacal opening. One cell present in the ectoderm of the embryo, near what is thought to be the cloacal opening was slightly darker in appearance than the surrounding cells (Fig. 63c) and thought to be anti-apoptotic. However no negative control was available for comparison.

The embryonic tissue was quite torn in the stage 25 embryo and the opening may have been a tear in the cloacal region and not the actual cloacal opening. No localization of Bax was apparent in this region (Fig. 64a) and was comparable to the negative control (Fig. 64c). In this embryo a few cells darker in appearance and thus thought to be immunolocalized with Bcl-2 were apparent around the cloacal opening (Fig. 64b).

The embryo at stage 26 of development had no Bax-positive cells visible in the cloacal region of the embryo (Fig. 65a) and was thus similar in appearance to the negative control (Fig. 65c). Although the cloacal opening was not visible in the section on which immunolocalization for Bcl-2 was performed, no labelled cells were seen in the cloacal region (Fig. 65b).

## 3.8 *IN SITU* HYBRIDIZATION FOR *BONE MORPHOGENETIC PROTEIN-4*

In order to determine the pattern of *BMP-4* expression in the proctodeal region of *Xenopus laevis* embryos, *in situ* hybridization was performed.

The agarose gels, on which the linearized DNA samples were run, indicated that the DNA of all the probes (Figs. 66, 67) was satisfactory for RNA transcription and that no contamination or degradation had occurred. The formaldehyde-agarose gel indicated that the *XCG-1* sense probe, the *BMP-4* antisense probe and the *BMP-4* sense probe were transcribed correctly and that they were viable to use for *in situ*

hybridization (Fig 68). The RNA transcribed from the first *XCG-1* antisense probe appeared to have degraded (Fig. 68), possibly due to contamination. The DNA of a fresh *XCG-1* plasmid was therefore linearized and a *XCG-1* sense probe and *XCG-1* antisense probe transcribed. These new RNA probes were checked on a formaldehyde-agarose gel (Fig. 69). The double bands of RNA that are visible on the gel indicated that perhaps the DNA of the *XCG-1* antisense probe didn't linearize properly. However this probe was deemed viable as the one band was in the correct position (personal communication with Dr A.J.G. Dickinson).

In order to ensure the efficacy of the technique, a known, highly specific gene, namely *XCG-1* was localized and the staining of the experimental embryos for *BMP-4* expression was compared with the staining for *XCG-1* expression. *XCG-1* is expressed in the cement gland, which is a prominent feature of the *Xenopus laevis* embryos by stage 21 and is located in the anterior region of the embryo. The staining for XCG-1 was specific and very intense (Fig. 70a), compared with the sense control (Fig. 70b).

As *BMP-4* is localized in the anterior region of the *Xenopus laevis* embryos, early on in development, stage 14 embryos were used as controls for *BMP-4* localization in the proctodeal region in later developed embryos. In stage 14 antisense control embryos, *BMP-4* stained strongly in both the anterior and posterior regions (Fig. 71a) compared with the sense control (Fig. 71b).

The pattern of *BMP-4* expression was then analysed in embryos at stages 22, 24 and 26 of development. At stage 22 there was intense *BMP-4* staining in the proctodeal region of the embryos (Fig. 72a, 72b) as well as in the anterior region of the embryos. This was compared to the sense control, where no staining was apparent (Fig. 72c). The embryos at stage 24 of development showed less intense staining of *BMP-4* around the cloacal opening (Fig. 73a, 73b) compared to that seen in stage 22 embryos. This was compared to the sense control, where no staining was apparent

(Fig. 73c). Very little or no staining was apparent in the region of the cloacal opening (Fig. 74a, 74b) of embryos at stage 26 of development, which were compared with the sense control, where no staining was seen (Fig. 74c).

Figure 4. A diagram illustrating the exterior distinguishing features of *Xenopus laevis* embryos at stages 21-26. a) An anterior view of a stage 21 embryo showing the closure of the neural tube and the secretory cement gland. b) A lateral view of a stage 22 embryo showing the distinct protrusion of the eyes. c) A lateral view of a stage 23 embryo showing the ventral outline as concave and a clear separation by a groove, of the jaw and gill areas. d) A lateral view of a stage 24 embryo where the gill area is more prominent than the jaw area and the tail bud is discernible. e) A lateral view of a stage 25 embryo showing the invagination of the ear vesicle and the beginning of fin formation. f) A lateral view of a stage 26 embryo indicating the protruding ear vesicle, the first sign of visible myotomes and showing the fin a little broader at the dorso-caudal end of body. (Taken from Nieuwkoop and Faber, 1967).

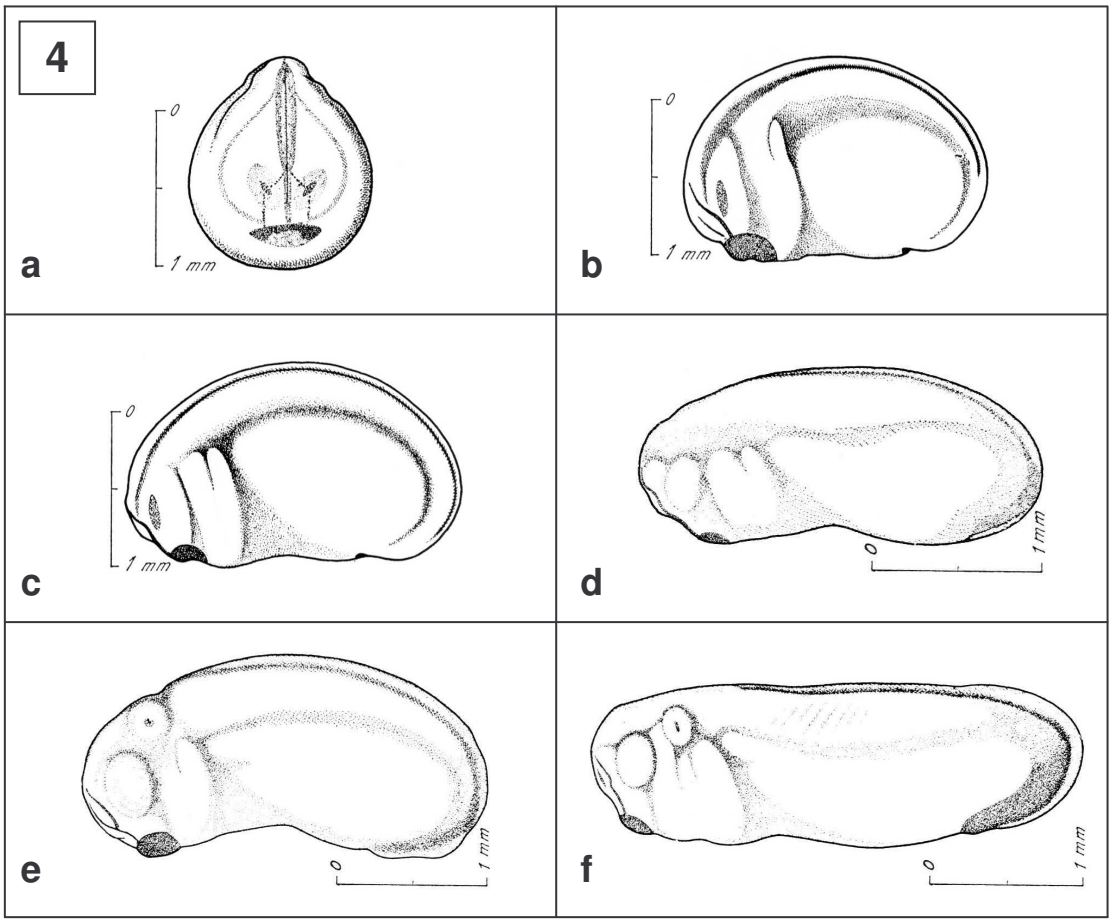
4
a
0
1 mm
b
0
1 mm
c
0
1 mm
d
0
1 mm
e
0
1 mm
f
0
1 mm

Figure 5. Images illustrating the development of the proctodeal depression, taken of three *Xenopus laevis* embryos over a time period of 4 hours. The embryos were placed on a stereomicroscope (Olympus) with transmitted light at 23ºC and images were captured with an Olympus digital camera. a) A ventral view of an embryo at stage 17 of development at the starting point of observation, showing the embryo initially round in shape with an open blastopore (black arrow). b) A ventral view of the embryo at approximately stage 18, 1 hour after the initial image was captured, illustrating the open blastopore (black arrow). c) A ventral view of the embryo at stage 19 of development, 2 hours after the initial image was captured. The embryo was elongated in appearance and the open blastopore (black arrow) was more ventrally positioned. d) A ventral view of the embryo at approximately stage 20, 3 hours after the initial image was taken, illustrating the blastopore (black arrow). e) A ventral view of an embryo at stage 21 of development at the starting point of observation, illustrating the slightly elongated embryo, closed blastopore and proctodeal depression (black arrow) on the posterior-ventral surface. f) A ventral view of the embryo 1 hour after the starting point of observation, at approximately stage 22 of development with a slightly enlarged proctodeal depression (black arrow). g) A ventral view of the embryo 2 hours after the starting point of observation at approximately stage 23 of development showing a more ventrally placed proctodeal depression (black arrow). h) A ventral view of the embryo 4 hours after the initial observation, at approximately stage 24 of development, in which the proctodeal depression (black arrow) is not very discernable. i) A ventral view of an embryo at stage 24 of development, at the starting point of observation, illustrating the proctodeal depression (black arrow). j) A ventral view of the embryo 1 hour after the initial observation, at approximately stage 25 showing a slightly narrow midsection of the embryo and not very discernable proctodeal depression (black arrow). k) A ventral view of the embryo at approximately stage 26 of development, 3 hours after the initial image was captured, illustrating the proctodeal depression (black arrow). l) A lateral view of the embryo between stages 26 and 27, 4 hours after the initial image was captured, showing the position of the cloacal opening (black arrow). 320X.


5
a
b
c
d
e
f
g
h
i
j
k
l

Figure 6. A representative lateral image of the posterior region of a stage 21 *Xenopus laevis* embryo illustrating a slight curvature of the outer ectoderm on the ventral surface, in the proctodeal region (PR). This is the region where the proctodeum will develop. 200X. Confocal microscopy.

Figure 7. A representative lateral image of the posterior region of a stage 22 *Xenopus laevis* embryo illustrating a small depression on the ventral surface, which is the proctodeum (P). 200X. Confocal microscopy.

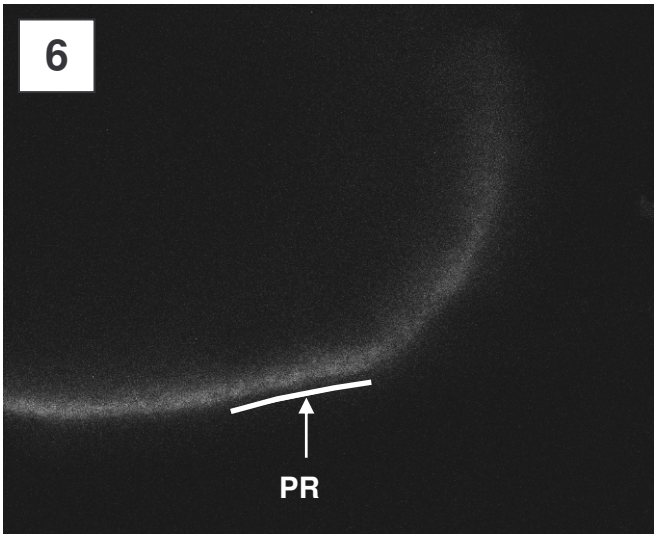
6
PR

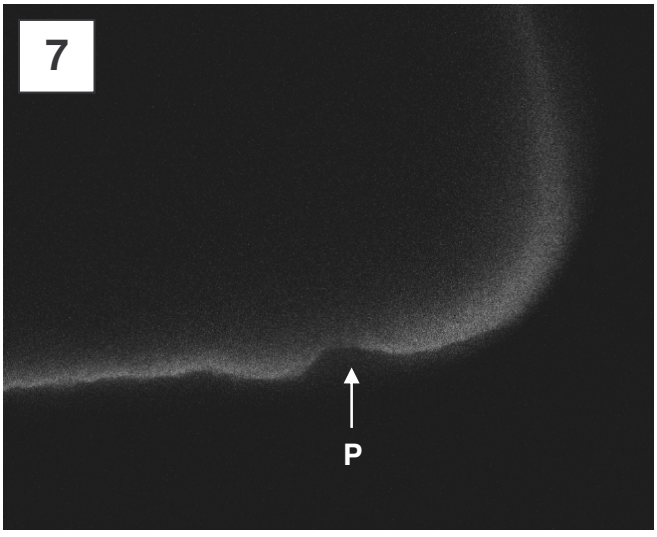
7
P

Figure 8. A representative lateral image of the posterior region of a stage 23 *Xenopus laevis* embryo illustrating the proctodeum (P), a small depression on the ventral surface. 200X. Confocal microscopy.

Figure 9. A representative lateral image of the posterior region of a stage 24 *Xenopus laevis* embryo illustrating the cloacal opening (CO) to the ventral surface of the embryo. The cloacal membrane has perforated, forming a free channel of communication between the hindgut (HG) and the exterior. 200X. Confocal microscopy.

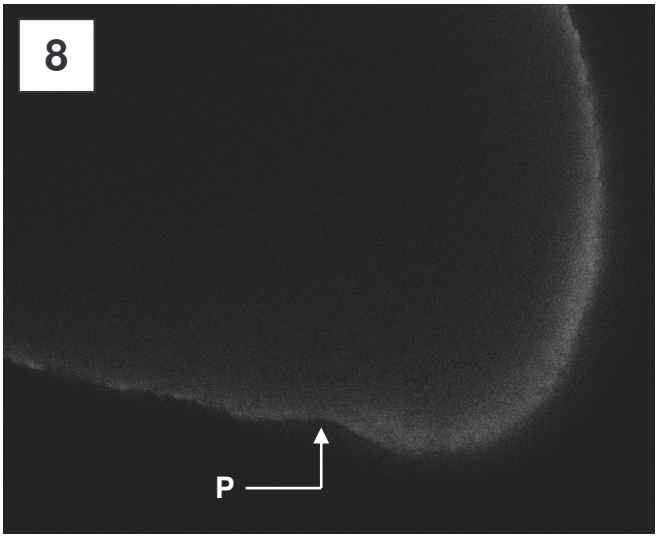
8
P

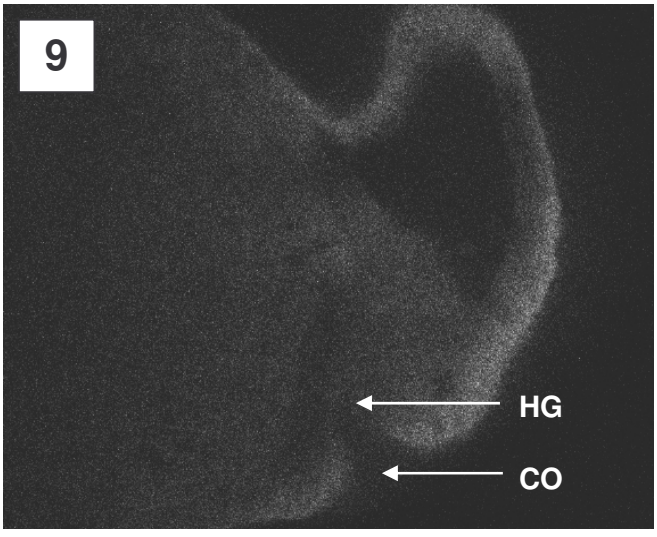
9
HG
CO

Figure 10. A representative lateral image of the posterior region of a stage 25 *Xenopus laevis* embryo illustrating the channel extending from the hindgut (HG) to the cloacal opening (CO) through which excretion will occur. 200X. Confocal microscopy.

Figure 11. A representative lateral image of the posterior region of a stage 26 *Xenopus laevis* embryo illustrating a slight increase in the size of the cloacal opening (CO) co-extensive with the hindgut (HG). The cells surrounding the cloacal opening appear to protrude forming a bulge. 200X. Confocal microscopy.

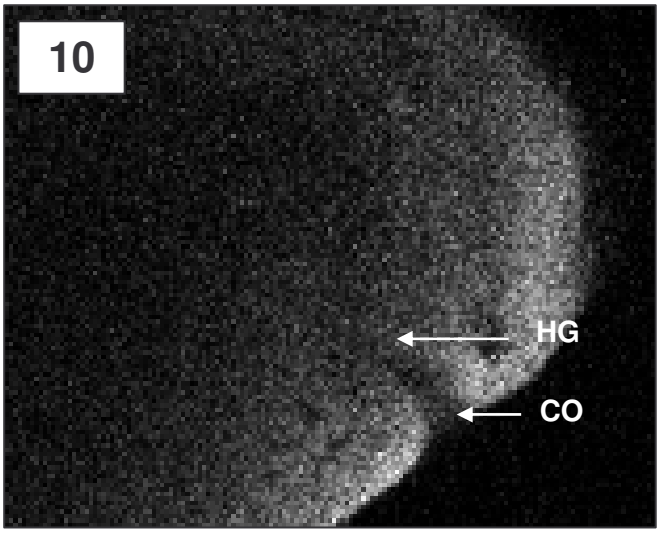
10
HG
CO

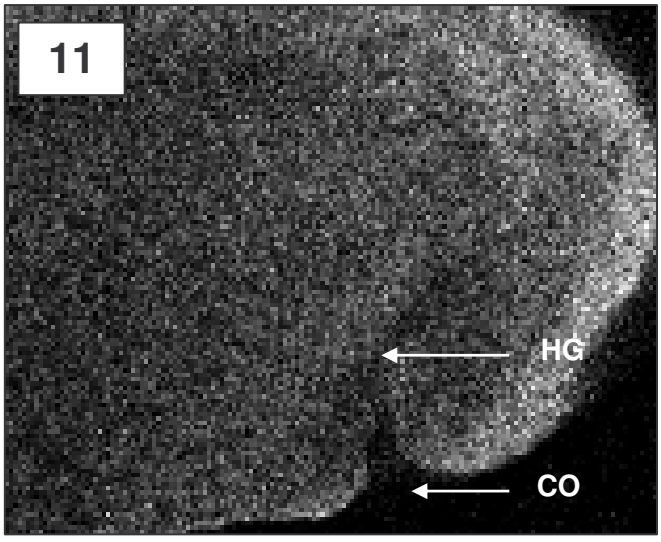
11
HG
CO

Figure 12. A representative scanning electron micrograph of the ventral surface of the posterior region of a stage 21 *Xenopus laevis* embryo. The blastopore (B) is not closed and is visible at the posterior end of the embryo. The area ventral to the blastopore is where the proctodeum is expected to develop. However at this stage the ectodermal surface appears smooth with no depression visible. 120X. (A-Anterior; P-Posterior).

Figure 13. A representative scanning electron micrograph of the surface ectodermal cells in the proctodeal region of a stage 21 *Xenopus laevis* embryo. Clear ectodermal cell are visible. A number of low cilia were dispersed across the ectodermal surface. 3 000X.

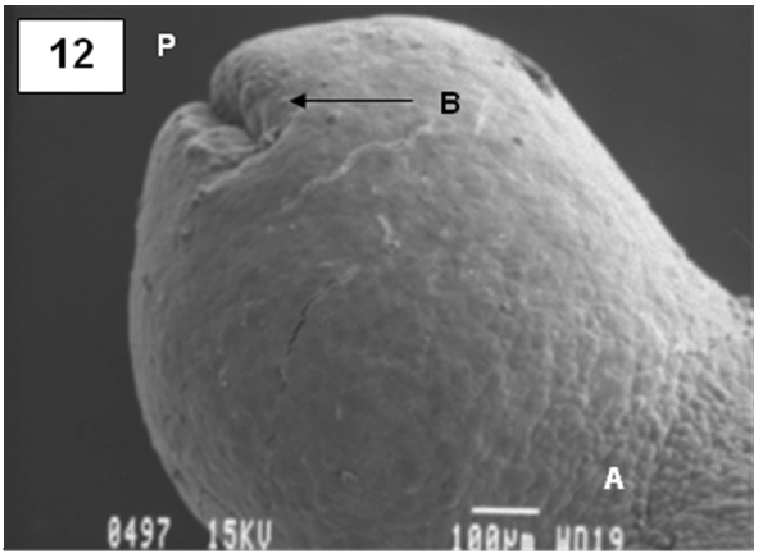
12
P
B
A
0497 15KV
100µm WD19

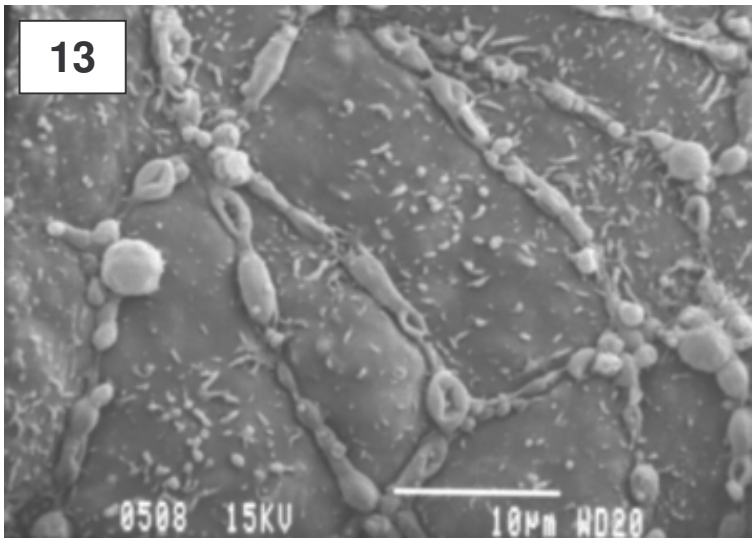
13
0508 15KV
10µm WD20

Figure 14. Representative scanning electron micrographs of the ventral surface of the posterior region of a stage 22 *Xenopus laevis* embryo, illustrating the proctodeum. a) The proctodeum (P) is visible as a marked depression. 130X. b) The proctodeum is slit-like in appearance with cilia (C) surrounding this depression. 600X. c) The clumping of rod-like structures in the proctodeal region was noted. 2 700X.

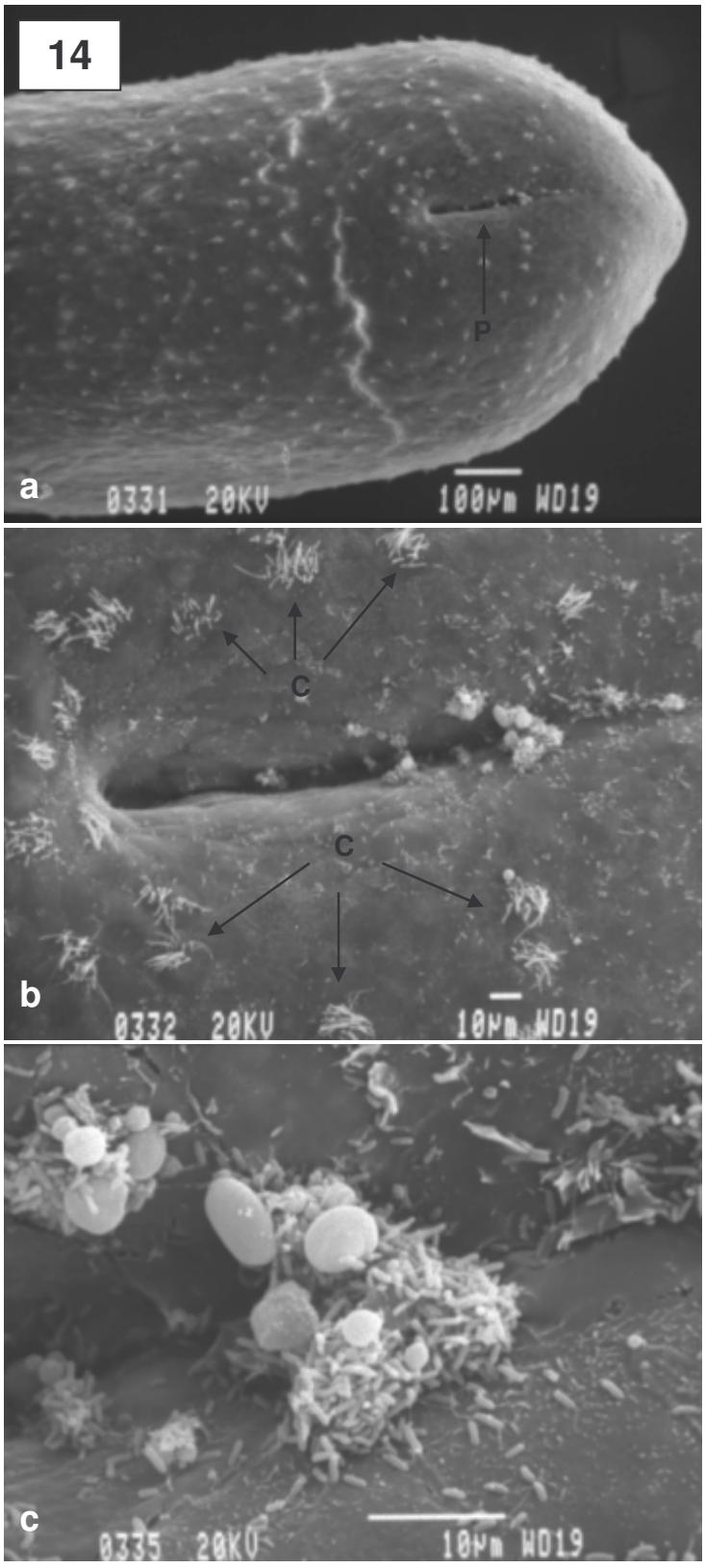
14
P
a
0331 20KV
100µm WD19
C
C
b
0332 20KV
10µm WD19
c
0335 20KV
10µm WD19

Figure 15. Representative scanning electron micrographs of the ventral surface of the posterior region of a stage 23 *Xenopus laevis* embryo, illustrating the proctodeum. a) The proctodeum (P) has widened during development and now appears oval in shape. 180X. b) The widened proctodeal depression has deepened and cilia (C) were evenly dispersed around this depression. 600X. c) The deepened proctodeal depression with distinct ectodermal cells, possibly becoming displaced to the interior. 1 900X.

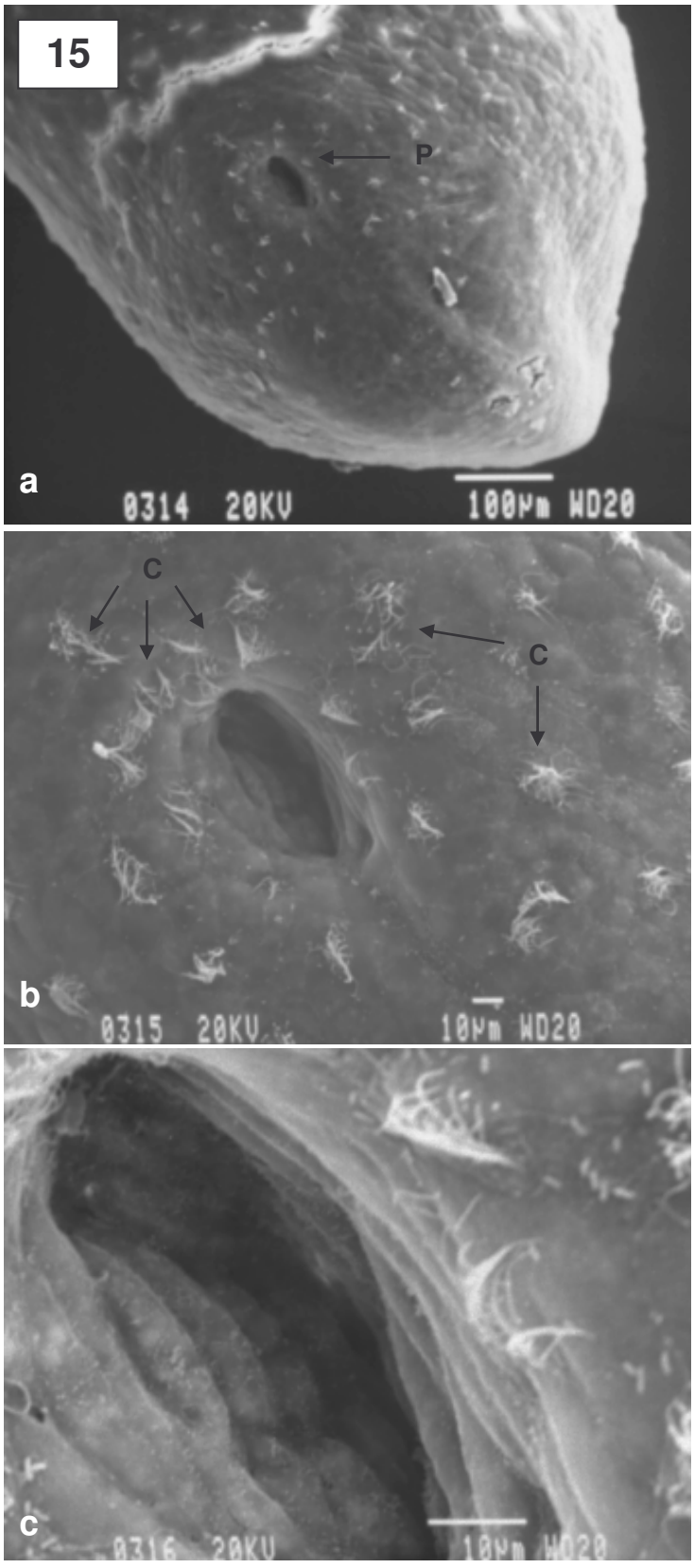
15
P
a
0314 20KV
100µm WD20
C
C
b
0315 20KV
10µm WD20
c
0316 20KV
10µm WD20

Figure 16. Representative scanning electron micrographs of the ventral surface of the posterior region of a stage 24 *Xenopus laevis* embryo, illustrating the cloacal opening of the embryo. a) The cloacal opening (CO) is clearly visible by this stage. 160X. b) The protrusion of cells around the cloacal opening is very prominent. Cilia (C) are concentrated around the cloacal opening. 600X. c) The cloacal opening, which is oval in shape, appeared to have deepened compared to the depression seen in the earlier stage embryos. 2 200X.

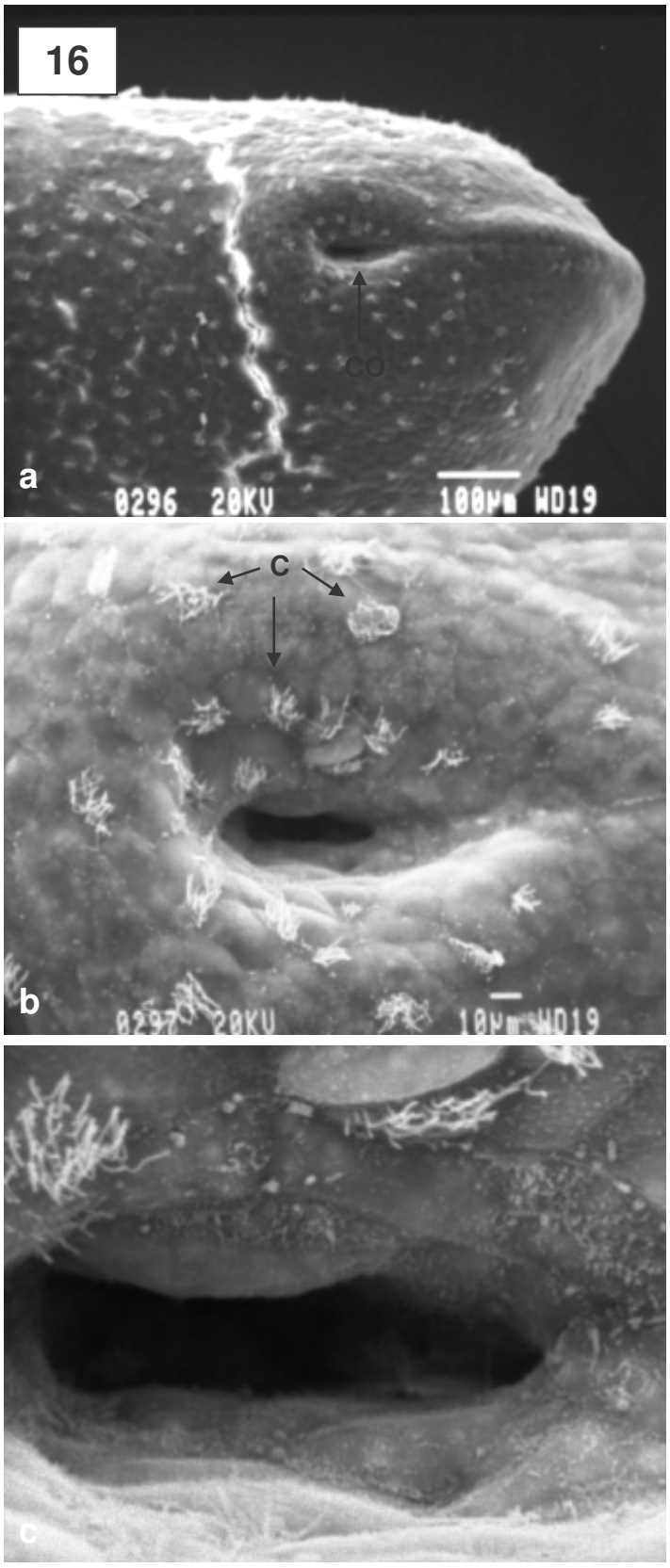
16
CO
a
0296 20KV
100µm WD19
C
b
0297 20KV
10µm WD19
c

Figure 17. A scanning electron micrograph of the cloacal opening on the posterior-ventral surface of a stage 24 *Xenopus laevis* embryo. The cloacal opening is not well defined and is very narrow in appearance. The ectodermal cells in this region are atypical as they are larger than those seen in numerous other embryos at stage 24 of development. Cilia were dispersed on the cells. However there are no cilia concentrated directly around the cloacal opening. 600X.

Figure 18. A representative scanning electron micrograph of the cloacal opening, on the posterior-ventral surface of a stage 25 *Xenopus laevis* embryo. A cellular "plug" is apparent in the cloacal opening of this embryo. "Plugs" such as this were found in a number of stage 25 and 26 embryos. 1 600X.

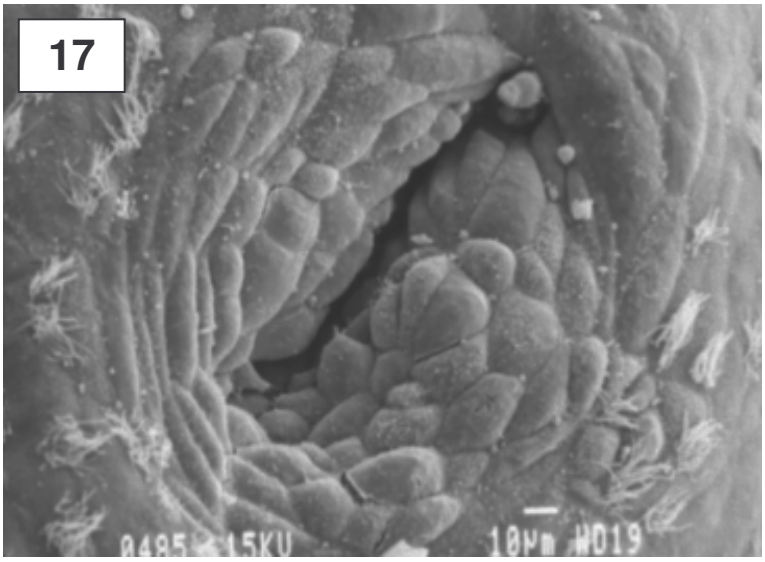
17
15KU
10μm WD19

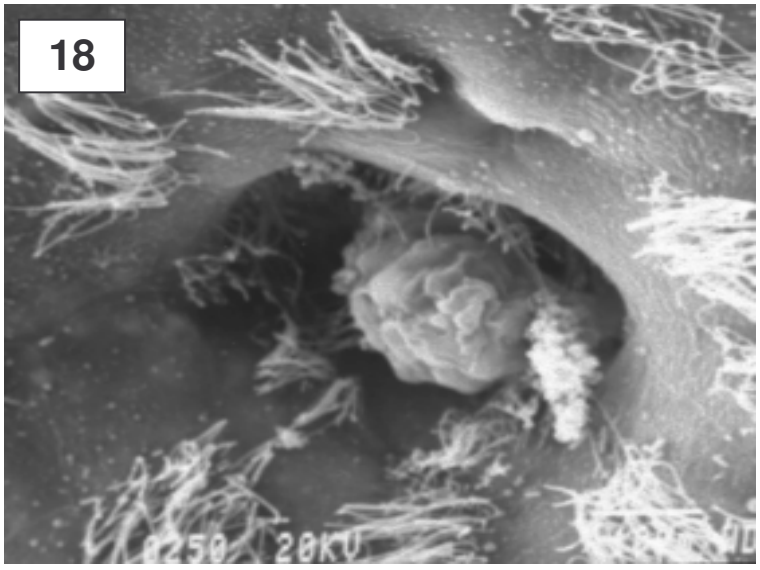
18
0250 20KU

Figure 19. Representative scanning electron micrographs of the ventral surface at the posterior region of a stage 25 *Xenopus laevis* embryo, illustrating the cloacal opening. a) The cloacal opening (CO) is more rounded and the protrusion of ectodermal cells around the cloacal opening is more pronounced than at stage 24. 150X. b) The cloacal opening has widened and cilia were dispersed around this opening. 1 300X.

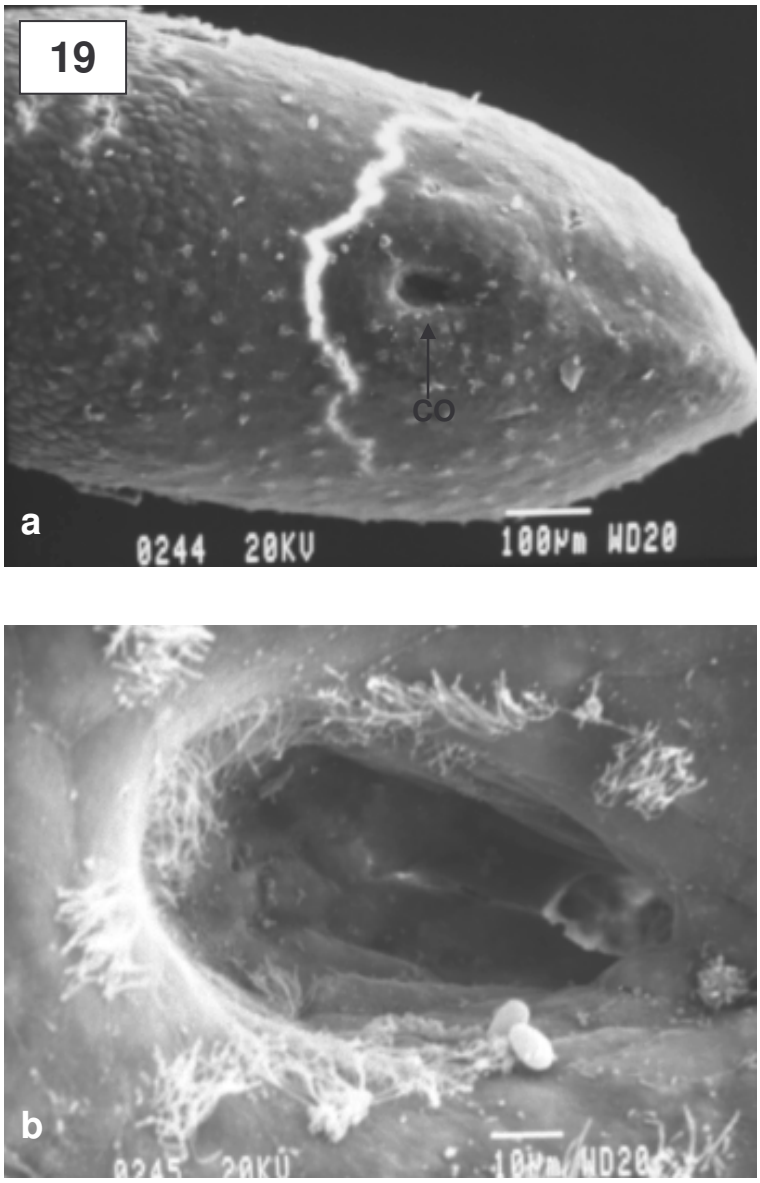
19
CO
a
0244 20KV
100µm WD20
b

Figure 20. Representative scanning electron micrographs of the ventral surface at the posterior region of a stage 26 *Xenopus laevis* embryo, illustrating the cloacal opening. a) The cloacal opening (CO) at this stage appears to be more ventrally placed due to development of the tail bud. 180X. b) The cloacal opening is round and prominent. 550X c) The round cloacal opening is dark and the interior structures not easily discernible, suggesting that the proctodeal depression had deepened and/or that the cloacal membrane had perforated forming a channel between the hindgut and the exterior. 2 200X.

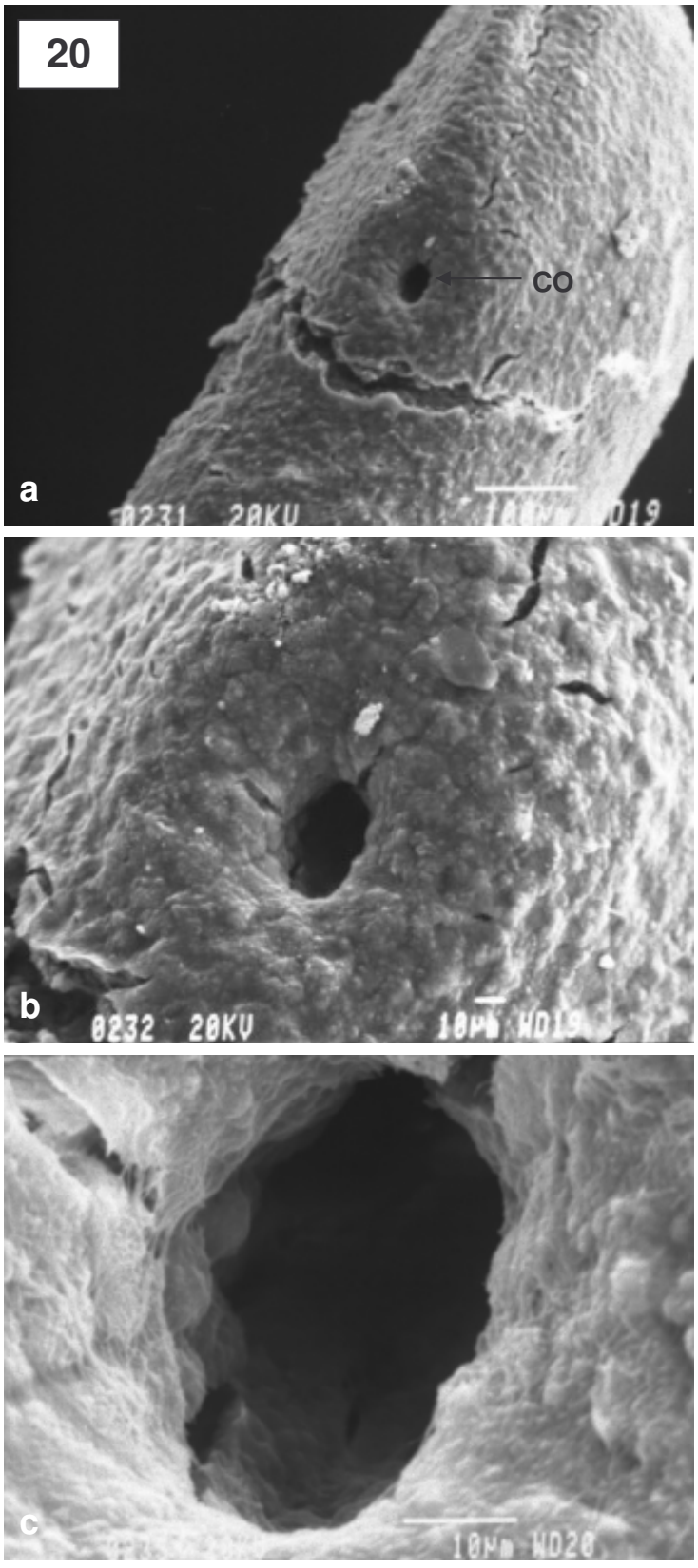
20
CO
a
0231 20KV
b
0232 20KV
c
10µm WD20

Figure 21. A representative scanning electron micrograph of elongated cilia of a stage 26 *Xenopus laevis* embryo. The cilia are numerous and are concentrated around the cloacal opening. 2 000X.

Figure 22. A representative scanning electron micrograph of cilia densely aggregated around the cloacal opening of a stage 26 *Xenopus laevis* embryo. 6 000X .

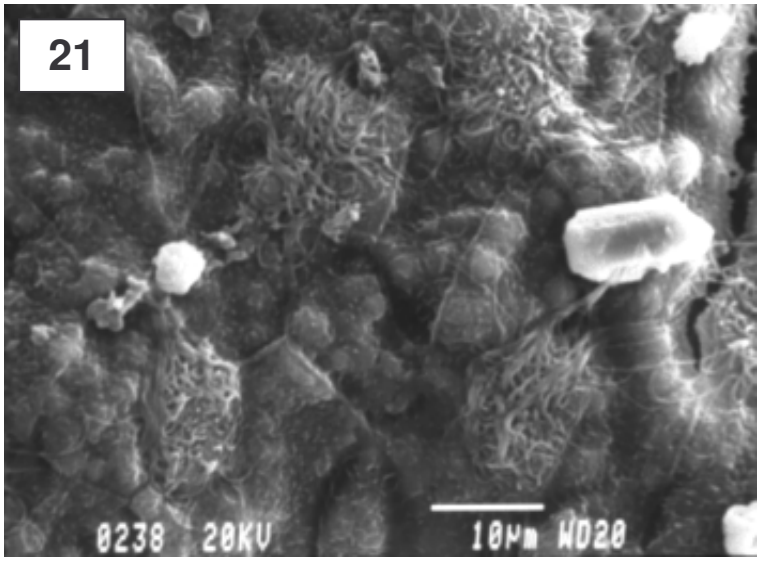
21
0238 20KV
10µm WD20

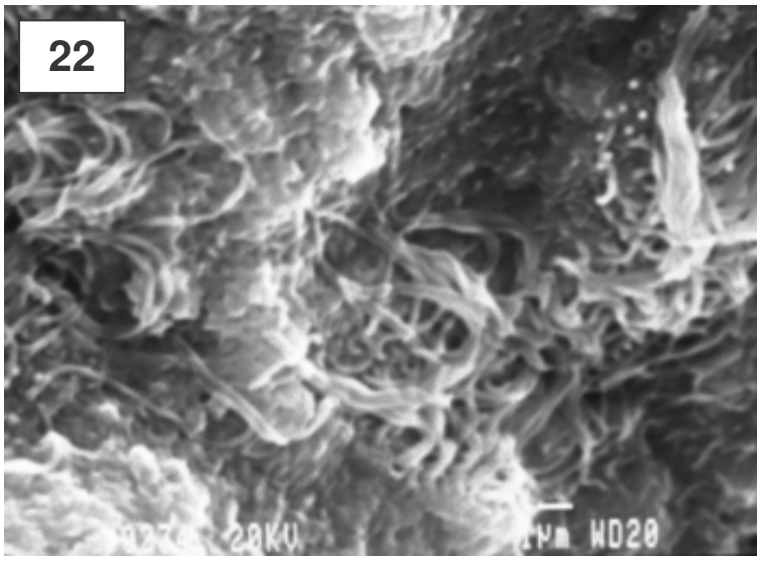
22
20KV
WD20

Figure 23. Representative photomicrographs of a sagittal section of the posterior region of a stage 21 *Xenopus laevis* embryo. The hindgut (HG), lined by large, yolky endodermal cells (EN) is visible with a slight indentation of the cuboidal surface ectoderm (EC) at the posterior-ventral region. This indentation is the proctodeum (P). a) 100X. b) 400X. Gill's haematoxylin and eosin.

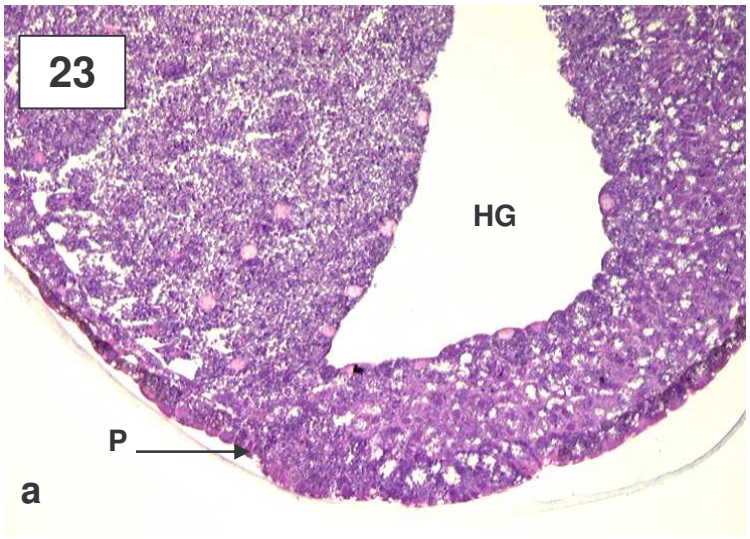
23
HG
P
a

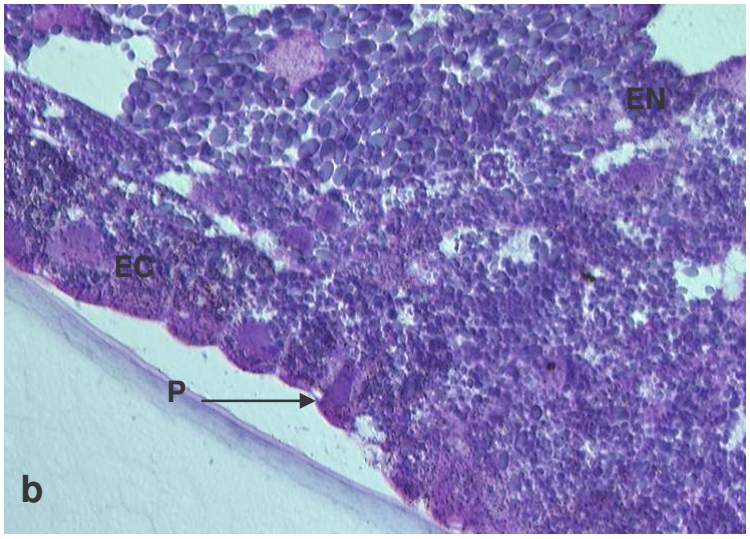
EN
EC
P
b

Figure 24. Representative photomicrographs of a sagittal section of the posterior region of a stage 22 *Xenopus laevis* embryo. The hindgut (HG), lined by large, yolky endodermal cells (EN) is visible aligned with a corresponding indentation of the surface ectoderm (EC) in the hindgut region. This indentation is the proctodeum (P). There is a decrease in thickness of cell layers from the indentation to the hindgut, compared to embryos at stage 21. a) 100X. b) 400X. Gill's haematoxylin and eosin.

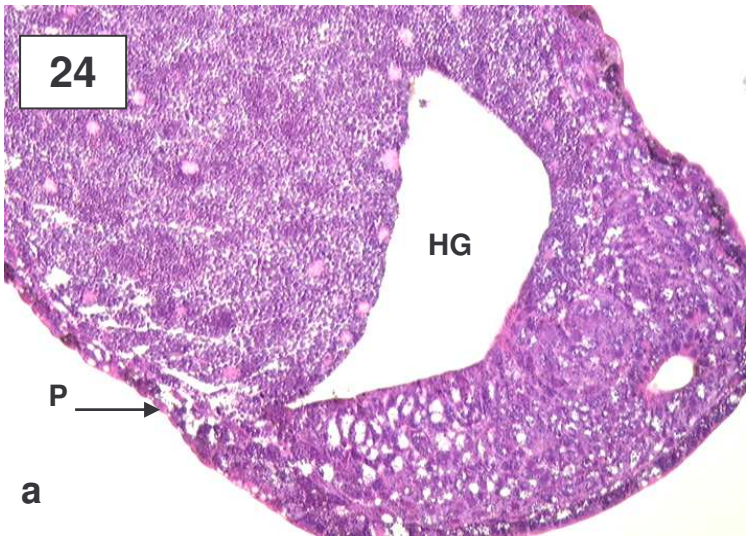
24
HG
P
a

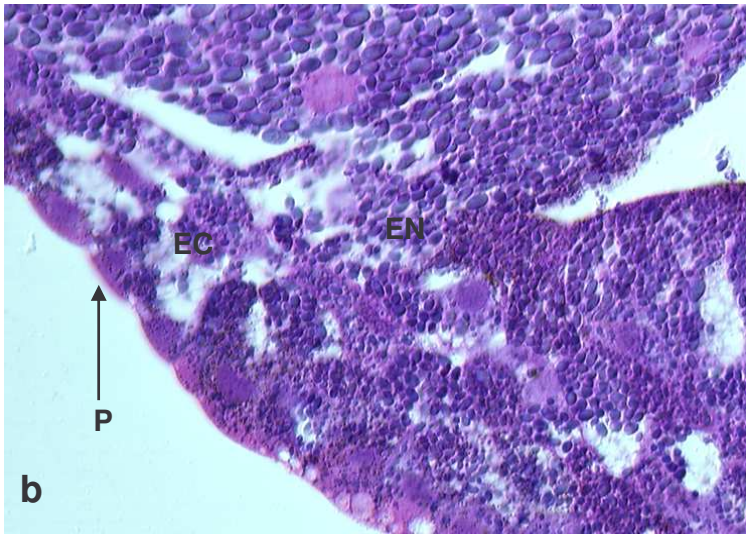
EC
EN
P
b

Figure 25. Representative photomicrographs of sagittal sections of the posterior region of a stage 23 *Xenopus laevis* embryo. a) The juxtaposing hindgut endoderm (EN) and surface ectoderm (EC) forming the cloacal membrane, separate the hindgut (HG) from the exterior. The indentation is the proctodeum (P). 400X. b) Thinning of the cloacal membrane (CM) with a prominent proctodeal depression (P) is visible. 400X. Gill's haematoxylin and eosin.

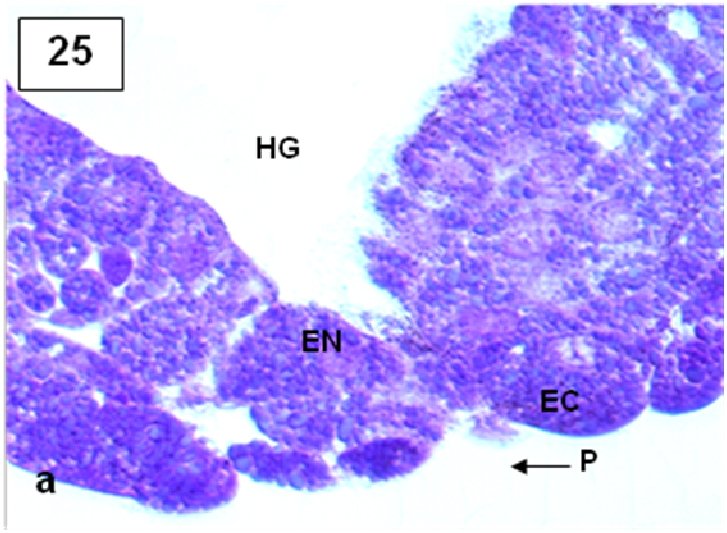
25
HG
EN
EC
P
a

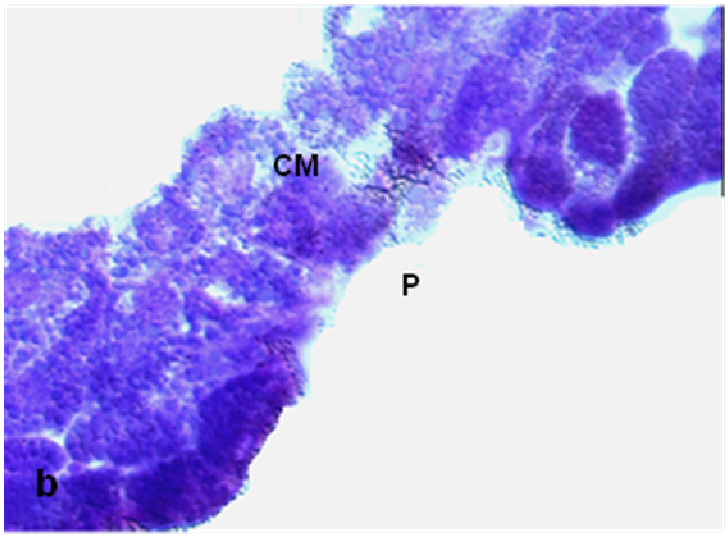
CM
P
b

Figure 26. Representative photomicrographs of a sagittal section of the posterior region of a stage 24 *Xenopus laevis* embryo. a) A free channel extends from the cloacal opening (CO) to the hindgut (HG). 100X. b) A vacuolated or secretory cell (VC) is apparent between the ectodermal cells around the cloacal opening (CO). Some flocculated substance is apparent in the cloacal opening. 400X. c) Numerous elongated cilia (C) are found in the cloacal region of the embryos. 630X. Gill's haematoxylin and eosin.

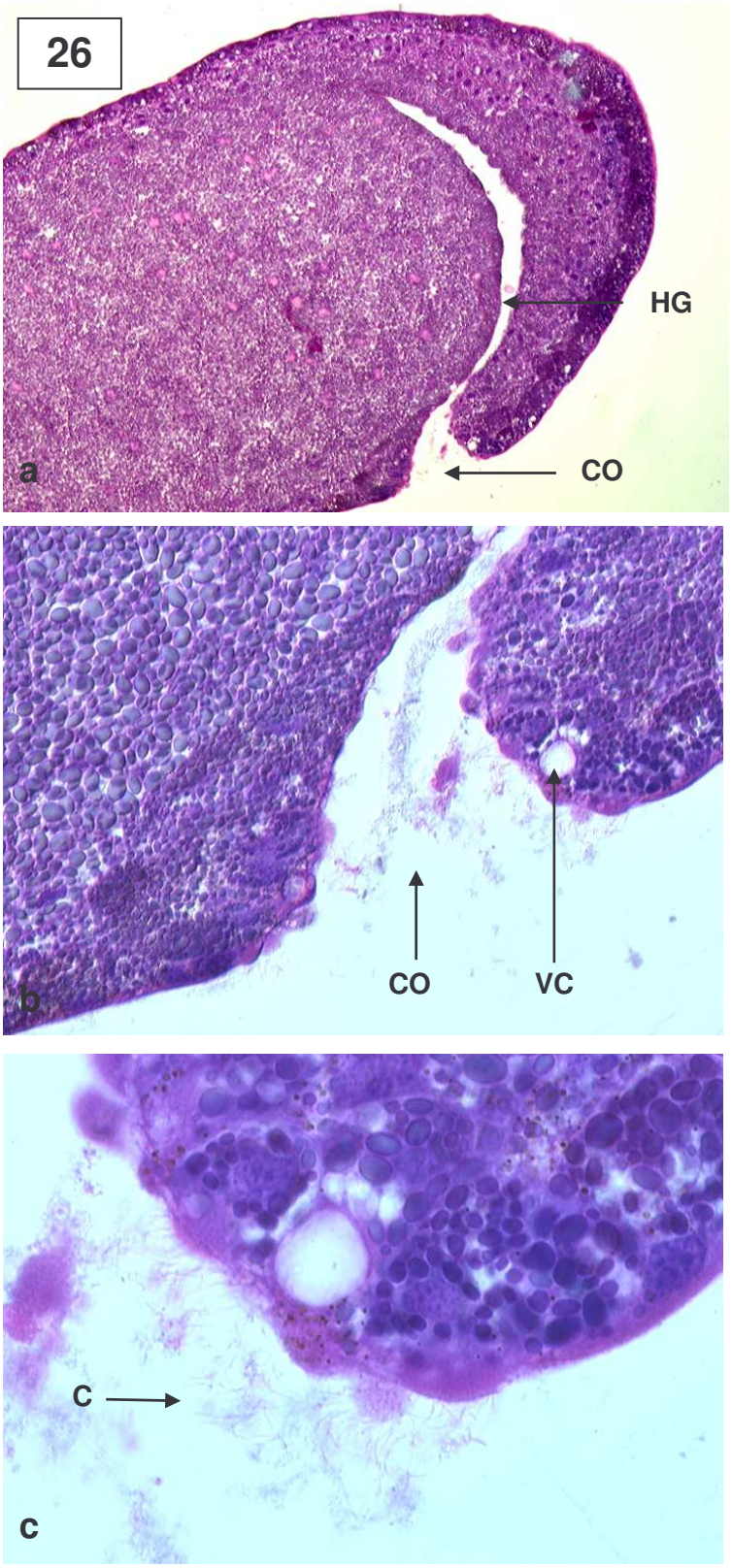
26
HG
CO
a
CO
VC
b
C
c

Figure 27. Representative photomicrographs of a sagittal section of the posterior region of a stage 25 *Xenopus laevis* embryo. a) The hindgut (HG) is continuous with the cloacal opening (CO). 100X. b) The cloacal opening (CO) is fairly wide and is continuous with the hindgut. 400X. c) Numerous vacuolated or secretory cells (VC) are scattered between the ectodermal cells around the cloacal opening. A possible secretory cell (AC) appears to be "blebbing." 630X. Gill's haematoxylin and eosin.

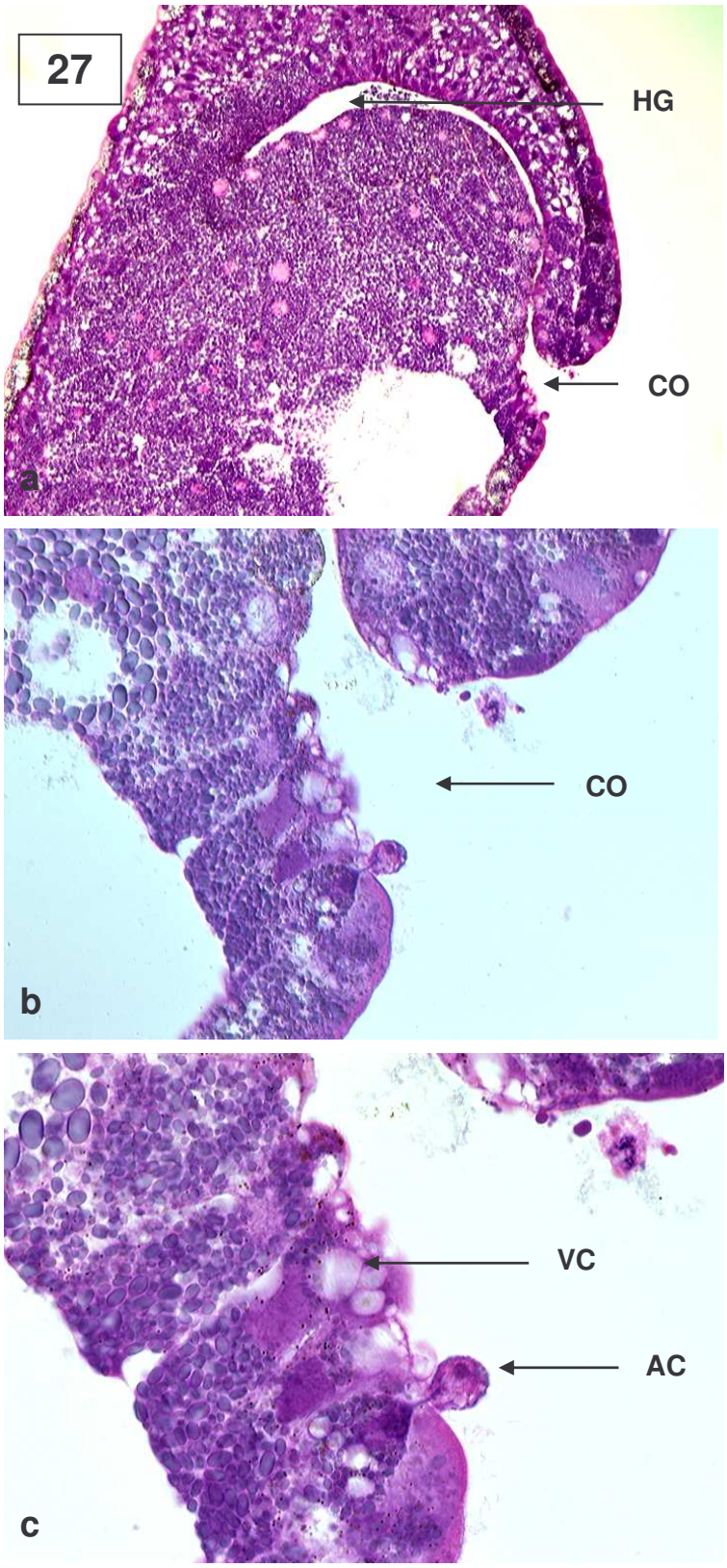
27
HG
CO
a
CO
b
VC
AC
c

Figure 28. Representative photomicrographs of a sagittal section of the posterior region of a stage 26 *Xenopus laevis* embryo. The hindgut (HG) is continuous with the cloacal opening (CO). a) 100X. b) 400X. Gill's haematoxylin and eosin.

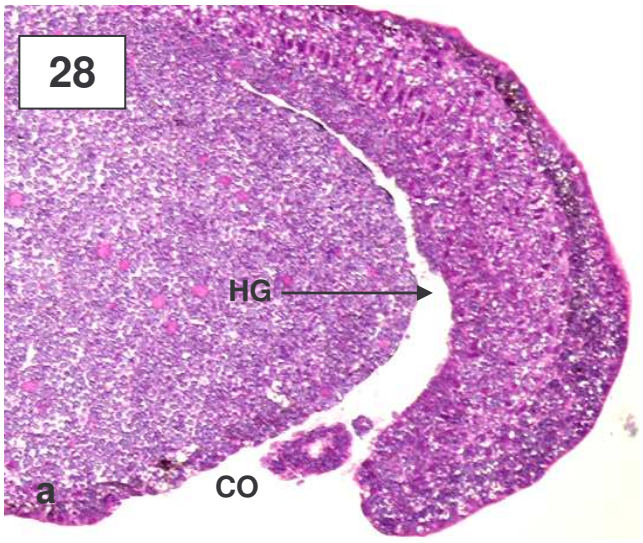
28
HG
a
CO

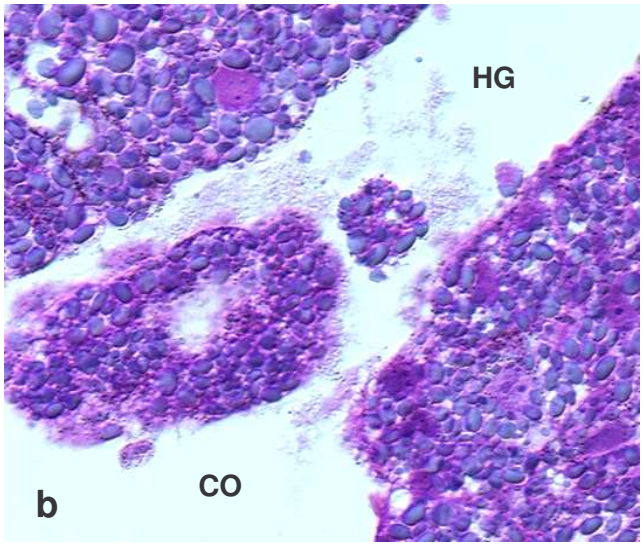
HG
CO
b

Figure 29. A representative photomicrograph of a sagittal section of the cloacal region of a stage 26 *Xenopus laevis* embryo. Numerous elongated cilia (C) are concentrated around the cloacal region and many vacuolated or secretory looking cells (VC) are apparent in this region. 630X. Gill's haematoxylin and eosin.

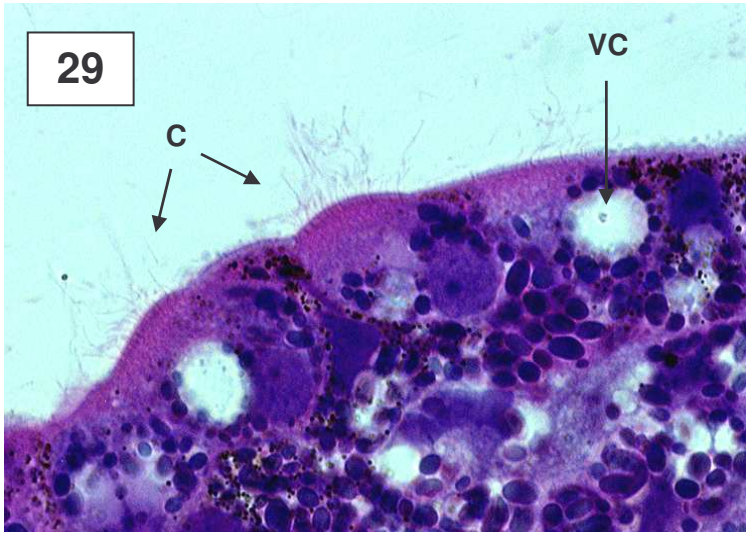
29
C
VC

Figure 30. A protein assay used to determine the presence of proteins in the *Xenopus laevis* embryonic samples. a) The embryonic sample was used undiluted and a blue reaction indicated the presence of proteins in the sample. b) The embryonic sample was used at a concentration of 1:10, but no reaction was produced.

Figure 31. A dot blot was used to determine the viability of the laminin antibody. a) A blue/grey reaction indicated the localization of the laminin protein, with the *Xenopus laevis* embryonic sample used undiluted and the laminin antibody applied at a concentration of 1:500. b) No reaction was seen when the *Xenopus laevis* embryonic sample was used at a concentration of 1:10 and the laminin antibody was applied at a concentration of 1:500. c) A blue/grey reaction indicated the localization of the laminin protein, with the *Xenopus laevis* embryonic sample used undiluted and the laminin antibody applied at a concentration of 1:1000. d) No reaction was seen when the *Xenopus laevis* embryonic sample was used at a concentration of 1:10 and the laminin antibody was applied at a concentration of 1:1000.

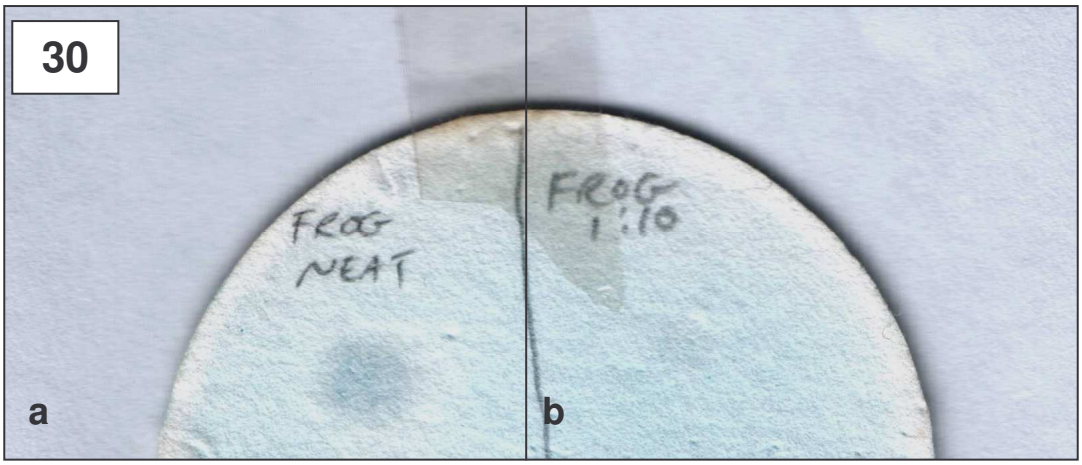
30
FROG
NEAT
FROG
1:10
a
b

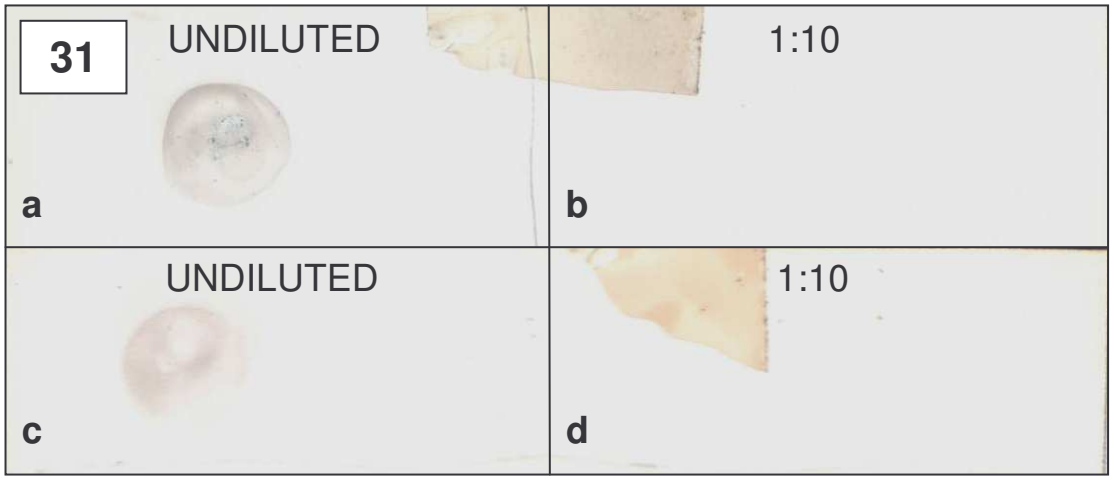
31
UNDILUTED
1:10
a
b
UNDILUTED
1:10
c
d

Figure 32. Representative photomicrographs of rat kidney used as a control for the immunolocalization of fibronectin. a) A positive control of rat kidney indicating the immunolocalization of fibronectin (black arrows), visualized as brown with DAB, in the basement membranes of the kidney tubules and glomeruli. No immunolocalization of fibronectin is visible in the kidney negative control sections in which the primary antibody was replaced with buffer (b); in which the secondary antibody was replaced with buffer (c) and in which the primary antibody was replaced with swine serum (d). 400X. Differential interference contrast microscopy.

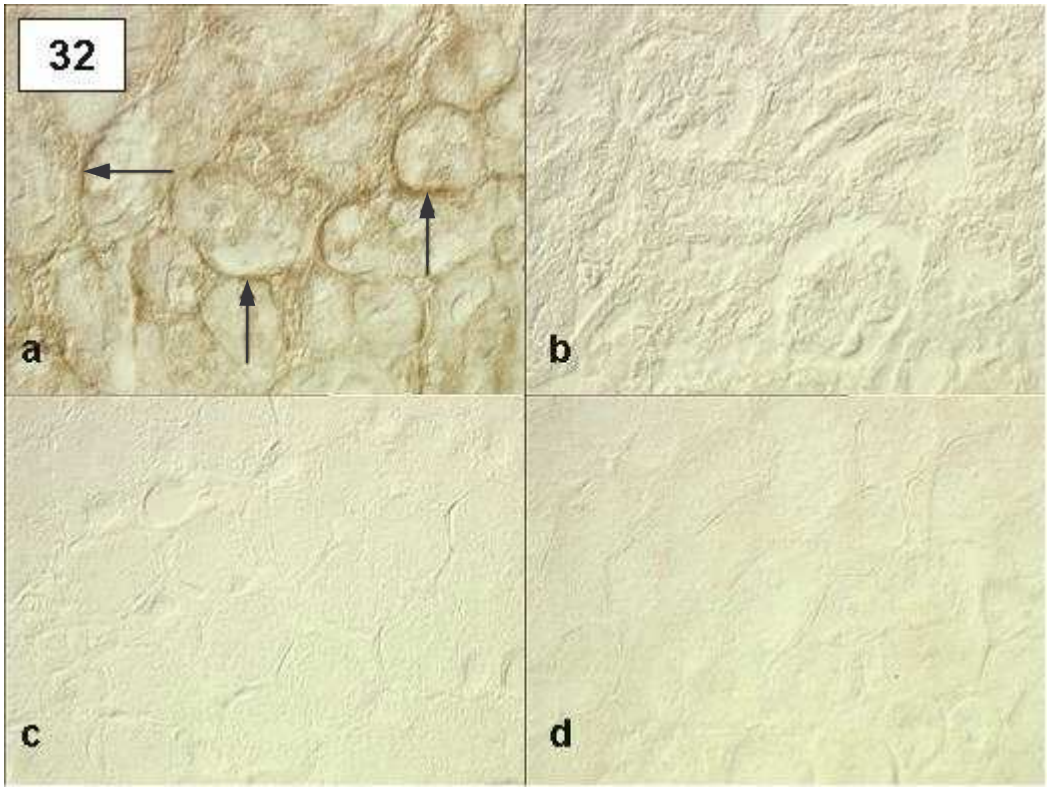
32
a
b
c
d

Figure 33. Representative photomicrographs of rat kidney used as a control for the immunolocalization of laminin. a) A positive control of rat kidney indicating the immunolocalization of laminin (black arrows), visualized as brown with DAB, in the basement membranes of the kidney tubules. No immunolocalization of laminin is visible in the kidney negative control sections in which the primary antibody was replaced with buffer (b); in which the secondary antibody was replaced with buffer (c) and in which the primary antibody was replaced with swine serum. 400X. Differential interference contrast microscopy.

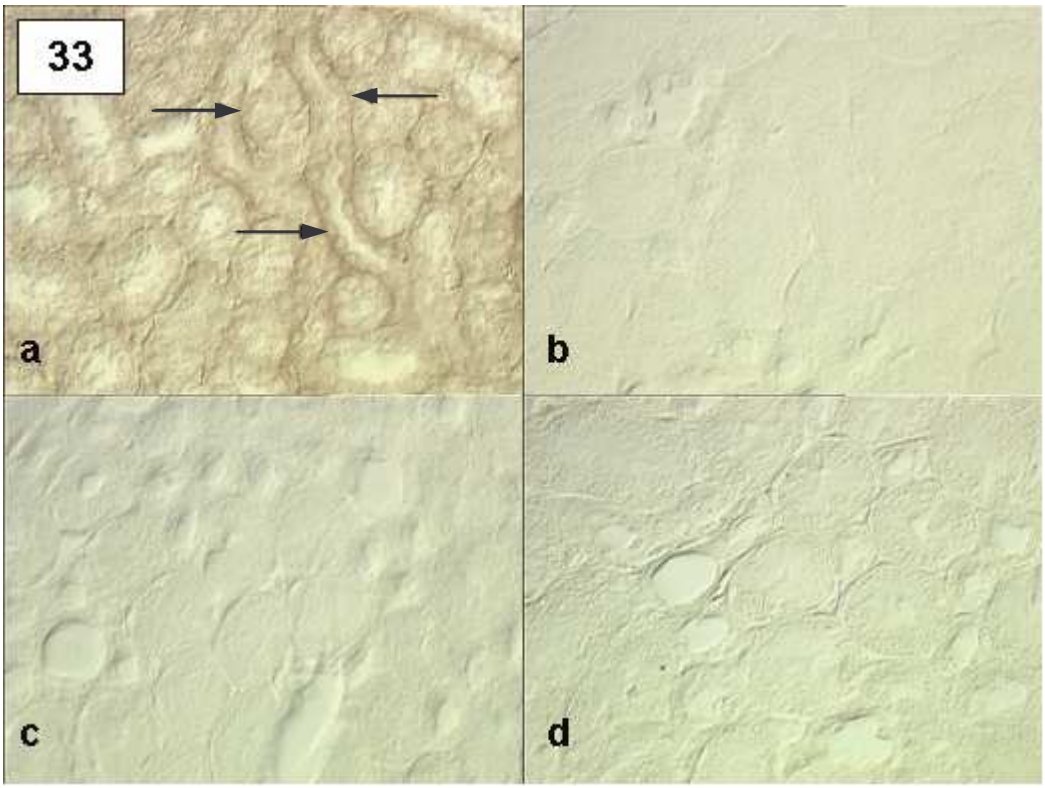
33
a
b
c
d

Figure 34. Representative photomicrographs of sagittal serial sections of the posterior region of a stage 21 *Xenopus laevis* embryo illustrating immunolocalization of the basement membrane components fibronectin and laminin. Fibronectin and laminin were visualized as brown with DAB. a) A topographical view of an embryonic section immunolocalized for fibronectin. 100X. b) A topographical view of a negative control section for fibronectin immunolocalization in which the primary antibody was replaced with buffer, showing no specific labelling. 100X. c) A topographical view of an embryonic section immunolocalized for laminin. 100X. d) A topographical view of a negative control section for laminin immunolocalization in which the primary antibody was replaced with buffer, showing no specific labelling. 100X. e) Interrupted immunolocalization of fibronectin (black arrows), possibly indicative of the discontinuous basement membrane between the proctodeal ectoderm and hindgut endoderm. 400X. f) A negative control for fibronectin immunolocalization in which the primary antibody was replaced with buffer, showing no specific labelling . 400X. g) Interrupted immunolocalization of laminin (black arrows), possibly indicative of the basement membrane between the proctodeal ectoderm and hindgut endoderm. 400X. h) A negative control for laminin immunolocalization in which the primary antibody was replaced with buffer, showing no specific labelling. 400X. Differential interference contrast microscopy. (HG-Hindgut; P-Proctodeum).

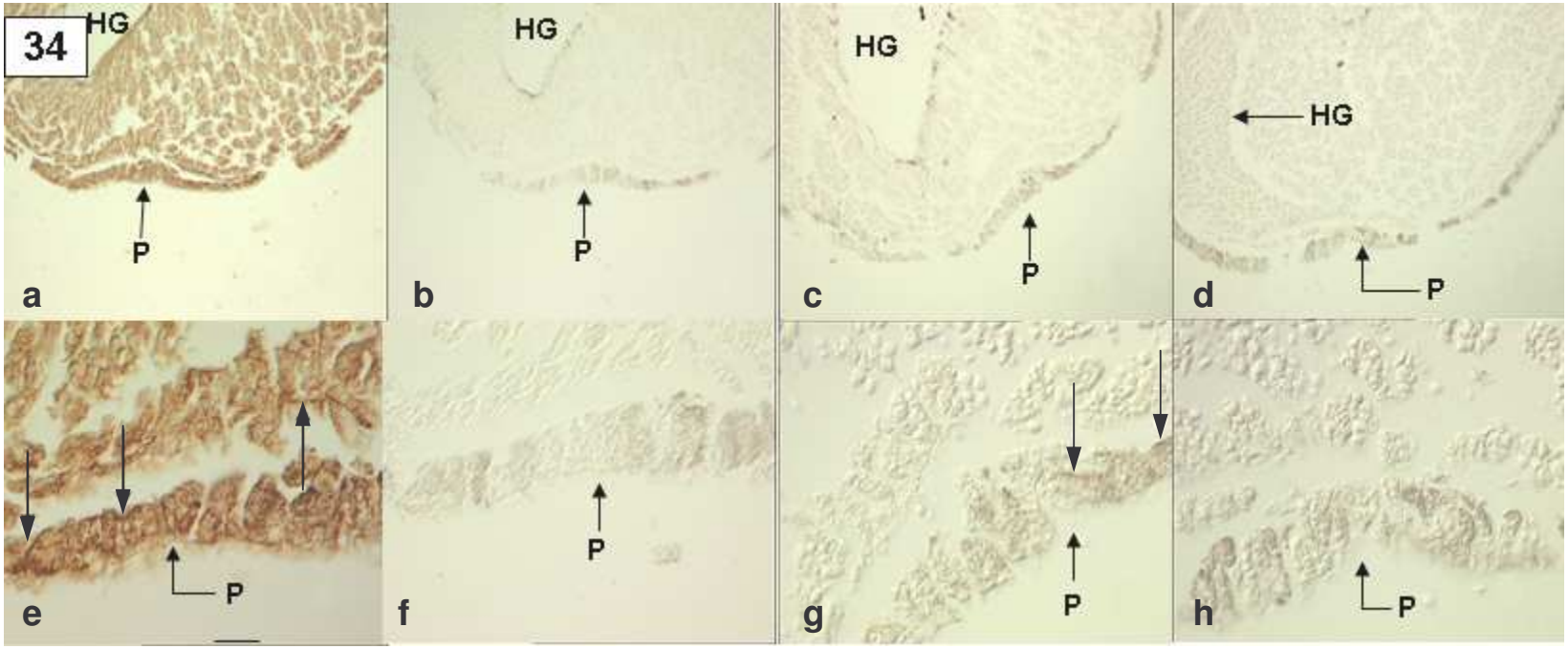
34
HG
P
a
HG
P
b
HG
P
c
HG
P
d
P
e
P
f
P
g
P
h

Figure 35. Representative photomicrographs of sagittal serial sections the posterior region of a stage 22 *Xenopus laevis* embryo illustrating immunolocalization of the basement membrane components fibronectin and laminin. Fibronectin and laminin were visualized as brown with DAB. a) A topographical view of an embryonic section immunolocalization for fibronectin. 100X. b) A topographical view of a negative control section for fibronectin immunolocalization in which the primary antibody was replaced with buffer, showing no specific labelling. 100X. c) Immunolocalization of fibronectin. 400X. d) A negative control for fibronectin immunolocalization in which the primary antibody was replaced with buffer, showing no specific labelling. 400X. e) Interrupted immunolocalization of fibronectin (black arrows), possibly indicative of the basement membrane between the proctodeal ectoderm and hindgut endoderm. 630X. f) A negative control for fibronectin immunolocalization in which the primary antibody was replaced with buffer, showing no specific labelling. 630X. g) A topographical view of an embryonic section immunolocalized for laminin. 100X. h) A topographical view of a negative control section for laminin immunolocalization in which the primary antibody was replaced with buffer, showing no specific labelling. 100X. i) Interrupted immunolocalization of laminin (black arrow), possibly indicative of the basement membrane between the proctodeal ectoderm and hindgut endoderm. 630X. j) A negative control for laminin immunolocalization in which the primary antibody was replaced with buffer, showing no specific labelling. 630X. Differential interference contrast microscopy. (HG-Hindgut; P-Proctodeum).

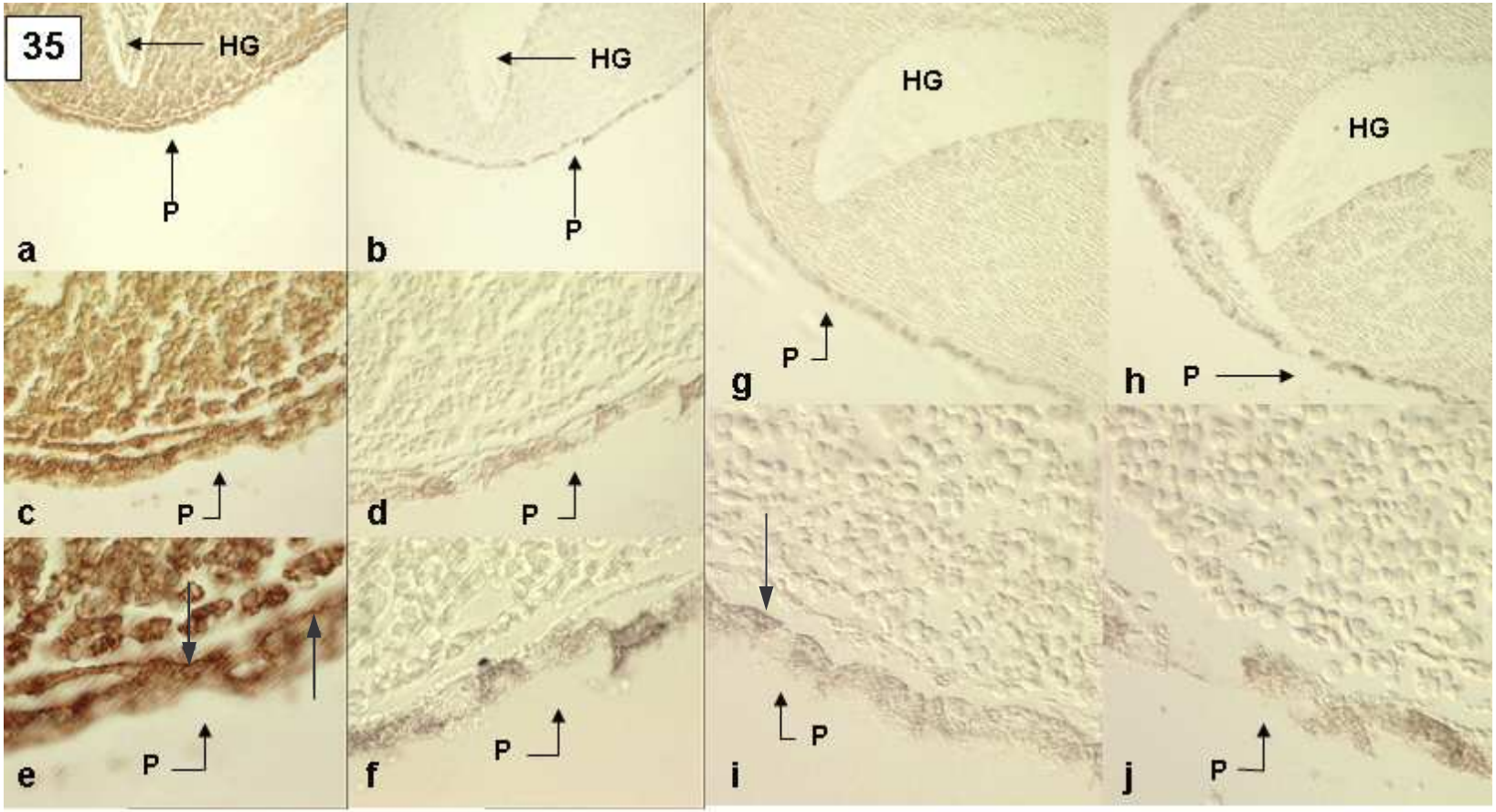
35
HG
P
a
HG
P
b
HG
P
g
HG
P
h
c
P
d
P
e
P
f
P
i
P
j
P

Figure 36. Representative photomicrographs of sagittal serial sections of the posterior region of a stage 23 *Xenopus laevis* embryo illustrating immunolocalization of the basement membrane components fibronectin and laminin. Fibronectin and laminin were visualized as brown with DAB. a) A topographical view of an embryonic section immunolocalized for fibronectin. 100X. b) A topographical view of a negative control section for fibronectin immunolocalization in which the primary antibody was replaced with buffer, showing no specific labelling. 100X. c) A topographical view of an embryonic section immunolocalized for laminin. 100X. d) A topographical view of a negative control section for laminin immunolocalization in which the primary antibody was replaced with buffer, showing no specific labelling. 100X. e) Immunolocalization of fibronectin, showing no specific labelling between the proctodeal ectoderm and hindgut endoderm. 400X. f) A negative control for fibronectin immunolocalization in which the primary antibody was replaced with buffer, showing no specific labelling. 400X. g) Immunolocalization of laminin, showing no specific labelling between the proctodeal ectoderm and hindgut endoderm. 400X. h) A negative control for laminin immunolocalization in which the primary antibody was replaced with buffer, showing no specific labelling. 400X. Differential interference contrast microscopy. (HG-Hindgut; P-Proctodeum).

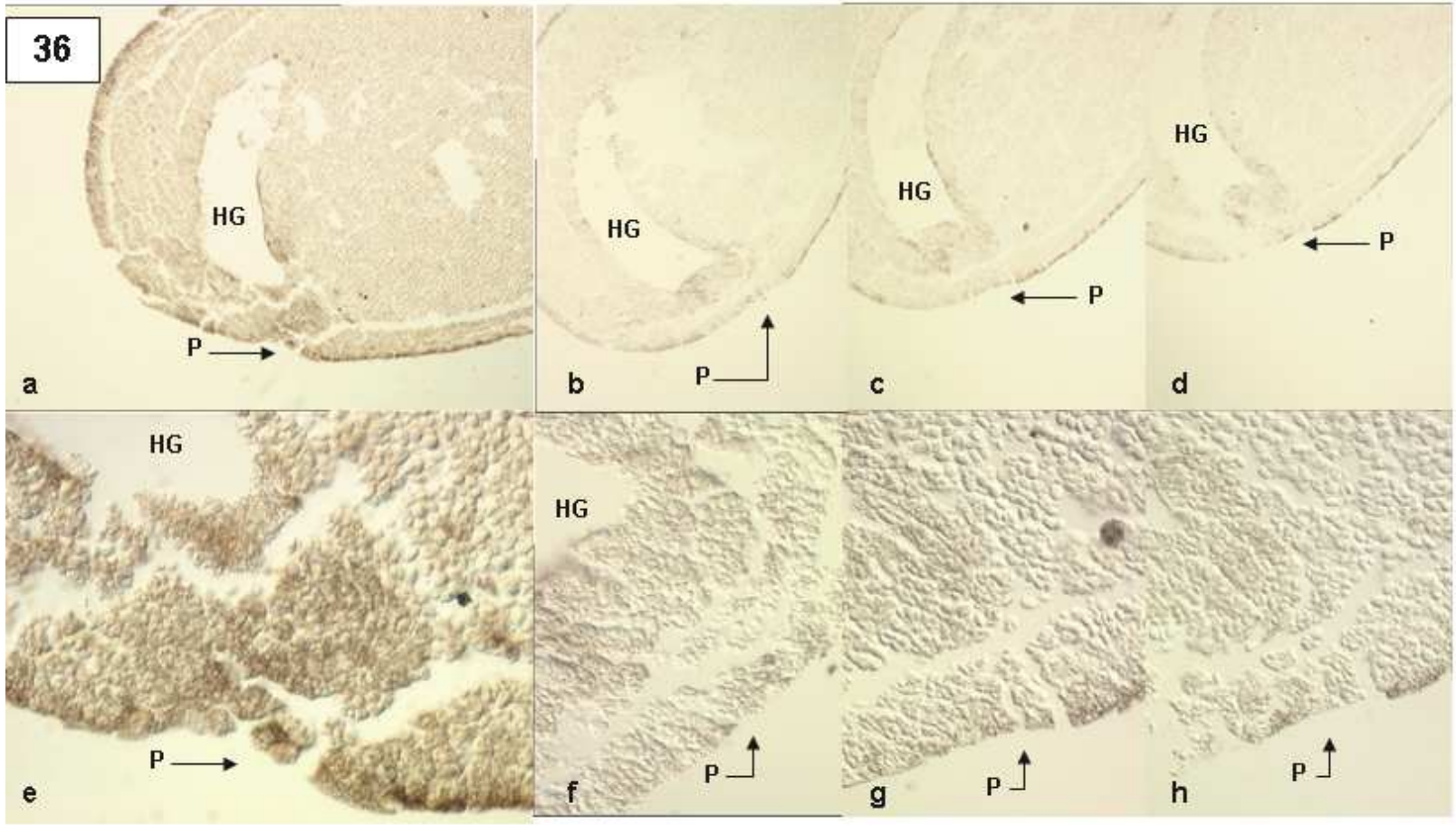
36
HG
P
a
HG
P
b
HG
P
c
HG
P
d
HG
P
e
HG
P
f
P
g
P
h

Figure 37. Representative photomicrographs of a sagittal section of the posterior region of a stage 24 *Xenopus laevis* embryo illustrating immunolocalization for fibronectin. No specific labelling can be seen. a) A topographical view. 100X. b) 400X. Differential interference contrast microscopy. (CO-Cloacal Opening; HG-Hindgut).

Figure 38. Representative photomicrographs of a sagittal section of the posterior region of a negative control section for fibronectin immunolocalization of a stage 24 *Xenopus laevis* embryo. The primary antibody was omitted and replaced with buffer in the immunohistochemical technique. a) A topographical view. 100X. b) 400X. Differential interference contrast microscopy. (CO-Cloacal Opening; HG-Hindgut).

Figure 39. Representative photomicrographs of sagittal serial sections of the posterior region of a stage 24 *Xenopus laevis* embryo, illustrating immunolocalization for the basement membrane marker, laminin. a) A topographical view, showing no specific labelling. 100X. b) A topographical view of a negative control section in which the primary antibody was replaced with buffer, showing no specific . 100X. c) No specific labelling can be seen. 400X. d) A negative control for laminin immunolocalization in which the primary antibody was replaced with buffer, showing no specific labelling. 400X. Differential interference contrast microscopy. (CO-Cloacal Opening; HG-Hindgut).

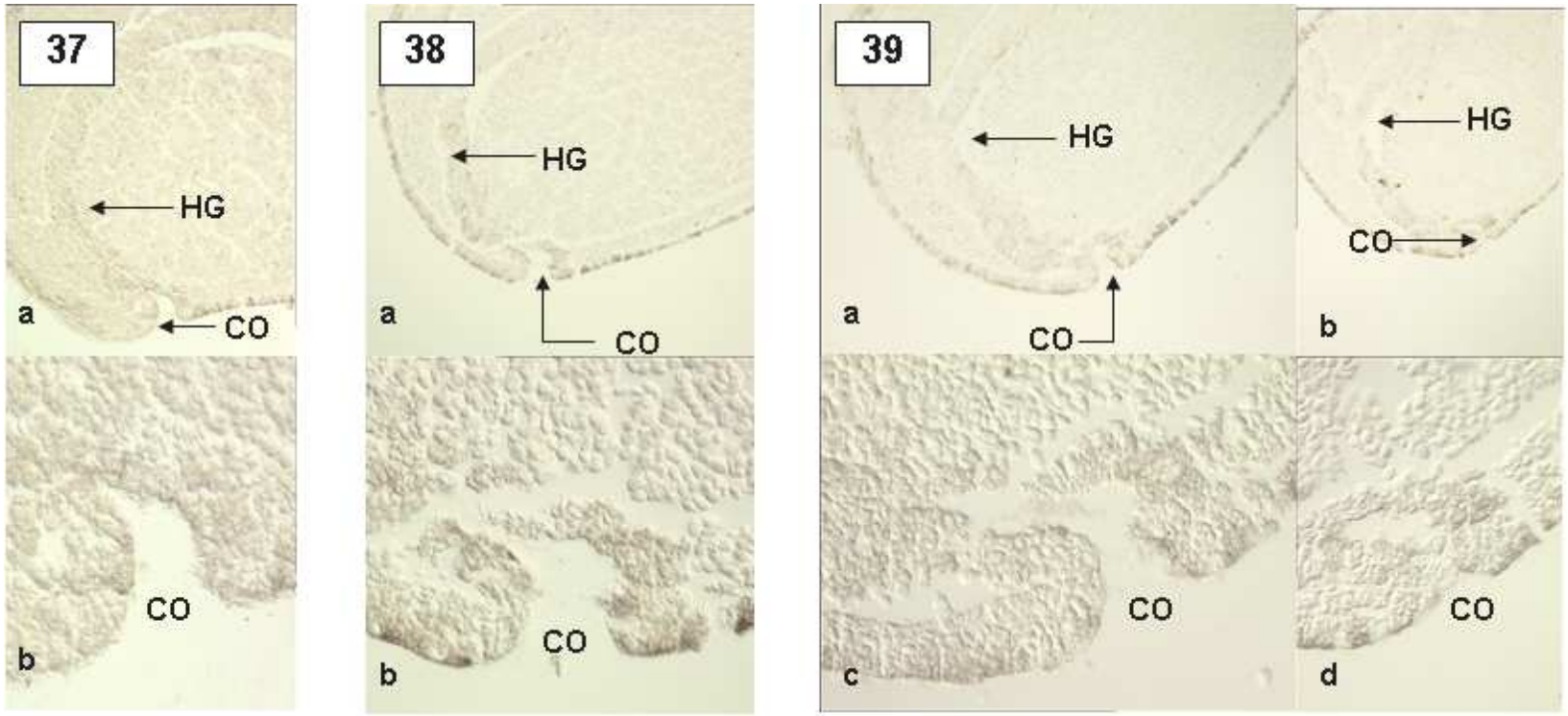
37
HG
a
CO
CO
b
38
HG
a
CO
CO
b
39
HG
a
CO
HG
b
CO
CO
c
CO
d

Figure 40. Representative photomicrographs of sagittal serial sections of the posterior region of a stage 25 *Xenopus laevis* embryo, illustrating immunolocalization for the basement membrane marker, fibronectin. a) A topographical view showing no specific labelling. 100X. b) A topographical view of a negative control section for fibronectin immunolocalization in which the primary antibody was replaced with buffer, showing no specific labelling. 100X. c) No specific labelling can be seen. 400X. d) A negative control for fibronectin immunolocalization in which the primary antibody was replaced with buffer, showing no specific labelling. 400X. Differential interference contrast microscopy. (CO-Cloacal Opening; HG-Hindgut).

Figure 41. Representative photomicrographs of sagittal serial sections of the posterior region of a stage 25 *Xenopus laevis* embryo, illustrating immunolocalization for the basement membrane marker, laminin. a) A topographical view, showing no specific labelling. 100X. b) A topographical view of a negative control section for laminin immunolocalization in which the primary antibody was replaced with buffer, showing no specific labelling. 100X. c) No specific labelling can be seen. 400X. d) A negative control for laminin immunolocalization in which the primary antibody was replaced with buffer, showing no specific labelling. 400X. Differential interference contrast microscopy. (CO-Cloacal Opening; CR-Cloacal Region; HG-Hindgut).

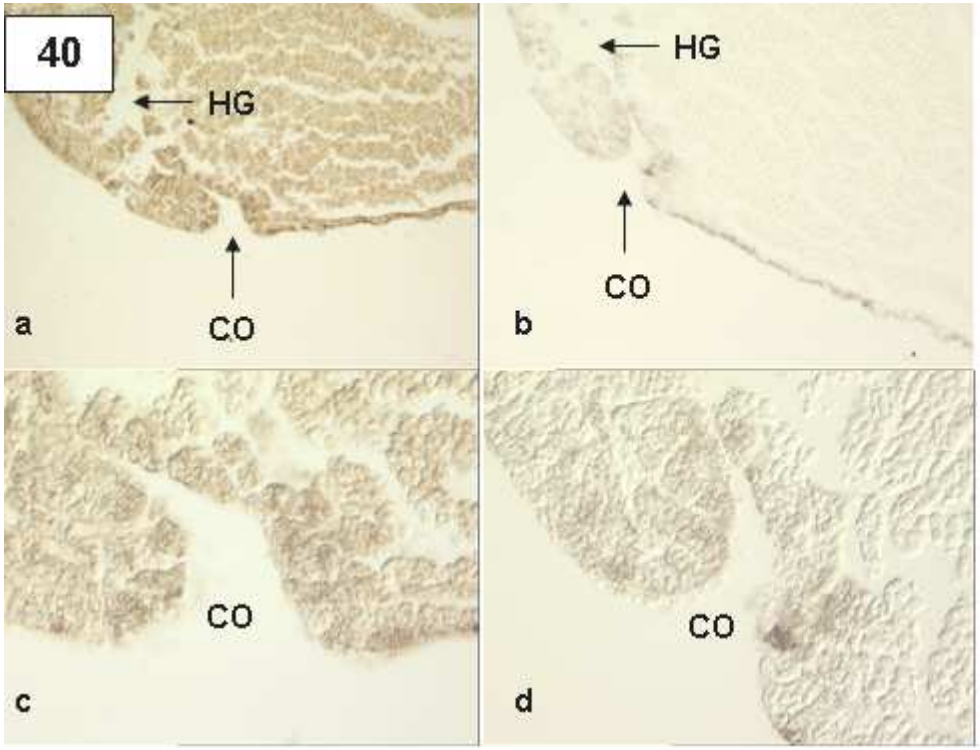
40
HG
CO
a
HG
CO
b
CO
c
CO
d

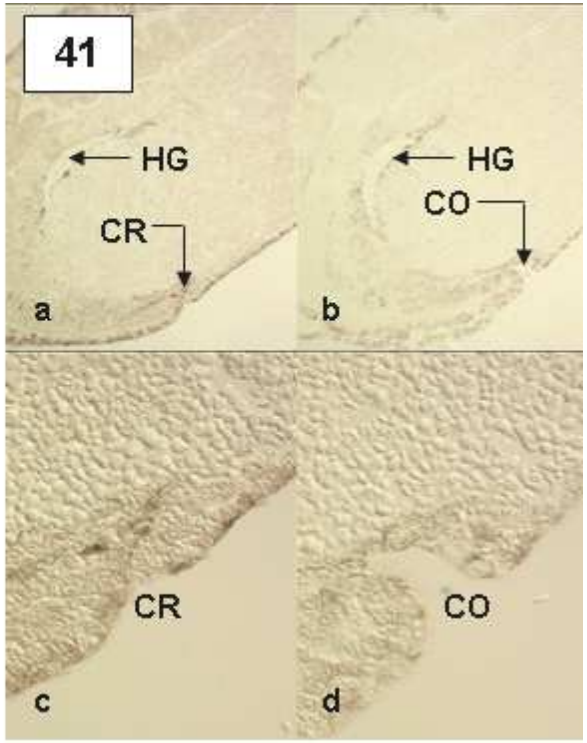
41
HG
CR
a
HG
CO
b
CR
c
CO
d

Figure 42. Representative photomicrographs of a sagittal section of the posterior region of a stage 26 *Xenopus laevis* embryo illustrating immunolocalization for fibronectin. No immunolocalization of fibronectin can be seen. a) A topographical view. 100X. b) 400X. Differential interference contrast microscopy. (CO-Cloacal Opening; HG-Hindgut).

Figure 43. Representative photomicrographs of a sagittal section of the posterior region of a negative control for fibronectin immunolocalization of a stage 26 *Xenopus laevis* embryo. The primary antibody was omitted and replaced with buffer in the immunohistochemical technique. a) A topographical view. 100X. b) 400X. Differential interference contrast microscopy. (CO-Cloacal Opening; HG-Hindgut).

Figure 44. Representative photomicrographs of sagittal serial sections of the posterior region of a stage 26 *Xenopus laevis* embryo, illustrating immunolocalization for the basement membrane marker, laminin. a) A topographical view, showing no specific labelling. 100X. b) A topographical view of a negative control section for laminin immunolocalization in which the primary antibody was replaced with buffer, showing no specific labelling. 100X. c) No specific labelling can be seen. 400X. d) A negative control for laminin immunolocalization in which the primary antibody was replaced with buffer, showing no specific labelling. 400X. Differential interference contrast microscopy. (CO-Cloacal Opening; CR-Cloacal Region; HG-Hindgut).

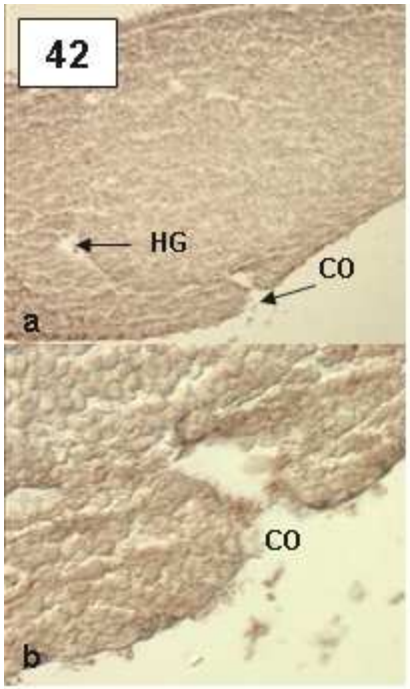
42
HG
CO
a
CO
b

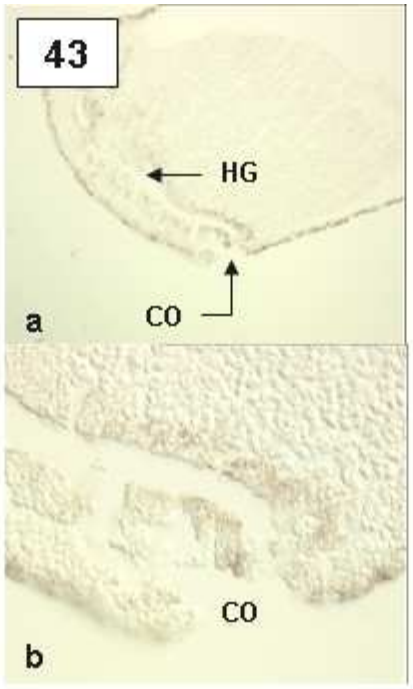
43
HG
CO
a
CO
b

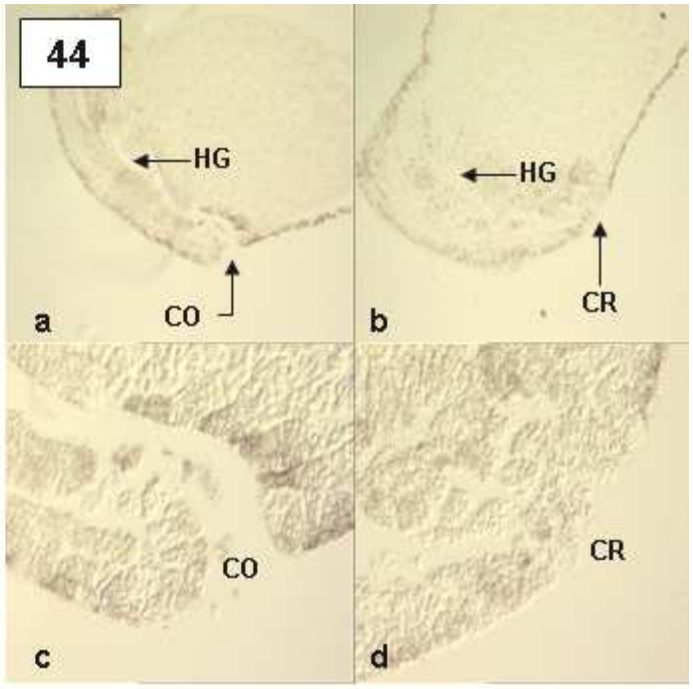
44
HG
CO
a
HG
CR
b
CO
c
CR
d

Figure 45. Rat testes used as a positive control for the TUNEL method for the identification of apoptosis. Apoptotic cells were visualized as brown cells, with DAB a) A positive control indicating apoptotic cells. 400X. b) A negative control in which the enzyme was omitted from the protocol. No reaction is visible. 400X. Differential interference contrast microscopy.

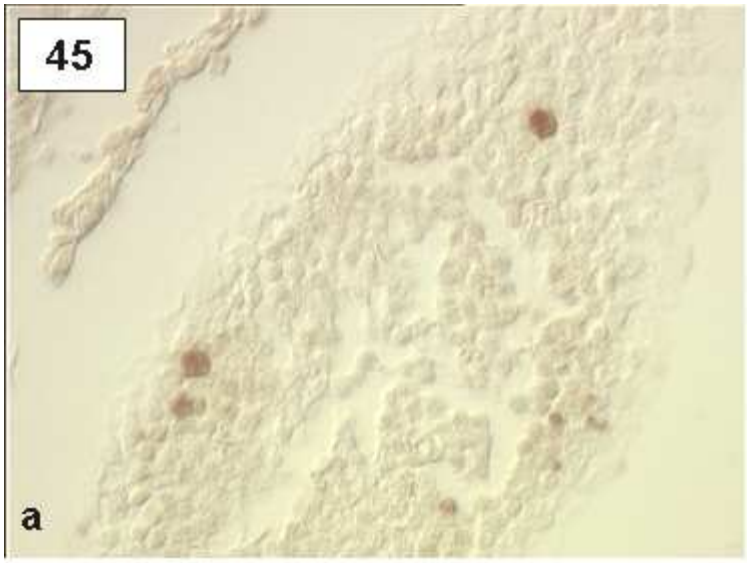
45
a


b

Figure 46. Lateral views of negative control *Xenopus laevis* embryos in which the enzyme was omitted from the TUNEL protocol to ensure the specificity of the labelling reaction. A lateral view, 50X (a) and sagittal section, 400X (b) of the posterior region of embryos at stage 21 of development illustrate no specific labelling. A lateral view (c) of the posterior region of an embryo at stage 22 of development illustrating the absence of specific labelling. 50X. A lateral view, 50X (d) of the posterior region and sagittal sections, 400X of the hindgut (HG) (e) and proctodeal ectoderm (EC) (f) of embryos at stage 23 of development, illustrating no specific labelling. A lateral view (g) of the posterior region of an embryo at stage 24, showing no specific labelling. A lateral view, 50X (h) and sagittal section, 400X (i) of the posterior region of embryos at stage 25 of development, showing no specific labelling in the hindgut region (HG). A lateral view (j) of the posterior region of an embryo at stage 26 showing no specific labelling. 50X. (Black Arrows-Proctodeal Region).

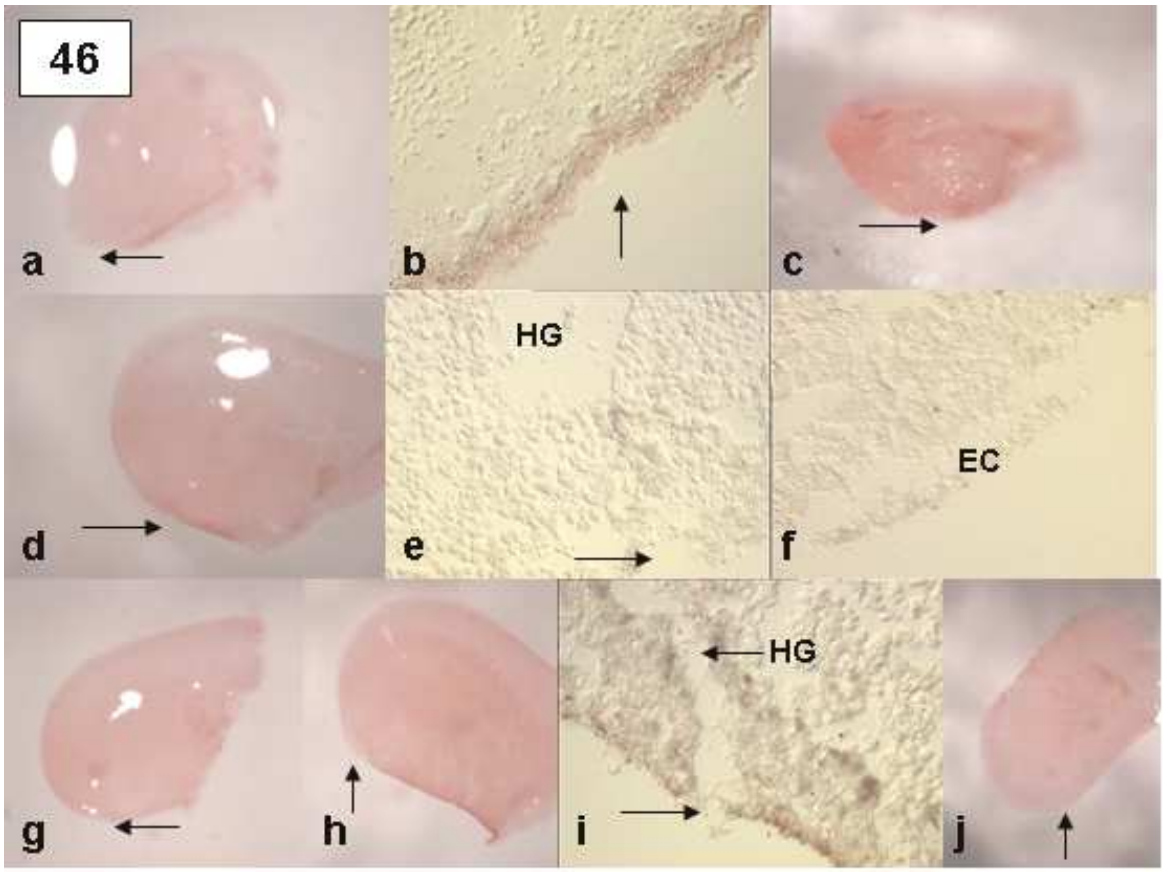
46
a
b
c
d
HG
e
EC
f
g
h
HG
i
j

Figure 47. Representative images of the posterior regions of *Xenopus laevis* embryos at stage 21 of development, labelled for apoptosis with the TUNEL method. Apoptotic cells were visualized as brown cells with DAB. a) A ventral view illustrating a few labelled cells (black arrows) scattered across the ectodermal surface of the embryo and in the region of the blastopore (B), which is not yet closed. The proctodeal depression is not visible and it is difficult to discern apoptotic cells in this region (PR). 50X. b) A sagittal section illustrating the proctodeal region (PR) and the hindgut (HG). High background staining or pigmentation is visible in the outer ectoderm with no specific labelling in the proctodeal region. 100X. c) A sagittal section showing no specific labelling in the proctodeal region (PR). There is some degree of background staining or pigment, which appears predominantly in the ectoderm. 400X.

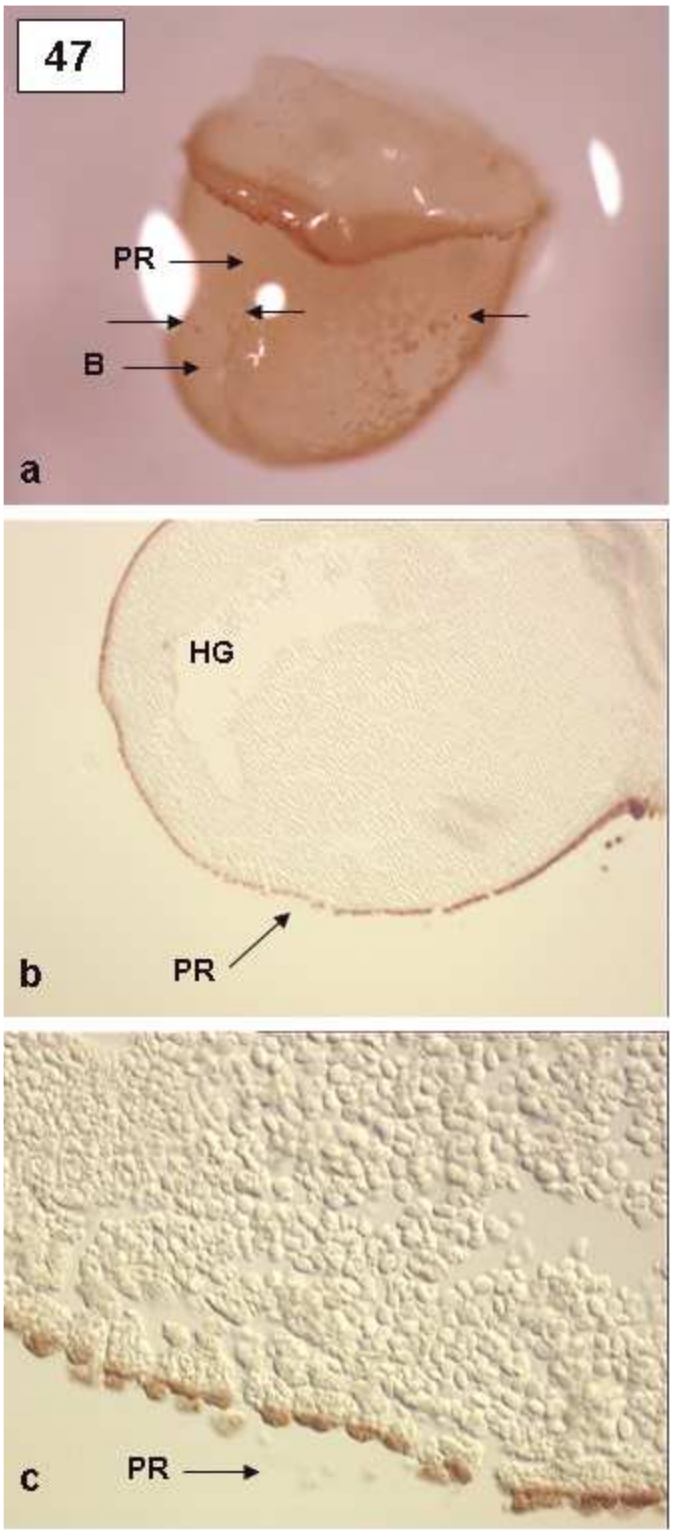
47
PR
B
a
HG
b
PR
c
PR

Figure 48. Representative images of the posterior regions of *Xenopus laevis* embryos at stage 22 of development, labelled for apoptosis with the TUNEL. The apoptotic cells were visualized as brown cells with DAB. a) A lateral-ventral view illustrating labelled cells (black arrows) in the surface ectoderm, which may appear brown due to tearing of the tissue. No specific labelling can be seen around the proctodeum (P), although there is a high degree of background staining making it difficult to differentiate any specifically labelled cells. 50X. b) A sagittal section illustrating labelled cells (black arrows) present in the ectoderm and dispersed throughout the posterior region, including the proctodeum (P). 100X. c) A sagittal section indicating a high proportion of labelled cells (black arrows) in the ectoderm of the proctodeum (P). 400X. (HG-Hindgut).

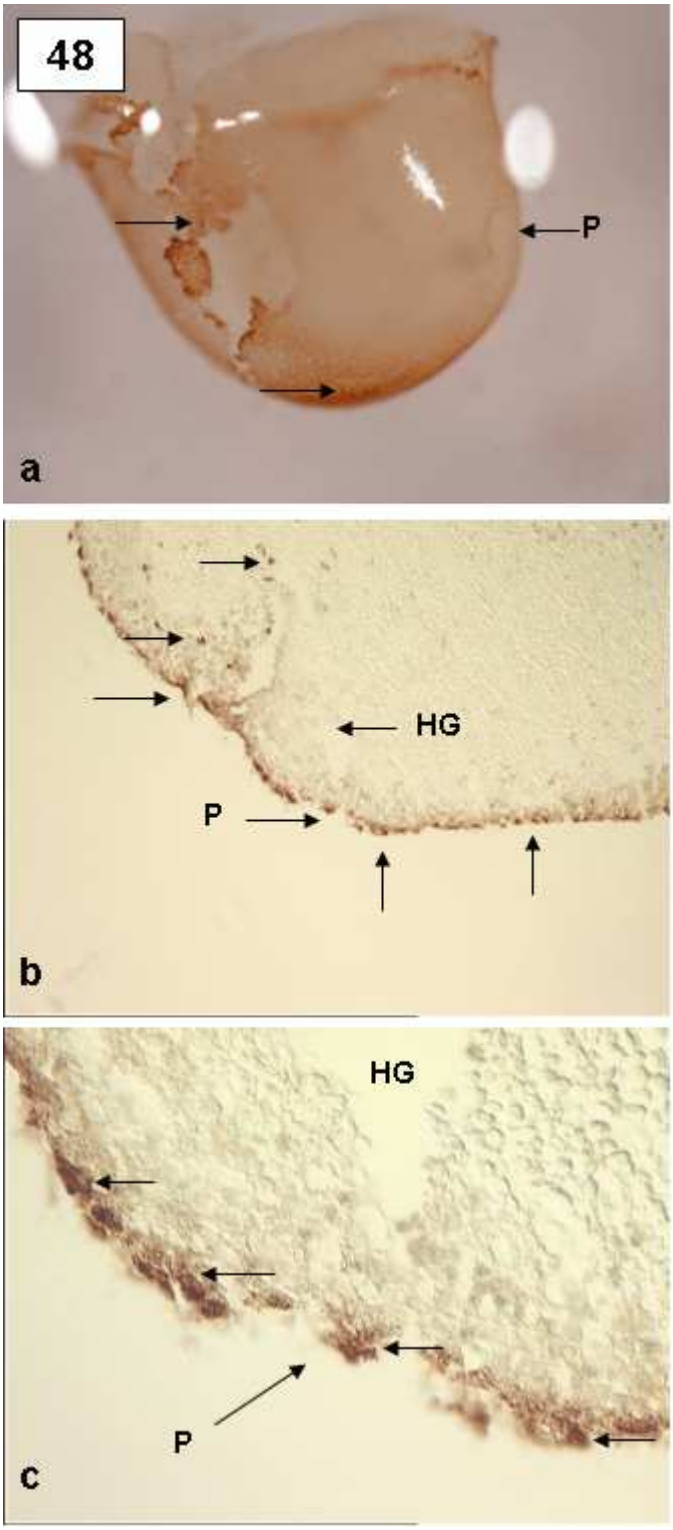
48
P
a
HG
P
b
HG
P
c

Figure 49. Representative photomicrographs of a sagittal section of the posterior region of a stage 22 *Xenopus laevis* embryo using the TUNEL method to label apoptosis. Some background staining is visible in the ectodermal cell layer. No specific labelling is visible in the proctodeum (P). a) 100X. b) 400X. (HG-Hindgut).

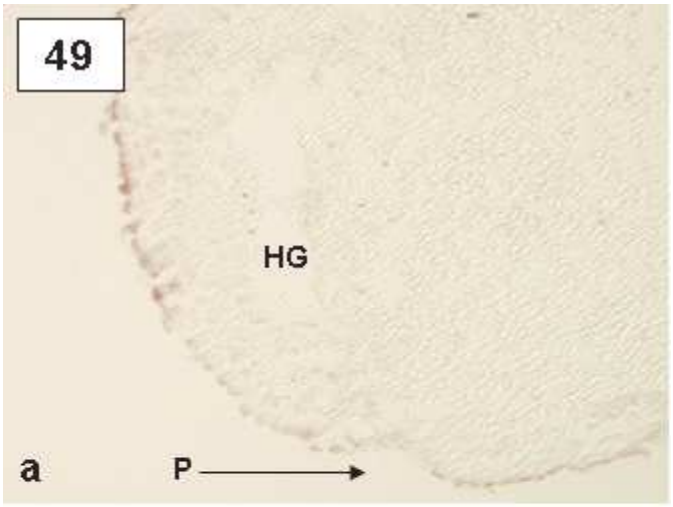
49
HG
a
P

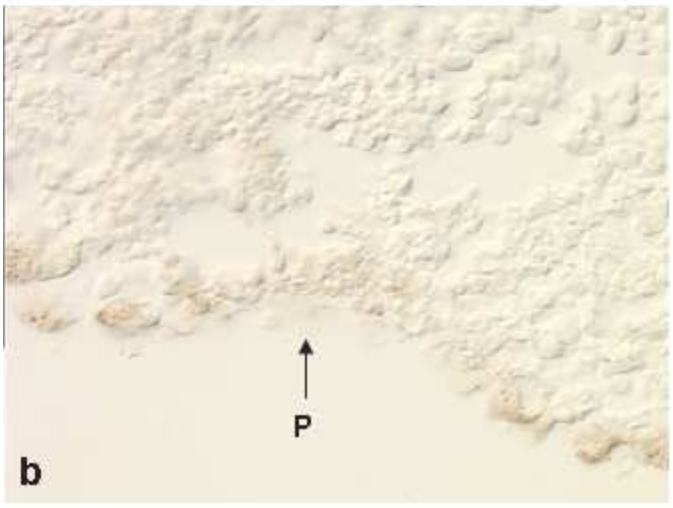
P
b

Figure 50. Representative posterior images of stage 23 *Xenopus laevis* embryos labelled for apoptosis, using the TUNEL method. Apoptotic cells were visualized as brown cells with DAB. a) A lateral-ventral view showing brown labelled cells located in the surface ectoderm (black arrows). It is difficult to distinguish any specifically labelled cells in the region of the proctodeum (P) as there is some background staining present. 50X. b) A sagittal section illustrating brown labelled cells (black arrows) dispersed in the outer ectoderm, including that of the proctodeum (P). 100X. c) A sagittal section showing the presence of a few labelled cells (black arrows) in the ectoderm of the proctodeum (P). 400X. (HG-Hindgut).

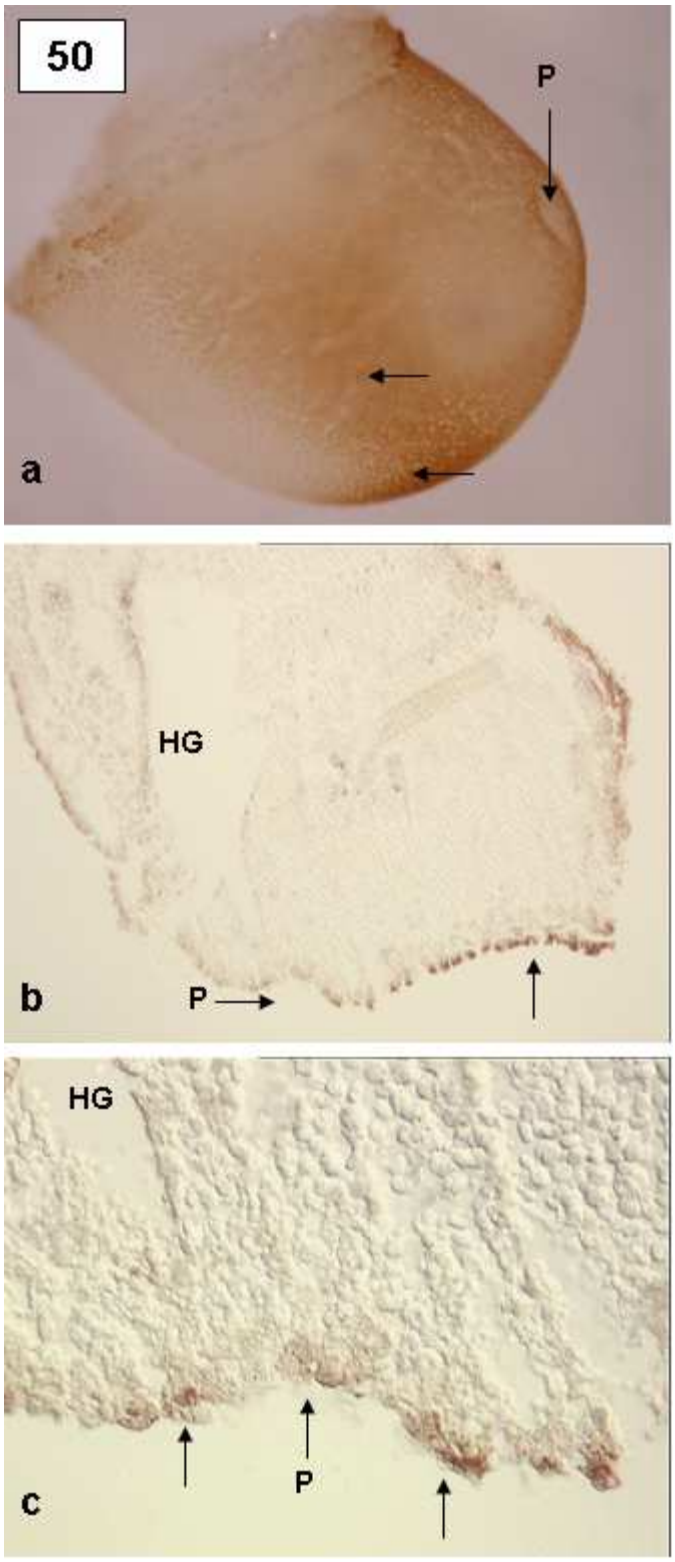
50
P
a
HG
b
P
HG
P
c

Figure 51. Representative photomicrographs of a sagittal section of the posterior region of a *Xenopus laevis* embryo at stage 23 of development, labelled for apoptosis using the TUNEL method. Apoptotic cells were visualized as brown cells with DAB. A few labelled cells (black arrows) can be seen in the endoderm of the hindgut (HG) and in the cloacal membrane (CM). a) 100X. b) 400X.

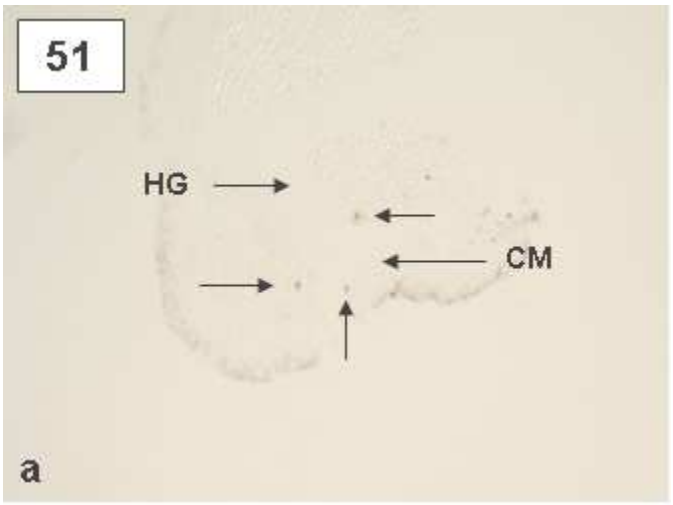
51
HG
CM
a

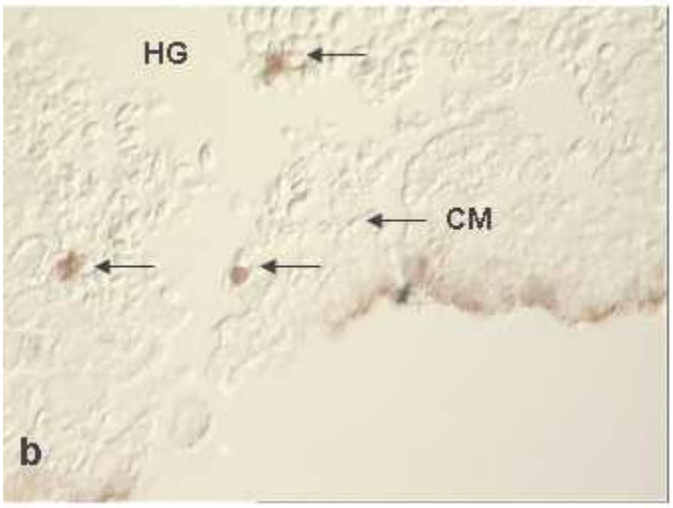
HG
CM
b

Figure 52. Representative photomicrographs of a sagittal section of the posterior region of a stage 23 *Xenopus laevis* embryo labelled for apoptosis, using the TUNEL method. No labelled cells are discernible in the region of the proctodeum (P), although some background staining is apparent. a) 100X. b) 400X. (HG-Hindgut).

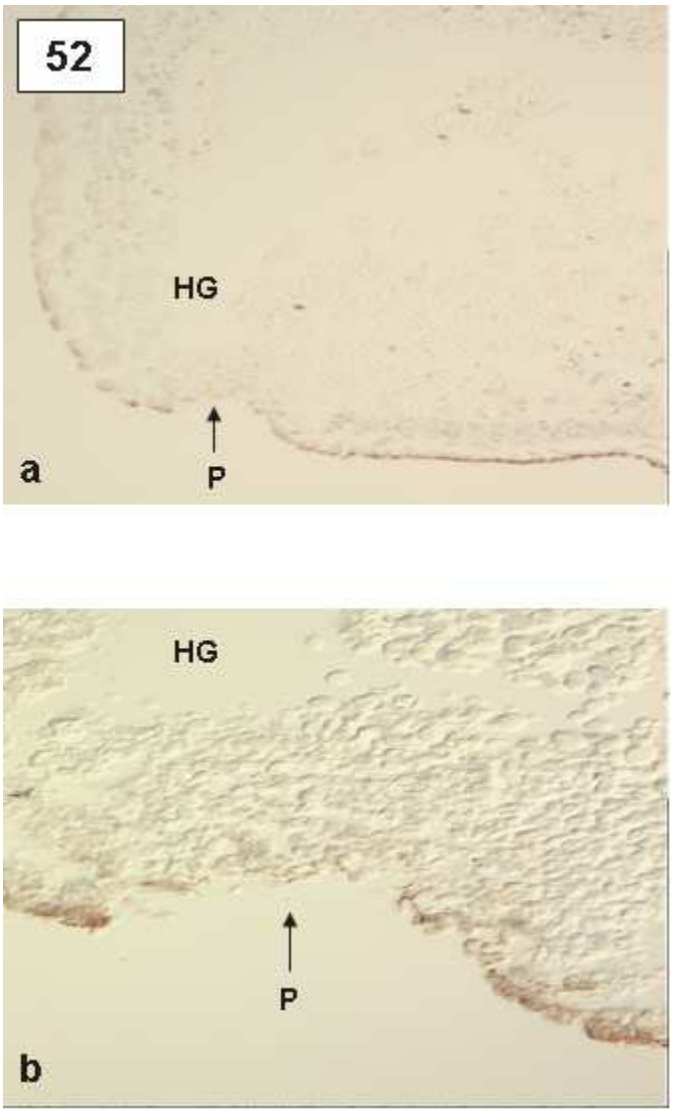
52
HG
P
a
HG
P
b

Figure 53. Representative images of the posterior regions of stage 24 *Xenopus laevis* embryos, labelled for apoptosis using the TUNEL method. Apoptotic cells were visualized as brown cells with DAB. a) A lateral-ventral view showing labelled cells (black arrows) in the surface ectoderm. It is difficult to distinguish any labelled cells around the cloacal opening (CO) as the background staining is quite high. 50X. b) A sagittal section indicating labelled cells (black arrows) present in the ectoderm, although not concentrated around the cloacal opening (CO). 100X. c) A sagittal section showing no specific labelling around the cloacal opening (CO). 400X. (HG-Hindgut).

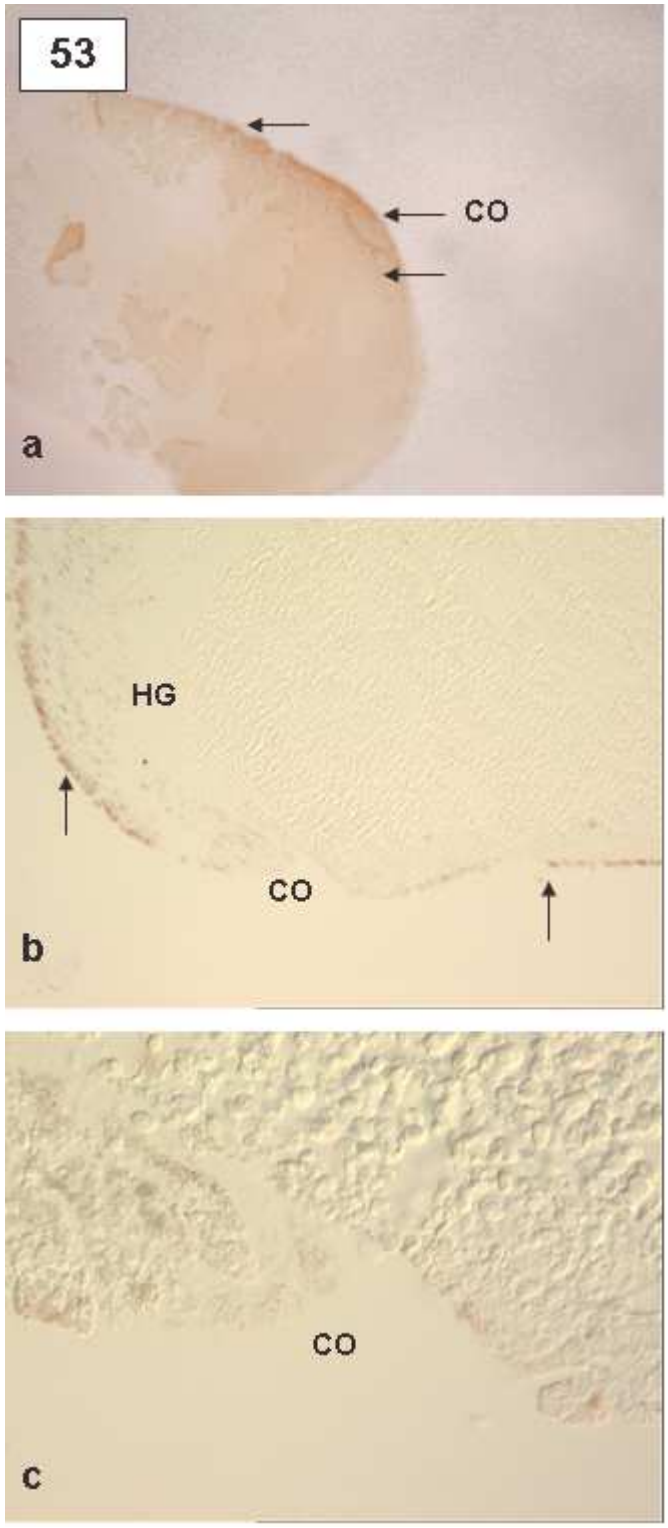
53
CO
a
HG
CO
b
CO
c

Figure 54. Representative images of the posterior regions of stage 25 *Xenopus laevis* embryos, labelled for apoptosis using the TUNEL method. Apoptotic cells were visualized as brown cells with DAB. a) A lateral-ventral view showing possible labelled cells (black arrows) in the surface ectoderm. It is difficult to distinguish any labelled cells around the cloacal opening (CO) as the background staining is quite high. 50X. b) A sagittal section indicating labelled cells (black arrows) present in the ectoderm around the cloacal opening (CO). 100X. c) A sagittal section indicating the presence of labelled cells (black arrows) in the ectoderm around the cloacal opening (CO).

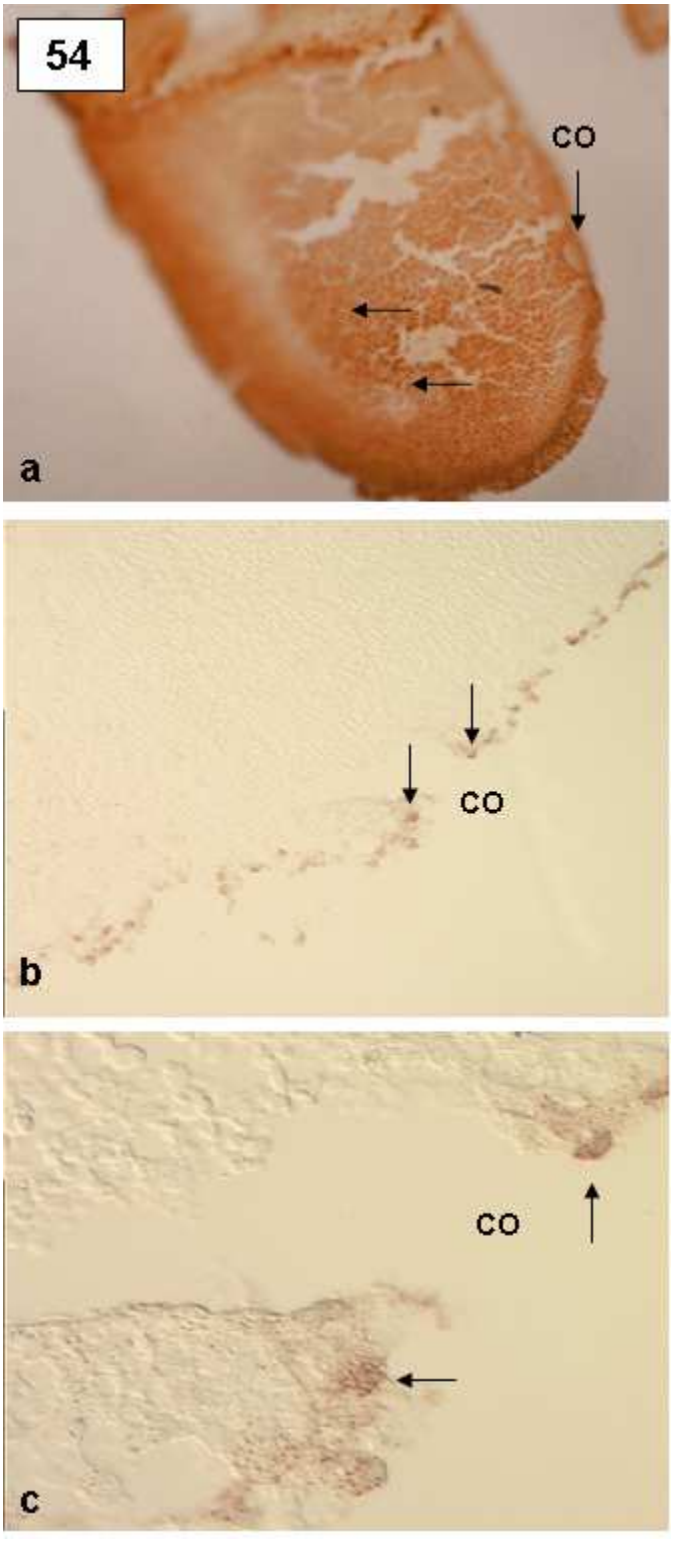
54
co
a
co
b
co
c

Figure 55. Representative photomicrographs of a sagittal section of the posterior region of a stage 25 *Xenopus laevis* embryo, labelled for apoptosis, using the TUNEL method. No specific labelling is visible in the region around the cloacal opening (CO), although there is some background staining visible. a) 100X. b) 400X.

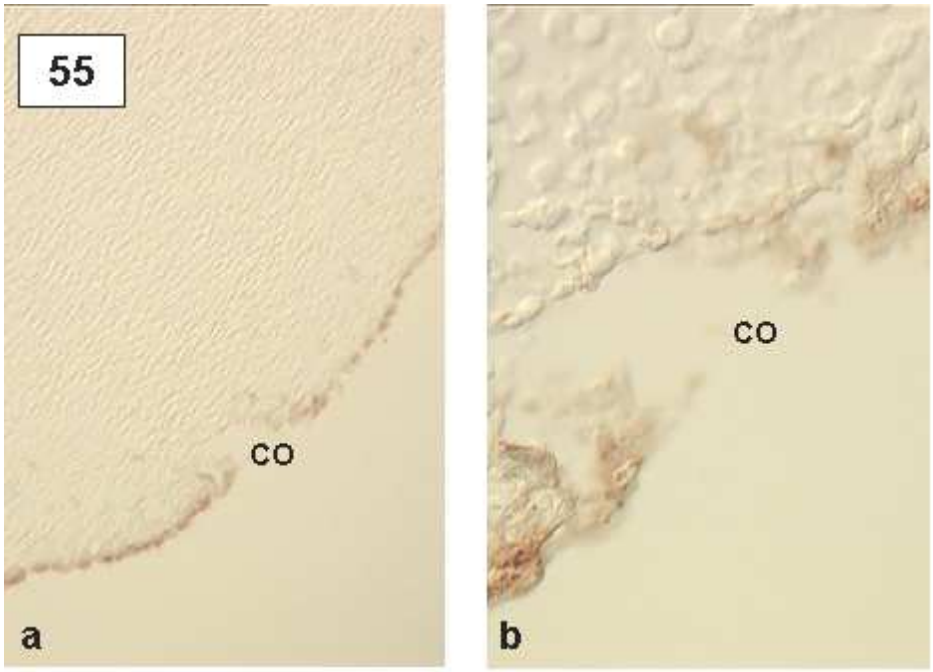
55
co
a
co
b

Figure 56. Representative images of the posterior regions of stage 26 *Xenopus laevis* embryos, stained for apoptosis using the TUNEL method. Apoptotic cells were visualized as brown cells with DAB. a) A lateral-ventral view showing possible labelled cells in the surface ectoderm (black arrows). No labelled cells are easily discernible around the cloacal opening (CO) due to the presence of some background staining. 50X. b) A sagittal section indicating labelled cells (black arrows) in the surface ectoderm, including that around the cloacal opening (CO). 100X. c) A sagittal section indicating the presence of number of labelled cells (black arrows) concentrated around the cloacal opening (CO). 400X.

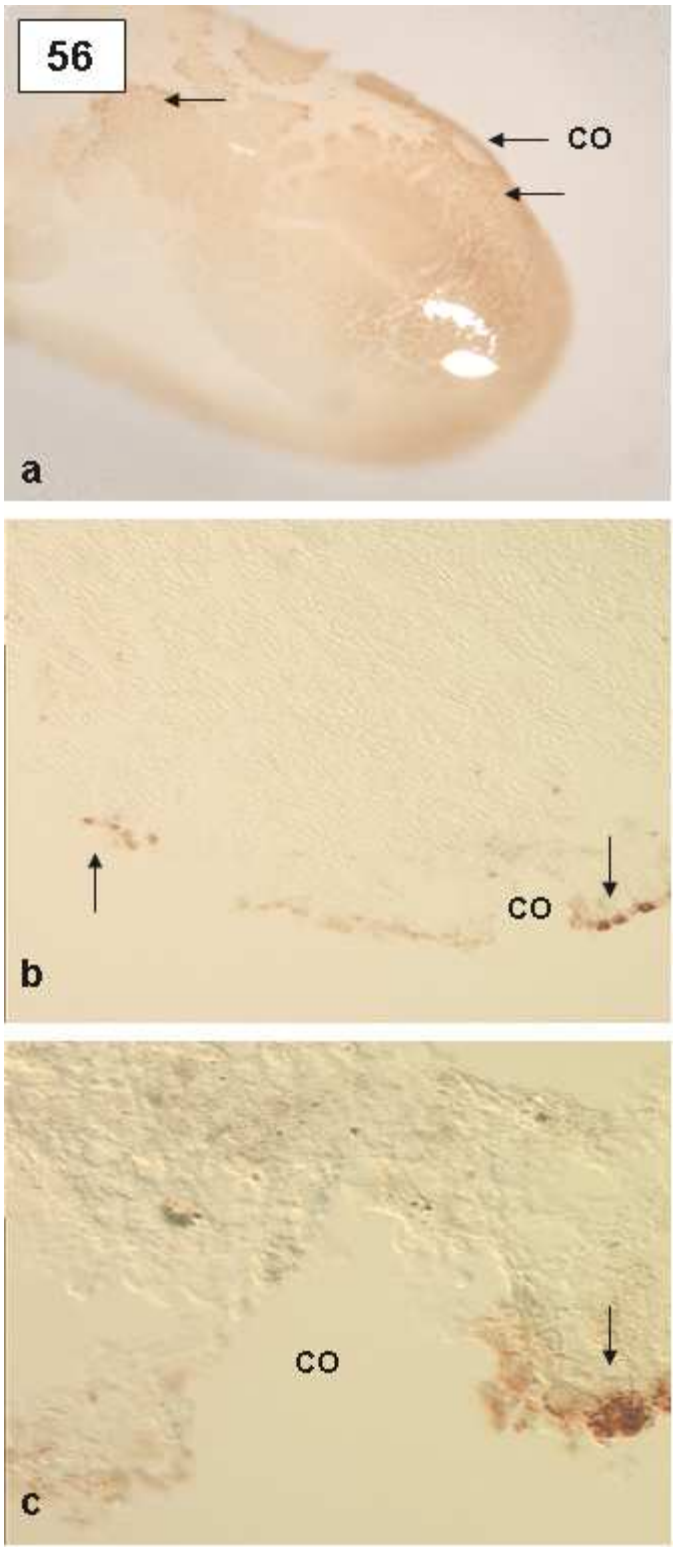
56
co
a
co
b
co
c

Figure 57. Representative photomicrographs of a sagittal section of the posterior region of a stage 26 *Xenopus laevis* embryo, labelled for apoptosis, using the TUNEL method. No specific labelling is visible in the region around the cloacal opening (CO). a) 100X. b) 400X.

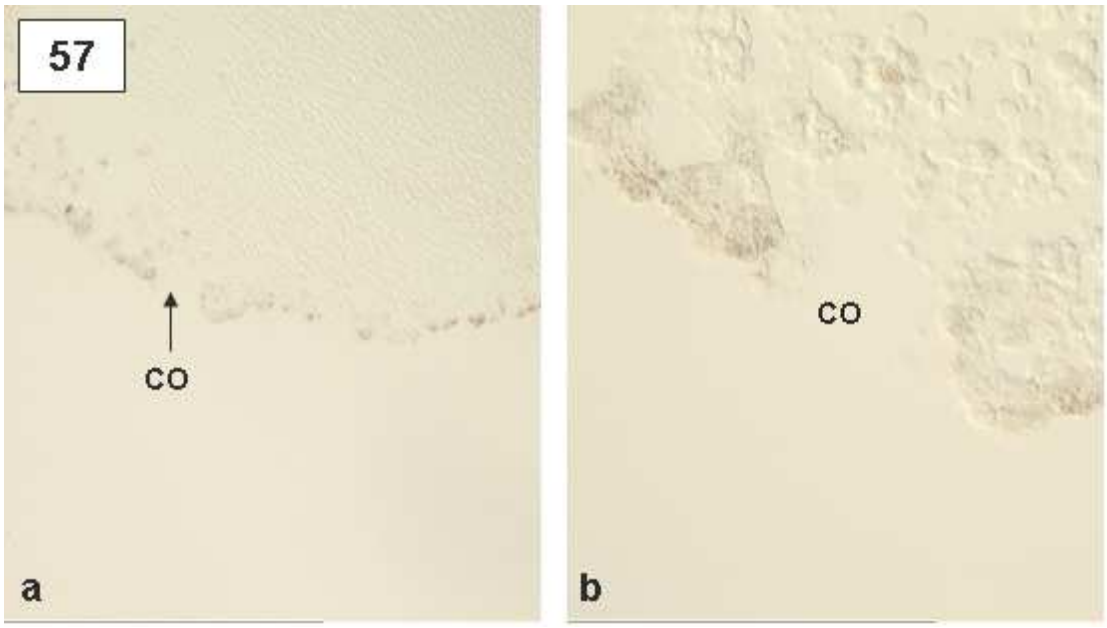
57
co
a
co
b

Figure 58. Representative photomicrographs of mouse colon localized for the pro-apoptotic protein Bax. a) A positive control illustrating Bax-positive cells, which appear brown as they were visualized with DAB. No immunolocalization of Bax is visible in the negative control sections in which the primary antibody was replaced with diluent (b); in which the secondary antibody was replaced with buffer (c) and in which the primary antibody was replaced with goat serum (d). 400X. Differential interference contrast microscopy.

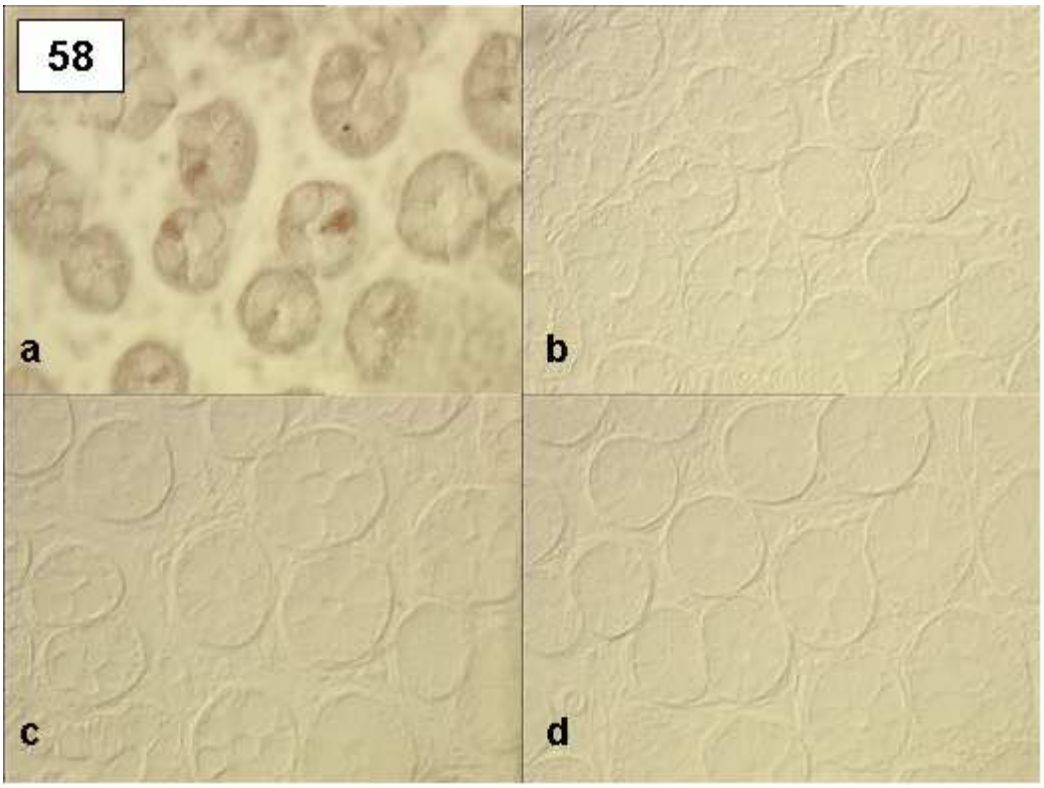
58
a
b
c
d

Figure 59. Representative photomicrographs of mouse colon localized for the anti-apoptotic protein Bcl-2. a) A positive control illustrating Bcl-2-positive cells, which appear brown as they were visualized with DAB. No immunolocalization of Bcl-2 is visible in the negative control sections in which the primary antibody was replaced with diluent (b); in which the secondary antibody was replaced with buffer (c) and in which the primary antibody was replaced with goat serum. Some background staining is present. 400X. Differential interference contrast microscopy.

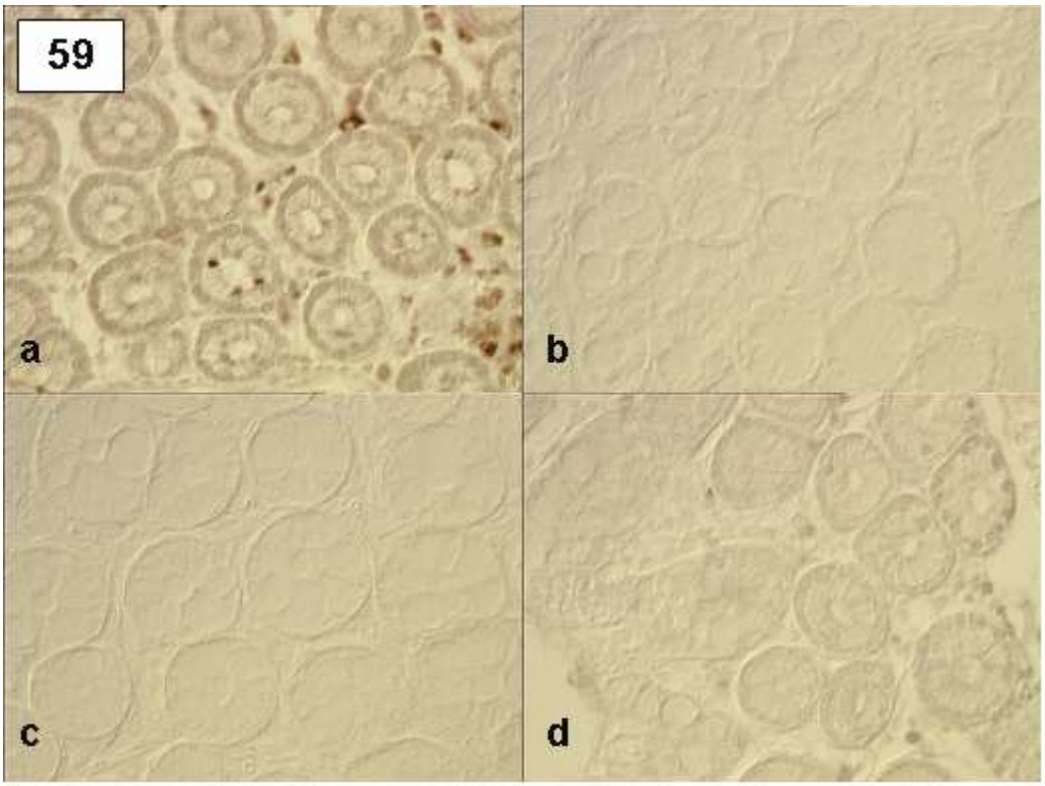
59
a
b
c
d

Figure 60. Photomicrographs of sagittal serial sections of the posterior region of a *Xenopus laevis* embryo at stage 21 localized for the Bax and Bcl-2 proteins. Bax-positive and Bcl-2-positive cells appear brown as they were visualized with DAB. a) Bax-positive cells (black arrows) are visible in the outer ectodermal layer of the embryo with a few cells specific for Bax localized to the proctodeal region (PR). 100X. b) 400X. c) 630X. d) Bcl-2-positive cells (black arrows) are found concentrated in the ectoderm of the proctodeal region (PR). 100X. e) 400X. f) A negative control whereby the primary antibody, anti-Bax was replaced with diluent, showing no specific labelling. 100X. g) 400X. Differential interference contrast microscopy. (HG-Hindgut)

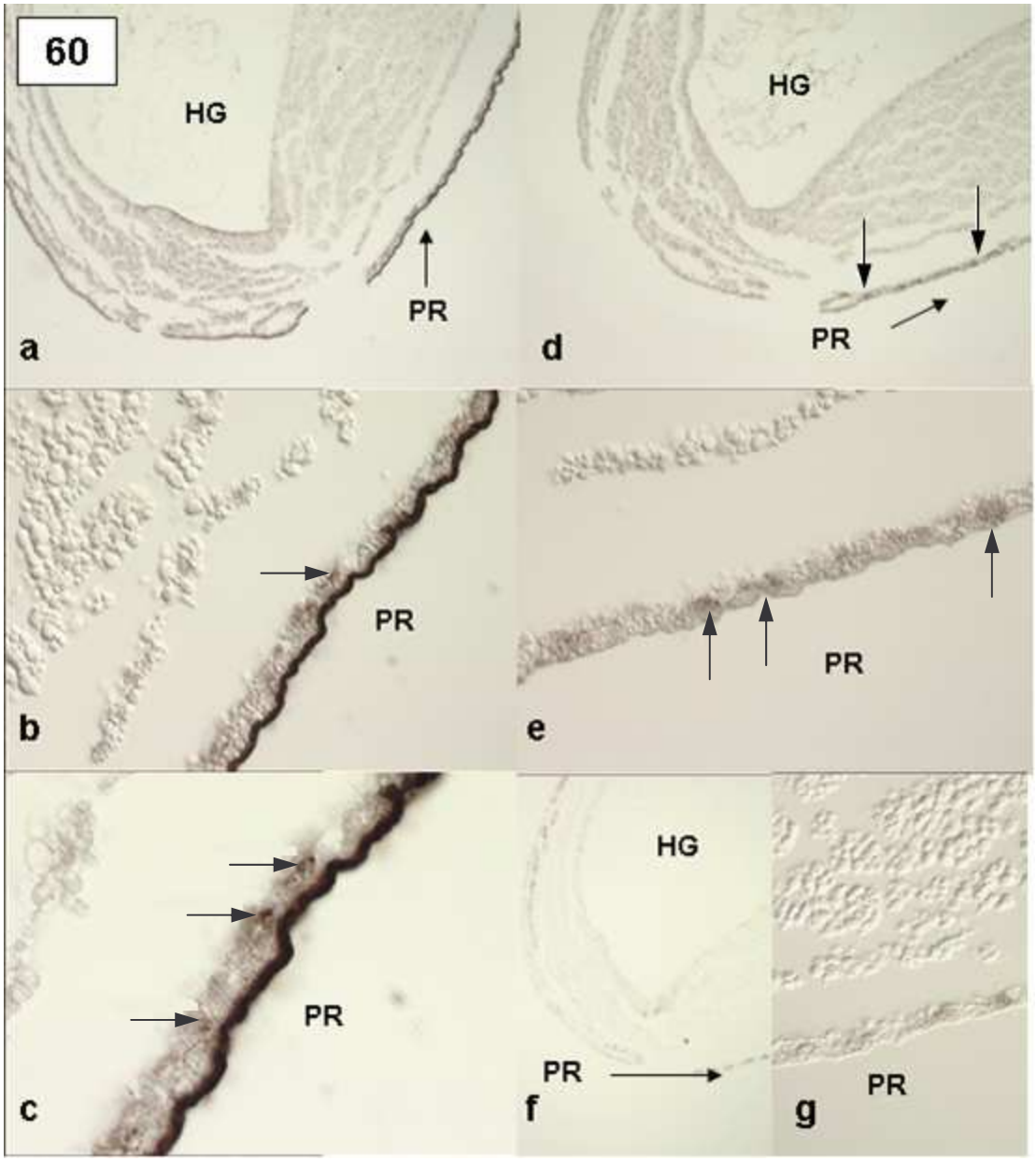
60
HG
PR
a
HG
PR
d
PR
b
PR
e
PR
c
HG
PR
f
PR
g

Figure 61. Photomicrographs of sagittal serial sections of the posterior region of a *Xenopus laevis* embryo at stage 22 localized for the Bax and Bcl-2 proteins. Bax-positive and Bcl-2-positive cells appear brown as they were visualized with DAB. a) A few brown labelled cells are visible in the outer ectoderm but no specific labelling for Bax can be seen in the proctodeal region. 100X. b) 400X. c) A few brown labelled cells are visible in the outer ectoderm but there is no specific labelling for Bcl-2 in the proctodeal region. 100X. d) 400X. e) A negative control, whereby anti-Bcl-2 was replaced with diluent, showing no specific labelling. 100X. f) 400X. Differential interference contrast microscopy. (HG-Hindgut; P-Proctodeum).

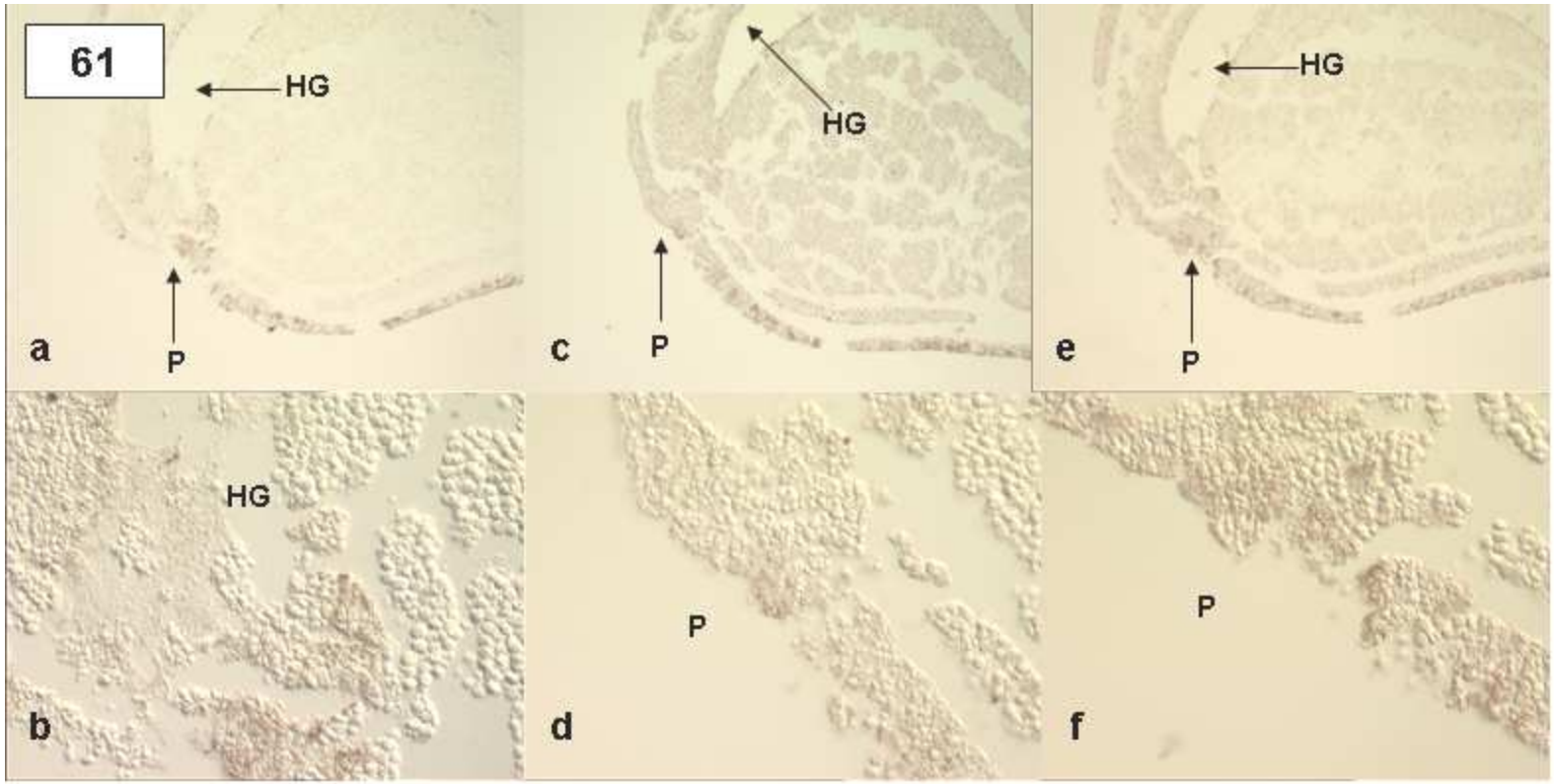
61
HG
P
a
HG
P
c
HG
P
e
HG
b
P
d
P
f

Figure 62. Photomicrographs of sagittal serial sections of the posterior region of a *Xenopus laevis* embryo at stage 23 localized for Bax and Bcl-2, which appear brown as they were visualized with DAB. a) Although the tissue is torn, Bax-positive cells (black arrows) are found intensely localized to the outer ectodermal layer with a few brown labelled cells in the hindgut (HG) endoderm and in the region of the proctodeum (P). 100X. b) 400X. c) Bcl-2-positive cells (black arrows) are found dispersed throughout the outer ectoderm of the embryo and are visible in the endoderm of the hindgut (HG) of the embryo. 100X. d) 400X. e) A negative control, whereby the anti-Bax was replaced with diluent, showing no specific labelling. 100X. f) 400X. Differential interference contrast microscopy. (HG-Hindgut).

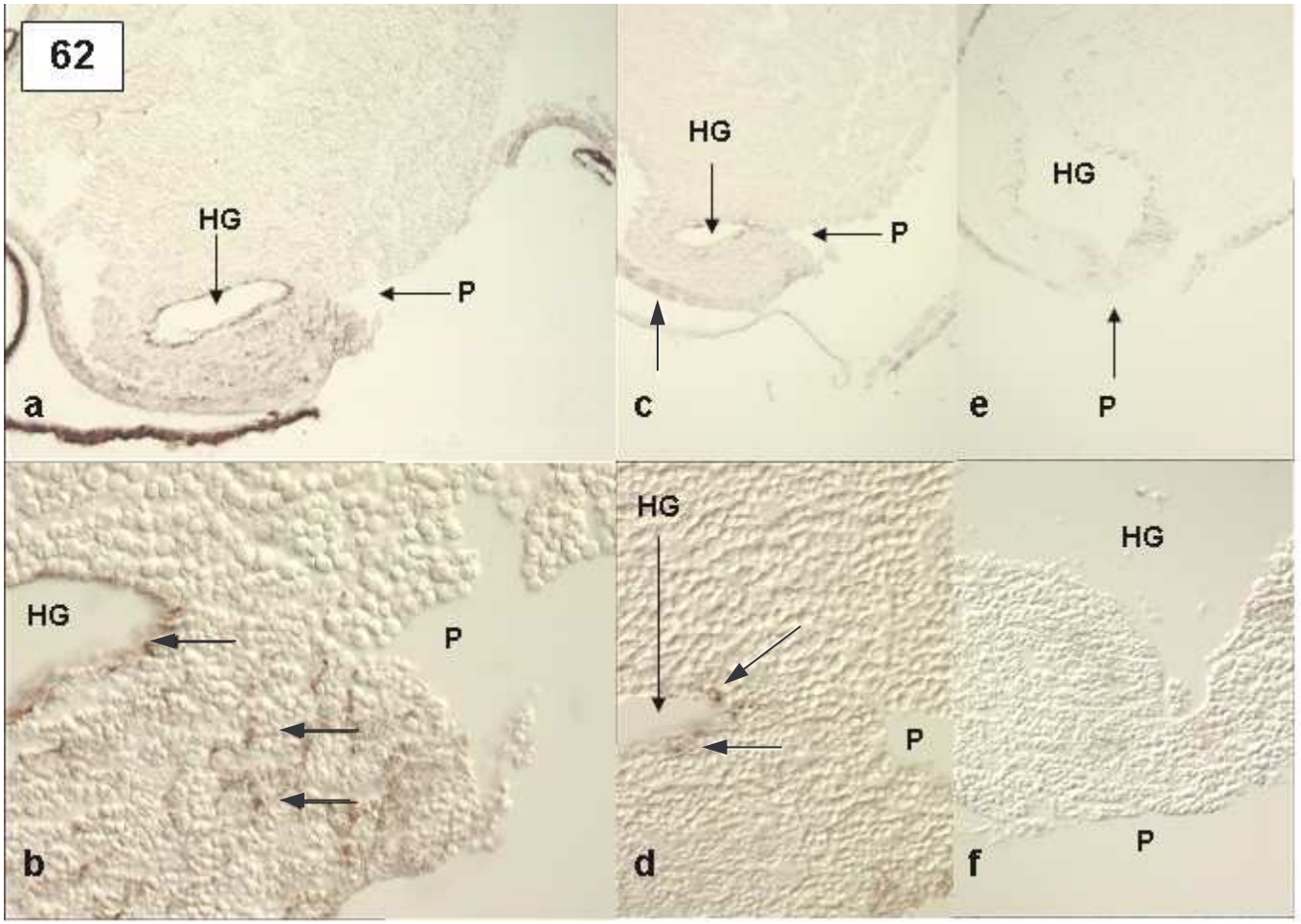
62
HG
P
a
HG
P
c
HG
P
e
HG
P
b
HG
P
d
HG
P
f

Figure 63. Photomicrographs of sagittal serial sections of the posterior region of a *Xenopus laevis* embryo at stage 24 localized for Bax and Bcl-2, which appear brown, as they were visualized with DAB. The embryo was not well sectioned and what appears to be the cloacal opening may in fact be a tear. a) Bax-positive cells (black arrows) are seen in the outer ectoderm of the embryo, including that of the cloacal region. 100X. b) 400X. c) A cell that is Bcl-2-positive (black arrow) is visualized as brown in the ectoderm in the cloacal region. 400X. Differential interference contrast microscopy. (CO-Cloacal Opening).

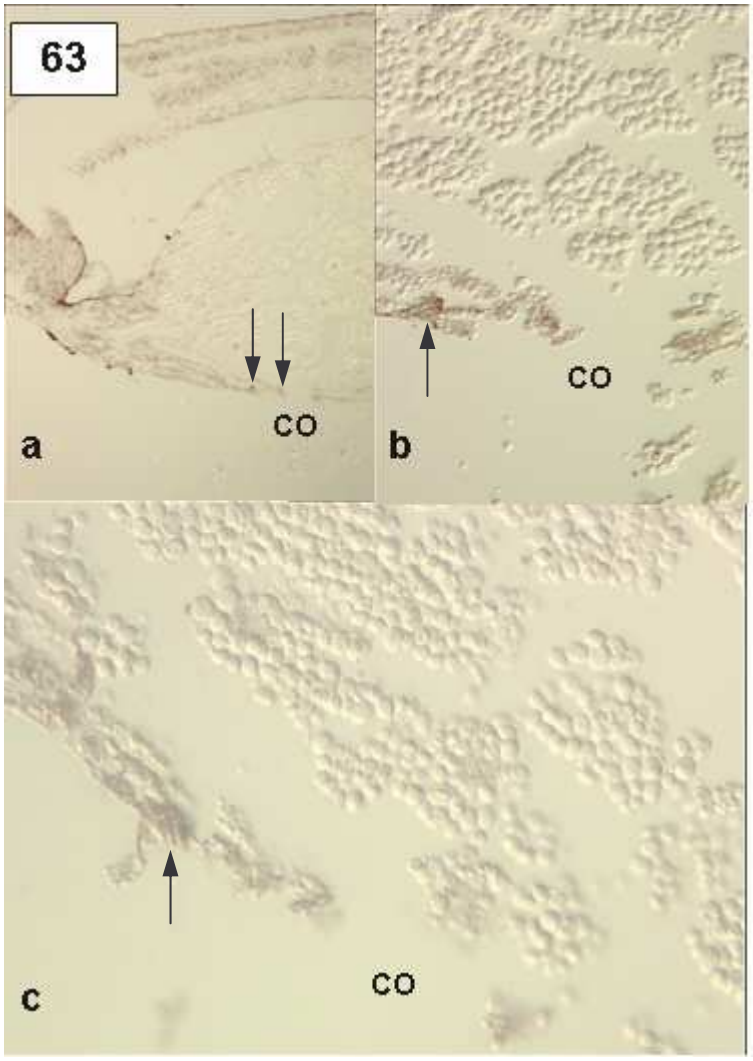
63
a
co
b
co
c
co

Figure 64. Photomicrographs of sagittal serial sections of the posterior region of a *Xenopus laevis* embryo at stage 25 localized for Bax and Bcl-2, which were visualized as brown with DAB. a) No Bax-positive cells are visible around the cloacal opening (CO). 400X. b) Although the cloacal opening is not visible in this section a small number of Bcl-2-positive cells (black arrow) are visible in the cloacal region (CR) region. 400X. c) A negative control, whereby anti-Bax was replaced with diluent, illustrating no specific labelling around the cloacal opening (CO). 400X. Differential interference contrast microscopy. (HG-Hindgut).

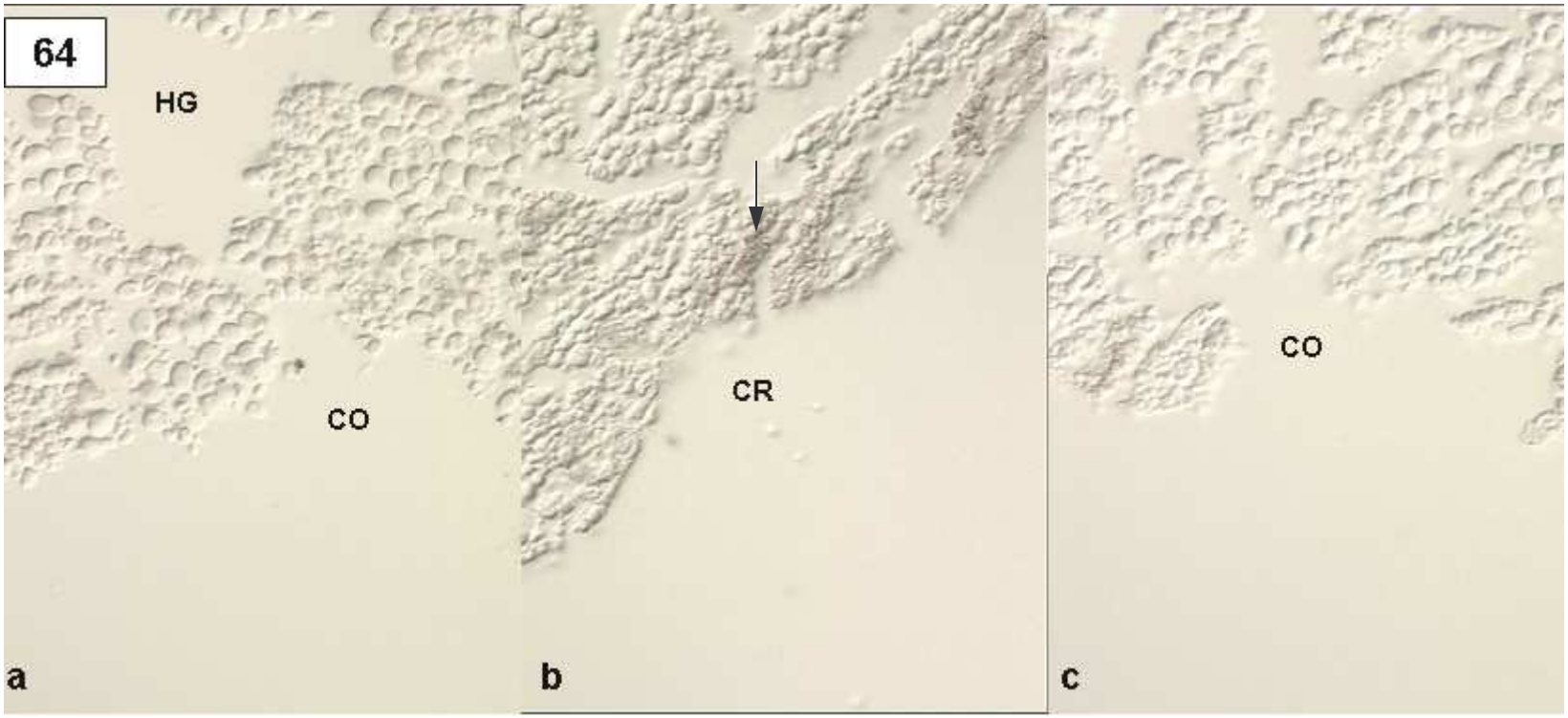
64
HG
CO
CR
CO
a
b
c

Figure 65. Photomicrographs of sagittal serial sections of the posterior region of a *Xenopus laevis* embryo at stage 26 localized for Bax and Bcl-2. a) No Bax-positive cells are visible around the cloacal opening (CO). 400X. b) This section does not show the cloacal opening but no Bcl-2-positive cells are visible in the cloacal region (CR). 400X. c) A negative control whereby anti-Bax was replaced with diluent, illustrating no specific labelling around the cloacal opening (CO). 400X. Differential interference contrast microscopy.

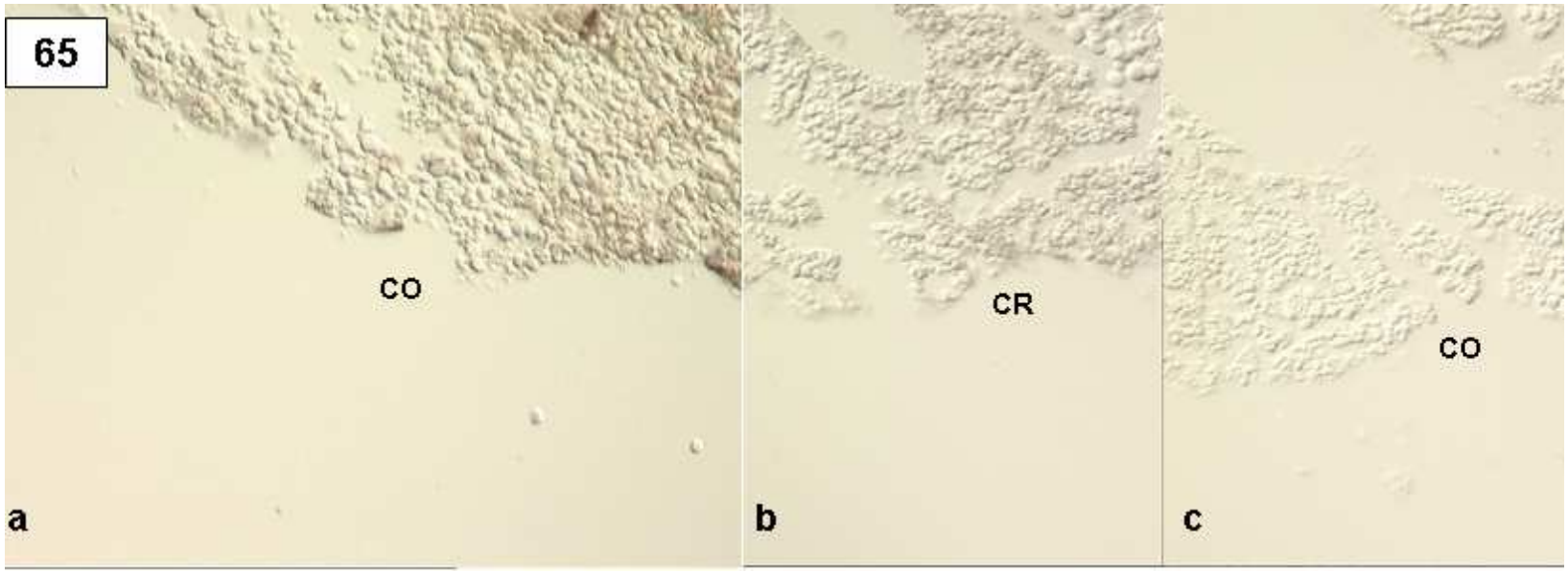
65
CO
CR
CO
a
b
c

Figure 66. DNA analysis by 1% agarose gel electrophoresis of the linearized *XCG-1* and *BMP-4* plasmids for probe preparation for *in situ* hybridization. The DNA ladder is shown in lane 1 and the linearized DNA of the plasmids in lanes 2-5. Lane 2-*XCG-1* antisense, lane 3-*XCG-1* sense, lane 4-*BMP4* antisense and lane 5-*BMP-4* sense.

Figure 67. DNA analysis by 1 % agarose gel electrophoresis of the linearized *XCG-1* plasmid for probe preparation for *in situ* hybridization. The DNA ladder is shown in lane 1, *XCG-1* antisense in lane 3 and *XCG-1* sense in lane 5.

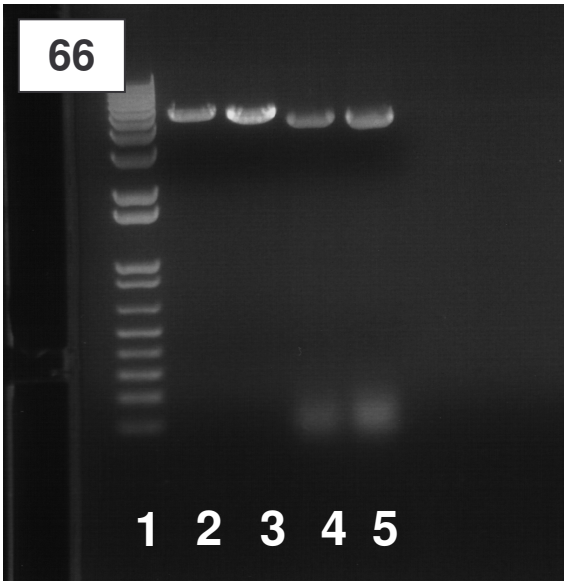
66
1 2 3 4 5

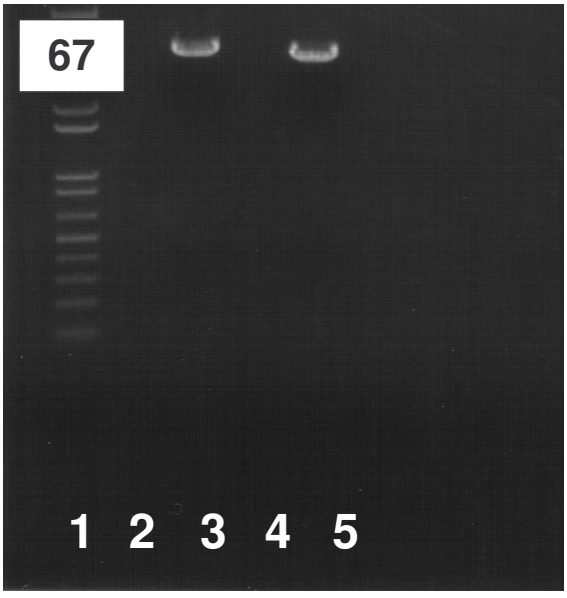
67
1 2 3 4 5

Figure 68. RNA analysis by 1% formaldehyde-agarose electrophoresis of the RNA probes transcribed from the linearized DNA. The RNA ladder is shown in lane 1 and the RNA probes in lanes 5-8. Lane 5-*XCG-1* antisense, lane 6-*XCG-1* sense, lane 7-*BMP-4* antisense and lane 8-*BMP-4* sense. (Lanes 3 and 4 illustrate unrelated RNA probes). It appears that the RNA degraded in the *XCG-1* antisense probe.

Figure 69. RNA analysis by 1% formaldehyde-agarose electrophoresis of the RNA probes transcribed from the linearized DNA. The RNA ladder is shown in lane 1. Lane 3-*BMP-4* antisense, lane 5-*XCG-1* antisense and lane 7-*XCG-1* sense. Although a double band is visible in lane 5 the one band is still in the correct place.

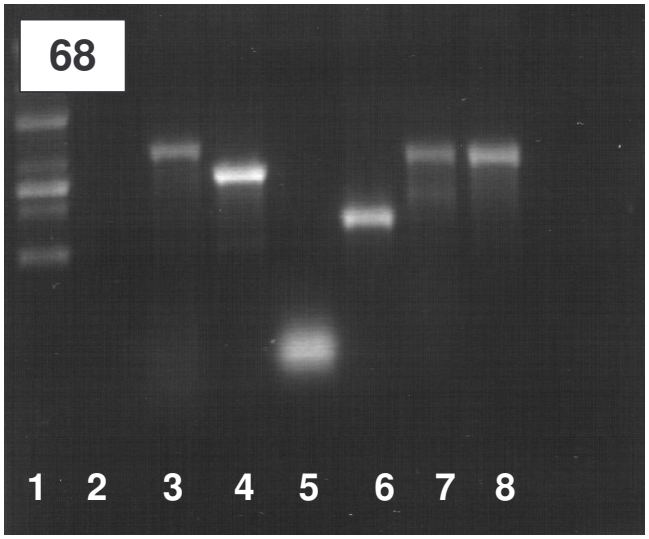
68
1 2 3 4 5 6 7 8

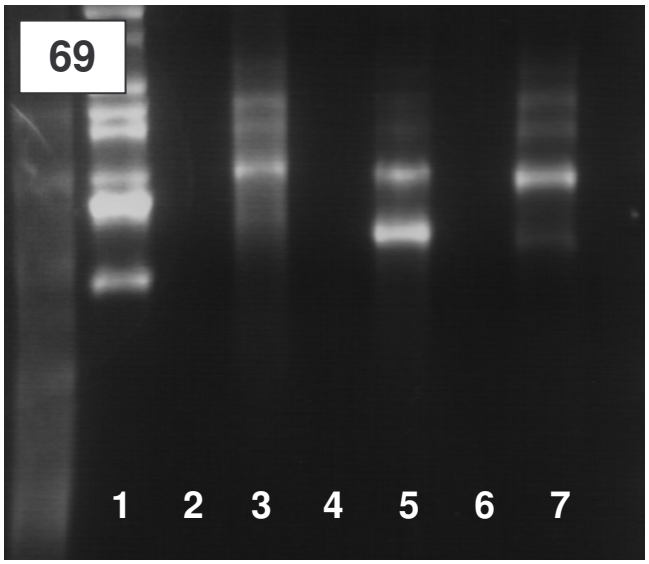
69
1 2 3 4 5 6 7

Figure 70. Representative lateral views of whole stage 26 *Xenopus laevis* embryos using *XCG-1* as a control probe for *in situ* hybridization. The staining reaction was visualized as blue/purple. *XCG-1* expression is specific to the cement gland. This control ensures the efficacy of the *in situ* hybridization technique. a) *XCG-1* expression (using the *XCG-1* antisense probe) is confined to the cement gland in the anterior region of the embryo. 40X. b) The *XCG-1* sense probe (the same sense as the mRNA) was used as another control, showing no staining for *XCG-1* gene expression. 40X. Stereomicroscopy. (A-Anterior; P-Posterior).


70
P
A
a

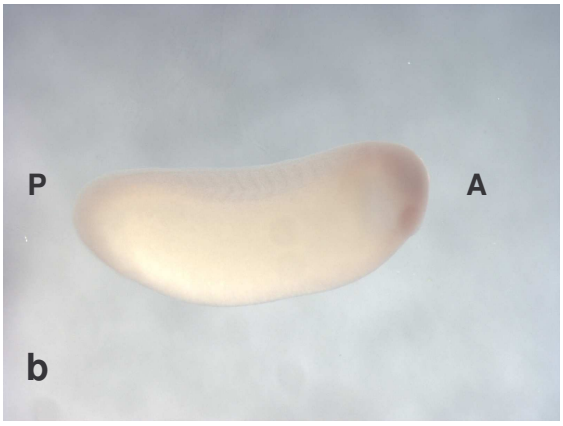
P
A
b

Figure 71. Representative ventral views of whole stage 14 *Xenopus laevis* embryos using the *BMP-4* probe for *in situ* hybridization. The staining reaction was visualized as blue/purple. These embryos were used as controls, as this gene is expressed both anteriorly and posteriorly in the early embryo. a) *BMP-4* expression (using the BMP-4 antisense probe) is localized to the anterior and posterior regions of the embryo. 40X. b) *In situ* hybridization performed using the *BMP-4* sense probe, as a control. 40X. Stereomicroscopy. (A-Anterior; P-Posterior).

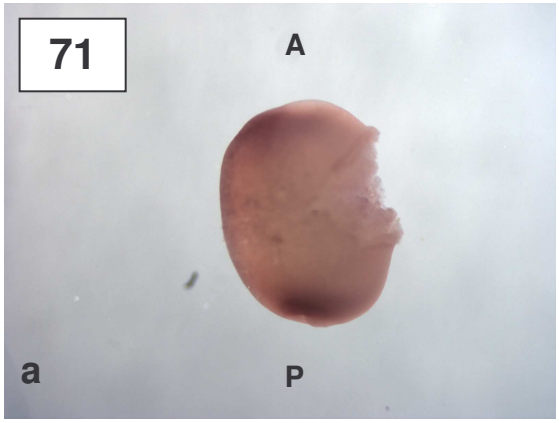
71
A
a
P

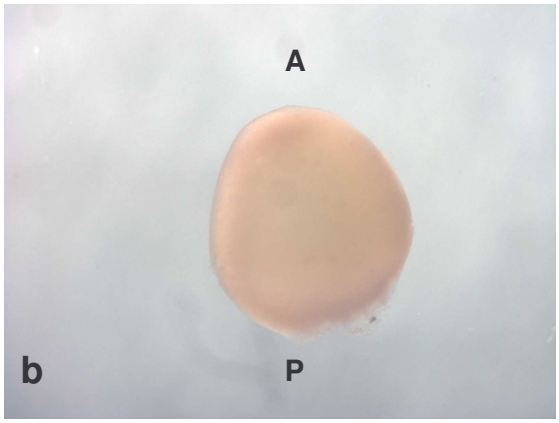
A
b
P

Figure 72. Representative images of whole *Xenopus laevis* embryos at stage 22 on which *in situ* hybridization was performed, using *BMP-4* sense and antisense probes. The staining reaction was visualized as blue/purple. a) A ventral view of *BMP-4* expression, showing strong gene expression localized to the anterior region and the proctodeum (black arrow) of the embryo. 40X. b) A lateral view of *BMP-4* expression, showing gene expression in the anterior region and proctodeal region (black arrow) of the embryo. 40X. c) A lateral view of an embryo using the *BMP-4* sense probe, as a control, showing no staining reaction. 40X. Stereomicroscopy. (A-Anterior; P-Posterior).

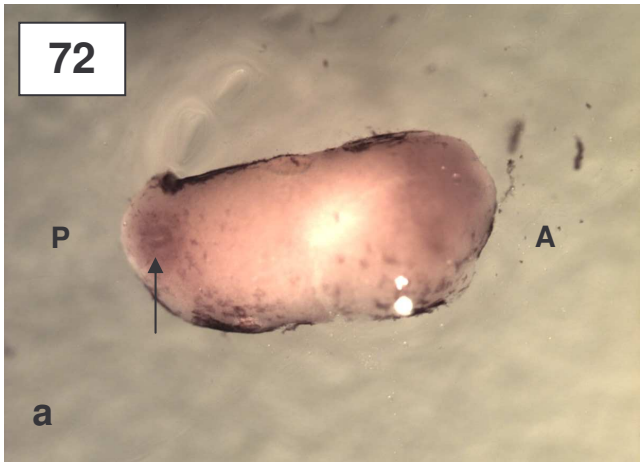
72
P
A
a

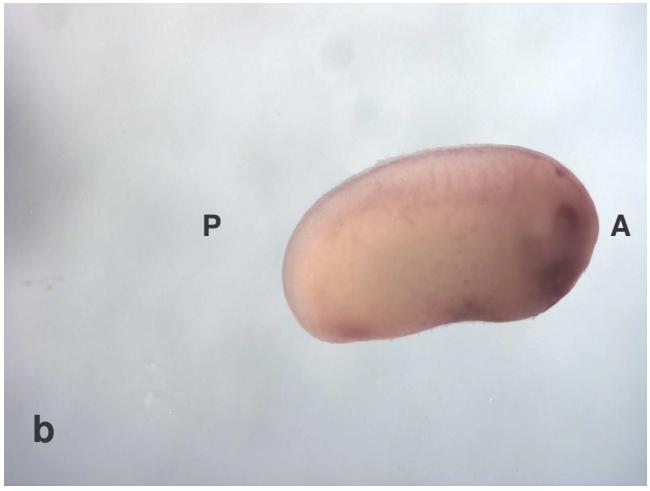
P
A
b

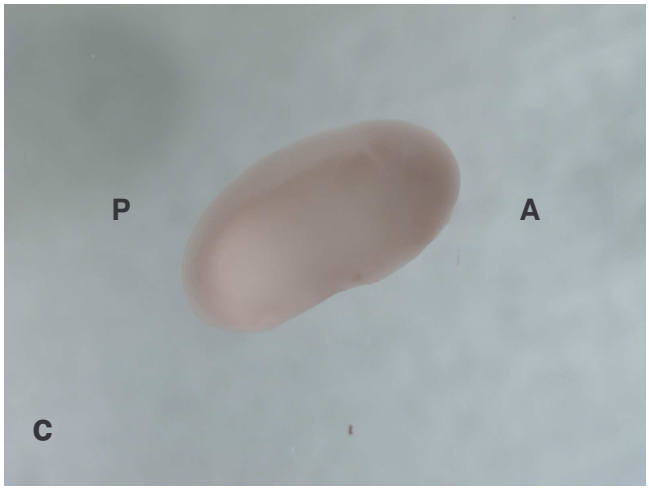
P
A
c

Figure 73. Representative images of whole *Xenopus laevis* embryos at stage 24 on which *in situ* hybridization has been performed, using *BMP-4* sense and antisense probes. The staining reaction was visualized as blue/purple. a) A ventral view of *BMP-4* expression, showing gene expression in the anterior region and cloacal region (black arrow) of the embryo, although it appears to have decreased in intensity compared to the stage 22 embryo. 40X. b) A lateral view of *BMP-4* expression, showing gene expression in the anterior region and cloacal region (black arrow) of the embryo. 40X. c) A lateral view of an embryo, using the *BMP-4* sense probe, as a control. No staining is apparent. 40X. Stereomicroscopy. (A-Anterior; P-Posterior).

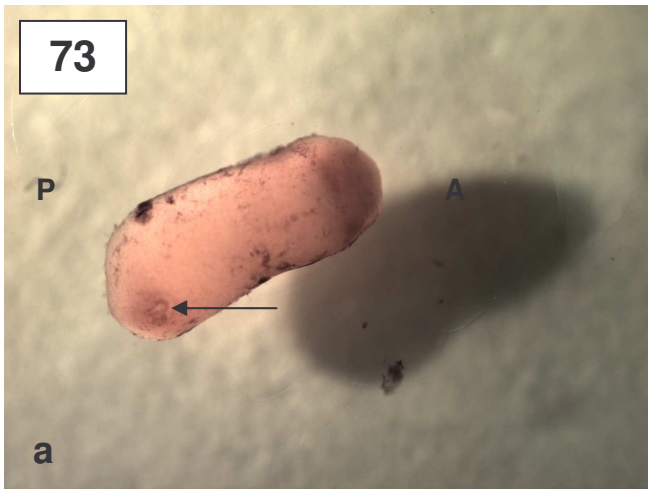
73
P
A
a

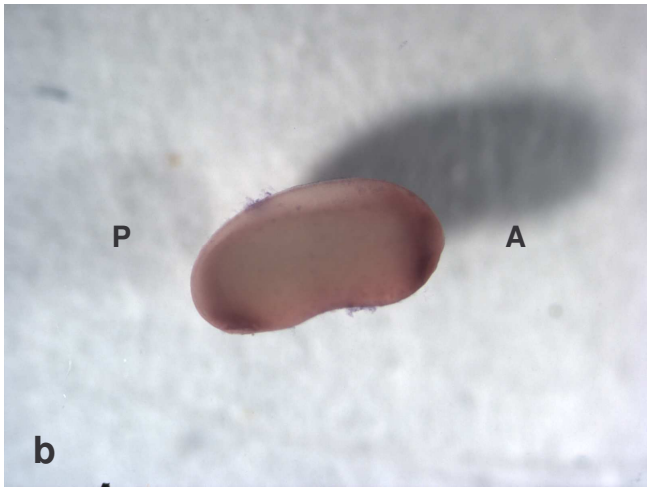
P
A
b

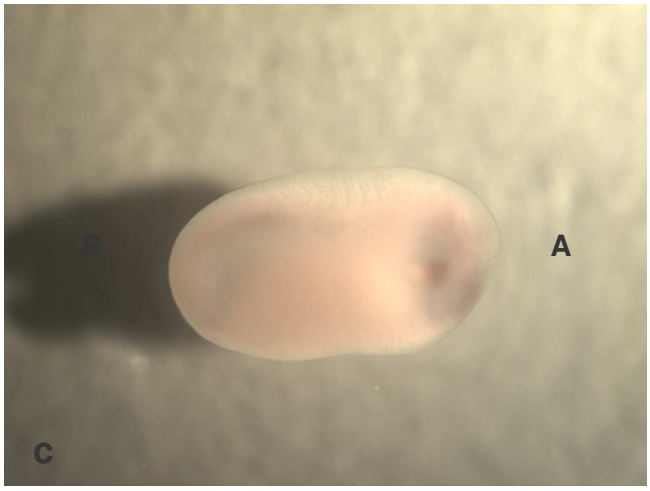
P
A
c

Figure 74. Representative images of whole *Xenopus laevis* embryos at stage 26 on which *in situ* hybridization has been performed, using *BMP-4* sense and antisense probes. The staining reaction was visualized as blue/purple. a) A ventral view of *BMP-4* expression, showing that the gene expression is still apparent in the anterior region but is markedly reduced and almost nonexistent in the cloacal region (black arrow). 40X. b) A lateral view, illustrating no *BMP-4* expression in the cloacal region. 40X. c) A lateral view of an embryo, using the *BMP-4* sense probe, as a control, showing no staining reaction. 40X. Stereomicroscopy. (A-Anterior; P-Posterior).

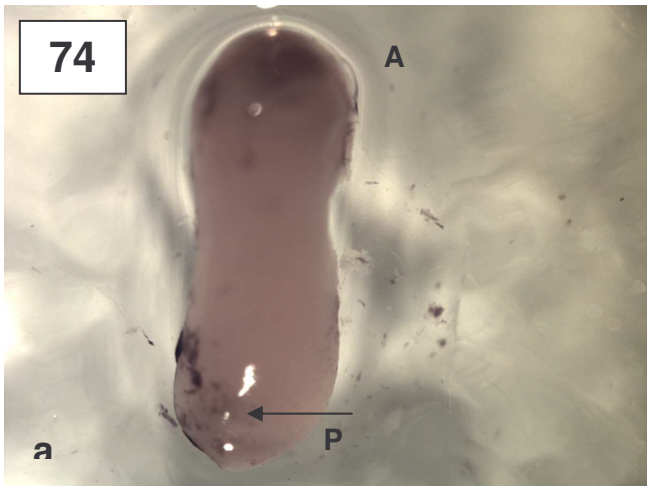
74
A
a
P

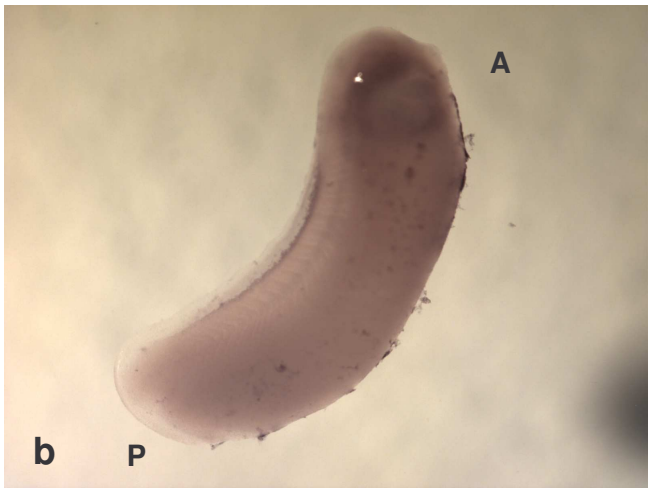
A
b
P

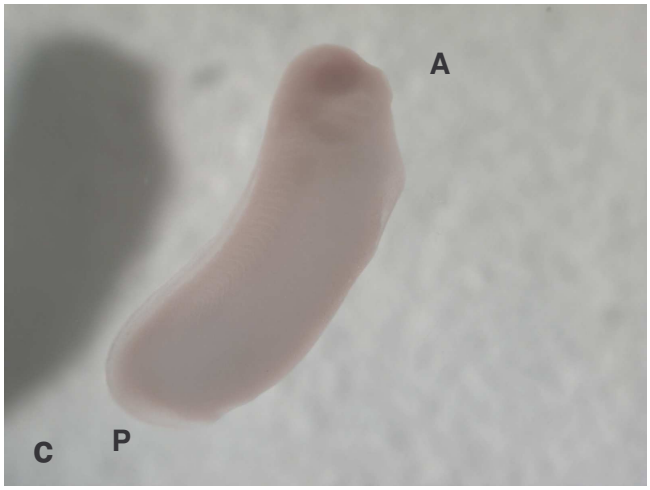
A
c
P

# 4

# DISCUSSION

This study incorporated the use of a variety of techniques enabling a greater understanding of some morphological, immunohistochemical and genetic aspects of development of the proctodeal region in *Xenopus laevis*.

## 4.1 MORPHOLOGY

Static images of *Xenopus laevis* embryos were captured using the confocal, scanning electron and light microscopes. However, there was difficulty in producing a continuous series of images following the development of the proctodeal region over a specific time period, as the embryos were very dense in appearance and the proctodeal region was not easily defined when viewed under the inverted phase contrast light microscope or confocal microscope. This problem of opacity has been an obstacle in investigations in the past and has been attributed to the huge volume of intracellular yolk platelets. These yolk platelets are filled with phospho-lipo-glycoproteins (Fagotto and Maxfield, 1994) and most prevalent during the initial stages of *Xenopus laevis* development, as they are thought to degrade in the later stages of development (Fagotto and Maxfield, 1994). These have an effect on light scattering, therefore making optical microscopy analysis more challenging (Papan *et al.* 2007).

Although continuous development of the proctodeal region was not visualized, images captured at time points during development showed the formation and development of the proctodeum. The initial proctodeal depression developed at stage 21, in the posterior-ventral region of the embryo, ventral to the blastopore. This has been illustrated in numerous experiments involving cell labelling, such as that by Tahara and Nakamura (1961), who found that the proctodeum and blastopore are

located side by side for a short period of time, after which the blastopore is covered with epidermis to form the neurenteric canal. In the current study the initial proctodeal depression was such a slight indentation that it was difficult to distinguish it in confocal images and in scanning electron micrographs at stage 21 of development. Histological sectioning however, provided a clearer image of this depression, which was apparent, at stage 21, earlier on in development than the stomodeum, which only becomes apparent at the late tailbud stage (approximately stage 32) (Watanabe *et al.*, 1984; Dickinson and Sive, 2006). This is in contrast to humans where the stomodeum develops before the proctodeum (Balinsky, 1965; Moore, 1988; Allan and Kramer, 2002). The proctodeal depression became more pronounced as development continued and although no measurement was made, the images, when compared to those available of stomodeal development, revealed that the proctodeum was smaller than the stomodeum in *Xenopus laevis*. The stomodeal depression in *Xenopus* was in turn found to be shallower (Watanabe *et al.*, 1984; Dickinson and Sive, 2006) than the stomodeal depression seen in urodela (Takahama *et al.*, 1988). The change in shape of the proctodeum, from a slit-like depression to one with a more oval appearance as seen in the present study, was characteristic of stomodeal development as well (Dickinson and Sive, 2006). The development of the proctodeum of *Xenopus laevis* embryos was also accompanied by the elongation of the whole embryo (Gont *et al.*, 1993), which is attributed to extensive endodermal cell movements and not to the development of the surrounding mesoderm (Horb and Slack, 2001).

The cloacal membrane thinned as development progressed in *Xenopus laevis* embryos in the current study, in a similar fashion to that of rats and humans (Penington and Hutson, 2002) and of the stomodeum of *Xenopus laevis* (Dickinson and Sive, 2006). The thinning of the ectodermal and endodermal layers in the stomodeal region of anurans which has been found to occur, leads to the formation of a buccopharyngeal membrane which is one to two cell layers thick (Watanabe *et al.*, 1984; Dickinson and Sive, 2006). However, in the present study, histological analysis of the

proctodeal region of *Xenopus laevis* did not show the cloacal membrane as thin as one or two cell layers thick. This may have been due to the plane of sectioning. In a stage 23 embryo however, a thin cellular layer was seen lying across the cloacal opening. This cellular layer may have constituted cells of the cloacal membrane which will undergo apoptosis or migrate to form the lining of the cloacal opening, therefore forming a channel between the hindgut and the exterior. Interestingly, the opposite was found to be true in the buccopharyngeal membrane of urodela where the membrane did not thin but thickened as development continued (Takahama *et al.*, 1988). During the thinning of the buccopharyngeal membrane in *Xenopus laevis*, the cells of the ectoderm and endoderm were found to intercalate (Dickinson and Sive, 2006). It was difficult to determine in the present study if ectodermal and endodermal cell layer intercalation was the case in the proctodeal region of *Xenopus laevis*, as even though the ectodermal and endodermal cell layers were quite distinct, they were also quite thick. There was difficulty in producing sections where direct apposition of the proctodeal ectoderm and hindgut endoderm was clearly evident, as was seen in the stomodeal region (Dickinson and Sive, 2006). This may have been due to the thickness or plane of sectioning. The ectodermal and endodermal cell layers became less distinct in the proctodeal region of *Xenopus laevis* in the current study as these layers thinned. This was also observed in the stomodeal region by Dickinson and Sive (2006). The mesoderm and endoderm were not always distinguishable from each other in the proctodeal region as seen by Florian (1933). Due to the plane of sectioning, mesoderm may have been seen "incorporated" into some histological sections creating the illusion of a thicker proctodeal region. Labelling of these cell layers individually, with dyes such as DiO or DiI (Dickinson and Sive, 2006) would make the distinction more apparent and allow for a more accurate analysis. These layers could also be identified using specific gene expression. For example, in a future study, the epidermis could be marked by the expression of *cytokeratin xk81* and the endoderm by the expression of *endodermin* (Zhang *et al.*, 1998; Dickinson and Sive, 2006).

The perforation of the cloacal membrane of *Xenopus laevis* embryos at stage 24, seen in histological and confocal images as well as scanning electron micrographs, is thought to be an important feature in the formation of the hindgut, as it creates a free channel linking the hindgut and the exterior. The importance of the perforation of a membrane has been demonstrated in the development of the "primary mouth" region in *Xenopus laevis* (Watanabe *et al.*, 1984; Dickinson and Sive, 2006), the hamster (Waterman, 1977) and the urodela (Takahama *et al.*, 1988). This perforation is imperative for normal development.

One embryo in the current study, at stage 24 of development, showed a variation in the morphological features of the proctodeum when viewed with the scanning electron microscope. The ectodermal cells around the cloacal opening were swollen and the opening had an unusually narrow appearance. This embryo may have been an example of normal variation or of a cloacal malformation.

The ectodermal cell layers in the proctodeal region of *Xenopus laevis* embryos often appeared as an outer layer and an inner layer. In frogs, these layers are known as the outer covering layer or periderm, and the inner sensory layer and constitute the entire epithelium (Balinsky, 1975). Different reactions were often found in these two layers in the present study, with the application of the terminal deoxynucleotidyl transferase mediated dUTP nick end-labelling (TUNEL) and immunohistochemical techniques. The flattened appearance of the outer ectodermal cell layer is possibly due to the keratinization of these cells, known to occur in *Xenopus* (Balinsky, 1975) although the exact stages at which this occurs are not clear in the available literature. These outer cells will eventually slough off. The cuboidal appearance of the inner ectodermal cell layer was similar to that of the ectoderm of the stomodeal region of urodela (Takahama *et al.*, 1988) and anurans (Watanabe *et al.*, 1984). The endodermal cells seen in histological sections in the present study, had a very different appearance to the ectodermal cells, as they were relatively large and round. This was in contrast to the endodermal cells of the stomodeal region in urodela,

which were found to be columnar and attached to each other by desmosomes and interdigitations (Takahama *et al.*, 1988). It was difficult to analyse the change in shape of the cells as the cloacal membrane became thinner, although they appeared to flatten slightly. This is in accordance with the chick buccopharyngeal membrane where the cells elongate and become flatter as the membrane thins (Waterman and Schoenwolf, 1980).

As well as showing characteristic features of proctodeal ectodermal and hindgut endodermal cells, histological analysis revealed the presence of vacuolated cells in the proctodeal ectoderm of *Xenopus laevis*. These cells could be actively involved in secretion, as secretory granules have been found in the foregut endoderm of urodela (Takahama *et al.*, 1988) or they may be apoptotic cells. Similar vacuoles were found at the tip of the urogenital sinus from gestational day 15 to 16 in rats (Qi *et al.*, 2000a) and were classified as apoptotic. A few cells were seen to be protruding into the cloacal opening in embryos at later stages of development. These "blebbing" cells are morphologically characteristic of apoptotic cells, and this can be confirmed with apoptotic detection techniques. In fact in the current studying, using the TUNEL technique and the immunolocalization of the pro-apoptotic protein Bax, possible apoptotic cells were found in this region, but were not necessarily the identical cells, as serial sections were not available for study here.

A specialized characteristic of the surface ectodermal cells of *Xenopus laevis*, seen in histological sections and under the scanning electron microscope in the present study was the presence of cilia. The cilia were found to be evenly dispersed across the ectoderm of the embryos and may be involved in the buoyancy of the *Xenopus laevis* embryos, as they are unable to swim in their early stages of development. The cilia were found to be concentrated on the ectodermal surface in the proctodeal region, especially once the cloacal membrane had perforated, as well as in the stomodeal region (Watanabe *et al.*, 1984). These cilia may act to ensure the removal of foreign particles from the cloacal opening during development. Whilst cilia were not

apparent in the chick, microvilli were prevalent in the cloaca and on the apical surface of the hindgut ectoderm of the hamster (Waterman, 1977; Yokouchi *et al.*, 1995).

The cellular "plugs" were noted in the cloacal opening of *Xenopus laevis* embryos in scanning electron micrographs and histological sections of the embryos once the cloacal membrane had perforated. These cellular "plugs" were distinct in the cloacal opening in the three-dimensional scanning electron micrographs and were thought to be apoptotic debris. Similar material was found in the urogenital sinus during cloacal septation of rats (Qi *et al.*, 2000a). However, due to the plane of sectioning, some of these "plugs" in the histological sections were possibly part of the lateral wall of the embryos. The "plugs" seen in the current study only occurred once the cloacal membrane had perforated and thus may be attributed to apoptosis of the cloacal membrane.

Smaller rod-like structures were also found in the cloacal opening of two embryos and were thought to be bacteria. These bacteria may have developed and been present in the solution in which the embryos were growing. However, as they were only seen in embryos in later stages of development once the cloacal membrane was known to have perforated, they may have been specific for gut development and formed part of the natural internal environment of the embryos. Although a role for bacteria in the cloacal opening of embryos does not appear to have been documented, many bacteria, such as the environmental pathogen *Mycobacterium ulcerans*, play an integral role in the development of organ systems in various embryos (Drancourt *et al.*, 2002).

In order to analyse the stomodeal region of the avian embryo in more detail Waterman and Balian (1980) used transmission electron microscopy. The authors used this technique to analyse the extracellular matrix between the ectoderm and endoderm of the buccopharyngeal membrane. This matrix was found to contain a flocculated material and it was proposed that this matrix may play a role in the

adhesion between the ectoderm and endoderm prior to direct cellular contact between these epithelia (Waterman and Balian, 1980). As many mechanisms and morphological characteristics have been found to be conserved between species, the results of the study by Waterman and Balian (1980) in the chick may bear some relevance to *Xenopus laevis*. Although such a technique was not performed in the current study, the results obtained by Waterman and Balian (1980) may be applicable to the proctodeal region of *Xenopus laevis* as well, as many aspects of stomodeal and proctodeal development have been found to be similar.

## 4.2 THE BASEMENT MEMBRANE BETWEEN THE PROCTODEAL ECTODERM AND HINDGUT ENDODERM

From investigations of the proctodeal and stomodeal regions in various embryos, it is known that the ectodermal and endodermal cell layers are directly juxtaposed (Balinsky, 1965). A basement membrane is present between the stomodeal ectoderm and foregut endoderm of *Xenopus laevis* (Dickinson and Sive, 2006) and is thought to play a role in stomodeal development and buccopharyngeal membrane dissolution. A similar concept may be applicable to the proctodeal region of *Xenopus laevis*. The basement membrane may be involved in initiating thinning of the ectodermal and endodermal cell layers composing the buccopharyngeal and cloacal membranes. These cell layers may also have a reciprocal relationship with the basement membrane as the thinning of the ectoderm and endoderm may give rise to changes in the basement membrane, which may lead to further development of the "primary mouth" and cloacal opening.

In order to investigate the role of the basement membrane in the proctodeal region in *Xenopus laevis*, the basement membrane markers fibronectin and laminin were immunolocalized. In this study discontinuous immunolocalization was sometimes observed in the region between the proctodeal ectoderm and the hindgut endoderm and is thought to be indicative of a basement membrane. High background staining

was present, especially in the sections where fibronectin was immunolocalized. This non-specific labelling may have contributed to the difficulty in detection of specific labelling of fibronectin and laminin and thus the basement membrane. The high background staining may have been due to the pigment which is highly concentrated in the ectoderm of the *Xenopus laevis* embryos and may have interfered with the reaction. Thus, for future studies the embryos should be bleached for immunohistochemistry as was carried out for the TUNEL technique to ensure that no false staining occurs and to decrease the background staining (Koga *et al.*, 2007). However, it is important to make certain that the bleaching does not interfere with the immunohistochemical reaction itself.

The discontinuous immunolocalization of fibronectin and laminin observed between the proctodeal ectoderm and hindgut endoderm in sections of stage 21 and 22 *Xenopus laevis* embryos, may indicate a disintegrating basement membrane. This was difficult to confirm with the histological study. A basement membrane in this region is, however, a feature common to the stomodeal region in avians (Waterman, 1985) and mammals (Takahama *et al.*, 1988) such as the hamster (Waterman, 1977) and thus is expected to occur in the proctodeal region of *Xenopus laevis*. Dickinson and Sive (2006) confirmed this finding and indicated the presence of a basement membrane between the stomodeal ectoderm and hindgut endoderm in *Xenopus laevis* using immunohistochemical techniques. However earlier morphological studies incorporating the use of transmission electron microscopy, found no basement membrane present in the stomodeal region in *Rana* frogs, when thinning of the ectodermal and endodermal cell layers occurred between the neural and hatching stages (Watanabe *et al*., 1984). This is interesting to note as the importance of the presence of a basement membrane has been shown by Murray and Edgar (2000), with the use of embryoid bodies derived from mouse embryonic stem cells. The laminin genes of these cells had been altered to prevent basement membrane deposition. No epiblast epithelium or archenteron was formed when laminin and therefore, basement membrane, deposition was absent. However, the addition of exogenous laminin

rescued basement membrane deposition and epiblast epithelium and a cavity developed (Murray and Edgar, 2000). As the loss of laminin function also leads to the death of embryos *in vivo*, laminin and therefore possibly the basement membrane can be said to be considered a survival signal as well as a death signal (Murray and Edgar, 2000). This study emphasizes the importance of laminin as a basement membrane protein, apparent from the present study where laminin was found to be a component of the basement membrane between the proctodeal ectoderm and hindgut endoderm in *Xenopus laevis*. As laminin immunolocalization was discontinuous and then absent in the stages prior to cloacal membrane perforation it is suggested that the basement membrane plays a role in cloacal membrane dissolution.

It was thought that the interrupted dark brown immunolocalization seen in this study between the proctodeal ectoderm and the hindgut endoderm was specific immunolocalization, based on the absence of this immunolocalization in negative immunohistochemical control sections. Therefore this indicates that the basement membrane was discontinuous at stages 21 and 22 of development in *Xenopus laevis*. Although the literature is not clear as to basement membrane immunolocalization at specific stages, the results from the current study indicate that the basement membrane may appear as a distinct, continuous entity in earlier stages of development than stage 21. This was the earliest stage of *Xenopus laevis* development analysed in the current study. Earlier stages of embryos should thus be analysed to test this hypothesis. As immunolocalization of the basement membrane markers, fibronectin and laminin, was discontinuous when the proctodeum developed and thinned, the basement membrane is thought to play a role in proctodeum formation and have an indirect role in cloacal membrane dissolution.

No evidence of fibronectin or laminin immunolocalization was seen in the proctodeal region of *Xenopus laevis* at stage 23 of development, indicating the absence of the basement membrane at this stage. Therefore it would appear that the disappearance of the basement membrane between the proctodeal ectoderm and the hindgut

endoderm occurs as the cloacal membrane thins, which is evident in hamster embryos (Waterman, 1977). It would thus, also seem, that the basement membrane perforates before the dissolution of the cloacal membrane, which occurs at stage 24. This was the sequence of events found to occur in the stomodeal region of *Xenopus laevis*, where the basement membrane between the stomodeal ectoderm and foregut endoderm had disappeared by stage 30 of development, before the breakdown of the buccopharyngeal membrane (Dickinson and Sive, 2006). From similar observations in mammals, it has been suggested that the basement membrane plays a role in inhibiting fusion of the stomodeal ectoderm and foregut endoderm (Dickinson and Sive, 2006) and that as the contact between the stomodeal ectoderm and foregut endoderm increases, a change in the secretion of the basement membrane is induced. The disappearance of the basement membrane is thought to occur by phagocytosis, for which the epithelium is responsible. This is then thought to ensure the fusion of the ectodermal and endodermal germ layers (Takahama *et al.*, 1988).

Fibronectin has been identified as a basement membrane marker and immunolocalized in the stomodeal region (Dickinson and Sive, 2006). High levels of this protein have also been found in the extracellular matrix of the buccopharyngeal membrane prior to ectoderm and endoderm intercalation in the chick (Waterman and Balian, 1980). In the chick, fibronectin was found to form a band in the stomodeal region, which became discontinuous as development proceeded. Therefore fibronectin was proposed to initially play a role in adhesion (Waterman and Balian, 1980) and maintenance of the ectodermal and endodermal cell layers in the stomodeal region (Miller *et al.*, 1993). As this band of fibronectin was found to become discontinuous, it was suggested that this protein facilitates the thinning and rupture of the buccopharyngeal membrane (Waterman and Balian, 1980). Unfortunately no transmission electron microscopy was performed in the current study but for future research, this would be a useful technique to define the exact role of fibronectin in the development of the proctodeum.

## 4.3 APOPTOSIS

In *Xenopus laevis* the perforation of the buccopharyngeal membrane and the loss of a basement membrane in the stomodeal region and in other developing regions, such as the heart (Miller *et al.*, 1993) have been associated with increased apoptosis or decreased cell proliferation (Trindade *et al.*, 2003; Dickinson and Sive, 2006). Not only does apoptosis appear to have a role in the perforation of the buccopharyngeal membrane of anurans, but it has also been localized to the buccopharyngeal membrane of avians (Waterman and Schoenwolf, 1980; Waterman and Balian, 1980) and the buccopharyngeal membrane of mammals (Waterman, 1977). It has also been localized to the cloacal membrane of rats (Penington and Hutson, 2002) and humans (Paidas *et al.*, 1999). It is thus reasonable to propose that the perforation of the cloacal membrane in *Xenopus laevis* may, at least in part, be due to apoptosis.

In the present study the most intensely labelled cells of the *Xenopus laevis* embryos were those in the outer ectodermal layer, when immunolocalized for the pro-apoptotic protein Bax. Cells in this layer were thought to be apoptotic, although it is unclear whether apoptosis can occur in all the cells in one layer at the same time. The large number of cells which were brown in colour may therefore indicate high background staining or non-specific labelling due to the presence of pigment granules. However, this was not apparent in the embryos localized for Bcl-2, in which an almost identical protocol to Bax localization was used or in the negative controls. It was thus thought that this labelling was specific for apoptosis. Apoptosis has been localized to the ectodermal cell layer in the tail region of *Xenopus* (Kerr *et al*., 1974) and is a known process to occur in the ectoderm of human skin and rat oesophagus (Gavrieli *et al.*, 1992). Apoptosis occurs as cells migrate from the epithelial basal layer to the apical surface. The ectodermal cells then become flattened in shape and their nuclei disintegrate as keratinization and differentiation take place (Gavrieli *et al.*, 1992; Jacobson *et al.*, 1997) and cytokeratins are produced (Slack, 1984). The results from such studies suggest that the hypothesis from the current study that the outer ectodermal cells undergo apoptosis is plausible.

No massive bursts of cell death were observed in the proctodeum or cloacal membrane in *Xenopus laevis*, in the current study. This was in contrast to the pattern of apoptosis found in the stomodeal region of *Xenopus laevis*, where there was an increased burst of cell death early on in stomodeum formation, at approximately stage 34, many hours before the dissolution of the buccopharyngeal membrane (Dickinson and Sive, 2006). As the buccopharyngeal membrane thinned and eventually perforated, there was a decrease in the number of apoptotic cells in this region (Dickinson and Sive, 2006). This pattern of apoptosis expression may be similar in the proctodeal region of *Xenopus laevis*. A massive burst of cell death may occur many hours before cloacal membrane dissolution at stage 24 of development. No burst of cell death was detected in the current study, although the earliest stage of embryos analysed were those at stage 21. Therefore, if a burst of cell death does occur it may take place in the embryos before stage 21, before the perforation of the cloacal membrane, which occurs by stage 24. As apoptosis was seen many hours prior to perforation of the buccopharyngeal membrane, Dickinson and Sive (2006) hypothesized that a loss of cell adhesion may induce apoptosis. Apoptosis is thus thought to play a role in the thinning of the buccopharyngeal membrane, but not in the actual perforation of the buccopharyngeal membrane.

Although perforation of the cloacal membrane had occurred by stages 24 and 25 of development in *Xenopus laevis*, labelled cells detected with DAB in both the TUNEL method and the immunolocalization of Bax, were visible. The labelled cells, possibly apoptotic, appeared in the ectoderm around the cloacal opening. These results relate to those seen from the histological sections, where at stages 24, 25 and 26 as well, many vacuolated cells and secretory cells were present. These cells were present in the ectoderm of the cloacal opening. Vacuolated cells also appeared in the buccopharyngeal membrane of urodela (Takahama *et al.*, 1988) and anurans such as *Rana* (Watanabe *et al.*, 1984) and the urogenital and cloacal membranes of rat embryos at day 14 of gestation (Qi *et al.*, 2000a). These vacuolated cells were also found to stain positively for acid phosphatase in the anurans and were thought to be

apoptotic cells (Watanabe *et al.*, 1984). In the current study, together with vacuolated cells, a few cells seen in the histological sections of embryos in later development when the cloacal membrane had perforated appeared to be protruding into the cloacal opening, from the ectoderm. These cells appeared to be "blebbing" off the surface ectoderm and were morphologically characteristic of apoptotic cells, thus contributing to the hypothesis that apoptosis plays a role in development of the proctodeum and cloacal membrane perforation.

In embryos at stages 24 to 25 of development a number of the cells in the cloacal region were Bcl-2 positive indicating that they were anti-apoptotic. As some apoptosis appeared to occur in the ectoderm of the cloacal region of the embryos, it was interesting to note the presence of some non-apoptotic cells in this region. Therefore, the majority of the cells may be fated to undergo apoptosis but not at the same time, or it is possible that not all the cells in the proctodeal region undergo apoptosis but migrate away from the cloacal membrane. Although Bcl-2 is not an indicator of proliferating cells and no mitotic figures were seen in the current study, apoptosis of epithelial cells has been found in conjunction with proliferating cells in the development of the *Xenopus laevis* small intestine (Ishizuya-Oka *et al.* 1997; Ishizuya-Oka *et al.*, 2006).

The ratio of Bax to Bcl-2 is thought to be important in analyzing tissue samples, as it gives some indication as to the prominence of the role of apoptosis. From various studies it appears that apoptosis may be disrupted by a decrease in Bax localization and not an increase in Bcl-2 expression (Krajewska *et al.*, 1996b). Due to the small sample size in this study, it was not possible to determine the ratio of positive Bax to Bcl-2 cells in the proctodeal region of *Xenopus laevis* embryos. It would be interesting however to investigate further the efficacy of the immunohistochemical technique in apoptosis detection and the roles the Bax and Bcl-2 proteins play in proctodeum formation and cloacal membrane dissolution in *Xenopus laevis*.

In the detection of apoptosis in the proctodeal region of *Xenopus* laevis in the current study, a number of difficulties were encountered, especially with the TUNEL method. The TUNEL technique is considered a highly specific labelling method as it labels DNA fragmentation, which occurs before the morphological features are identified thereby allowing for early detection of apoptosis (Erenpreisa *et al.*, 1997). However it is also considered to have a number of downfalls, such as specificity and sensitivity (Labat-Moleur *et al.*, 1998). The results for apoptosis detection using the TUNEL technique in the current study were inconsistent and must be interpreted with care, even though the labelled cells in the embryonic sections were comparable to the clear apoptotic cells in the rat testes, used as a positive control. Thus, assays for the pro-apoptotic protein Bax and anti-apoptotic protein Bcl-2 were performed in order to substantiate the results obtained with the TUNEL method. The background staining with the immunohistochemical technique was not as high as with the TUNEL method. The labelling was more specific and the non-specific labelling reduced with the immunohistochemical technique compared with the TUNEL method. However, as only one embryo per stage was used for the Bax and Bcl-2 analysis, this was insufficient to determine whether the results obtained were representative.

With the TUNEL technique, high background staining and non-specific labelling was generally localized to the ectoderm and may have been due to the high concentration of pigment granules in this cell layer. These pigment granules are found in the cytoplasm of the basal cells of the epidermis and have peroxidase activity within them (Ito and Otsuki, 1998) and found to produce false reactions when DAB is used as a chromagen in various techniques. The embryos were bleached prior to the application of the TUNEL method to try and reduce this effect. However, the embryos used for the immunolocalization of the Bax and Bcl-2 proteins involved in apoptosis were not bleached. Therefore, for future studies the embryos should be bleached to negate pigment granules as an extraneous variable and in the case of the TUNEL method, the embryos should be bleached for a longer period of time. It may

also be more appropriate to use a fluorescent chromagen, instead of DAB to visualize immunolocalization or labelling.

Further indications of apoptosis included the presence of a flocculated substance or cellular "plugs" in the cloacal openings of later stage embryos, namely stages 25 and 26. In some of the histological sections, the flocculated substance was thought to be an area of the lateral wall, due to the plane of sectioning. However, from analysis of the histological sections and scanning electron micrographs it is believed that the flocculated material may be debris from apoptosis of cells of the cloacal membrane. Similar remnants of the anuran buccopharyngeal membrane have been observed in the "primary mouth" opening and attached to the surrounding epithelium (Watanabe *et al.*, 1984). Cell death has been assumed to be responsible for the debris associated with this region in hamsters (Waterman, 1977) and has been associated with the epithelial debris found in the anal region of rat embryos at day 12.5 of gestation (Qi *et al.*, 2000a). Thus, apoptosis may be responsible, in part at least, for dissolution of the cloacal membrane, as well as the buccopharyngeal membrane in *Xenopus laevis*.

However, apoptosis may not be the only process important in the dissolution of the buccopharyngeal and cloacal membranes. It is hypothesized, as although apoptosis was present in the stomodeal region of the chick (Waterman and Schoenwolf, 1980), hamster (Waterman, 1977) and urodela (Takahama *et al.*, 1988) vast amounts of cell death were not obvious. It has been postulated therefore that apoptosis is not the main mechanism responsible for the buccopharyngeal membrane dissolution but that cellular reorganization (Waterman, 1985; Miller *et al.*, 1993) and cell differentiation (Takahama *et al.*, 1988) may play a more important role.

As acid phosphatase-positive lysosomes were found to be present in the buccopharyngeal membrane of anurans, it has been suggested that these also play a role in the degeneration of membranes (Watanabe *et al.*, 1984) and may be included in cloacal membrane dissolution. The thinning of the buccopharyngeal membrane

and thus the weak attachment of the stomodeal ectoderm and foregut endoderm seen in embryonic development, including that of anurans, may be another mechanism responsible for the dissolution of the membrane (Watanabe *et al.* 1984). The tension and physical forces (Waterman, 1977; Hensey and Gautier; 1998) which may be active or passive (Miller *et al.*, 1993), may also aid in the breakdown of the buccopharyngeal and cloacal membranes. In rats, the weakened cloacal membrane was thought to collapse under pressure from the adjacent mesenchyme (Miller *et al.*, 1993; Qi *et al.*, 2000a). These forces may also be created by neural crest cells participating in the formation of the facial features around the buccopharyngeal membrane (Dickinson and Sive, 2006). Although neural crest cells are not present in the proctodeal region of *Xenopus laevis* embryos, a similar tension may be created by forces and contribute to the breakdown of the cloacal membrane. These mechanisms, together with apoptosis and various other unknown processes, may be responsible for the breakdown of the buccopharyngeal and cloacal membranes.

Taking into consideration the advantages and obstacles of the TUNEL method and the sample number in the immunolocalization of Bax, the results of the current study suggest that that there is a decrease in apoptosis in the proctodeal region as development of the *Xenopus laevis* embryos continues and once perforation of the cloacal membrane has occurred. This directly correlates with a decrease in BMP-4 expression found in the proctodeal region in the current study suggesting BMP-4 may play a role in the apoptosis and dissolution of the cloacal membrane.

## 4.4 GENE EXPRESSION

One BMP, namely BMP-4 is known to be expressed in the early stages of *Xenopus* development in both the anterior and posterior regions of the embryos and is localized to the proctodeum, as well as the heart and the eye, in the early tailbud stages (Karaulanov *et al.*, 2004). The expression pattern of BMP-4 was thus investigated over the period of development of the proctodeum.

High levels of BMP-4 expression were found at stage 14 and stage 22 of *Xenopus laevis* development and the expression was localized to the ectoderm. The ectodermal layer, especially in the neurula and tailbud stage embryos is known to have a high keratin concentration and has been associated with the highest concentrations of BMP-4 (Dale and Jones, 1999), which in the proctodeal region appears from the current study to be before stage 26 of development.

The results from the current study indicate that *BMP-4* expression was prominent in the proctodeal region of the *Xenopus laevis* embryos at stage 22 of development. The expression decreased in the proctodeal region as development continued and by stage 26, little to no expression was visible in the cloacal region. The results of the present study therefore suggest that *BMP-4* may play a role in the development of the proctodeum at stages 22 and 23. It may also be important in the dissolution of the cloacal membrane at stage 24, as at this stage *BMP*-4 expression is still quite prominent. Therefore, BMP-4 is thought to play an important role in the normal development of the proctodeal region in *Xenopus laevis*. The importance of BMPs in normal development was demonstrated in the development of the tail region and ventral fin, which is thought to be the most sensitive to decreases in BMP signalling in zebrafish (Pyati *et al.*, 2005).

As the BMPs have been implicated in apoptosis (Goltzené *et al.*, 2000), for example by activating the MAP kinase pathway (Dale and Jones, 1999), *BMP-4* may induce apoptosis, which in turn may play a role in the thinning and eventual perforation of the cloacal membrane. The expression of BMP-4 in the proctodeal region appears to correspond to that obtained from the results using the TUNEL and Bax method. This possibly indicates a relationship between programmed cell death and BMP-4 expression in this region in *Xenopus laevis*.

BMP-4 has in the past been localized to the ventral mesoderm as well as the ectoderm in zebrafish (Pyati *et al.*, 2006). However it appears that ectodermal differentiation is

the most sensitive to misexpression of BMP-4, as when Angerer *et al.* (2000) injected low concentrations of BMP-4 mRNA into sea urchin embryos, the epithelium of the archenteron was induced to form squamous cells. As BMP-4 expression occurred in the proctodeal region of *Xenopus laevis* embryos, it may be involved in ectodermal signalling and possibly in the ectodermal invagination during development of the proctodeum.

The involvement of BMP signalling in normal patterning of the hindgut was shown in zebrafish by Pyati *et al.* (2006) who used *in situ* hybridization labelling methods and transgenics. The zebrafish larvae with reduced BMP signalling could not excrete waste properly and these embryos thus presented morphologically with cloacal malformations (Pyati *et al.*, 2006). Zebrafish mutants with increased BMP expression showed excessive cell death in the proctodeal region and also presented with cloacal malformations (Pyati *et al.*, 2006). Cloacal defects were only found to be induced in embryos from the 80% epiboly stage to the 10 somite stage, but no effect was seen in embryos with misexpression of BMP in later stages (Pyati *et al.* 2006). As these cloacal malformations are only apparent when misexpression of BMP occurs in a certain time period, this indicates that BMP is not vital throughout development of the proctodeum and is only important for a short period of time. The importance of *BMP* expression in the proctodeal region has also been shown by the use of embryos with the *swirl* mutation. In these embryos, *BMP* is down-regulated and the embryos present with severe posterior and ventral malformations (Dale and Jones, 1999). Therefore, the pattern of BMP-4 expression, seen in the proctodeal region of *Xenopus laevis* in the current study may be essential for normal development.

As the expression of BMPs has been associated with apoptosis and the disruption of the BMP pathway has increased the rate of programmed cell death, BMP-4 may have a direct relationship with apoptosis. BMP-4 may therefore play an important role in conjunction with other genes and mechanisms in development of the proctodeal

region and dissolution of the cloacal membrane. As the mechanisms of BMP-4 have been found to be evolutionarily conserved (Dale and Jones, 1999), the role of BMP-4 in proctodeum formation may be similar in different organisms.

## 4.5 ANORECTAL MALFORMATIONS

From the current study on the development of the proctodeum and breakdown of the cloacal membrane in *Xenopus laevis* a more comprehensive view of normal development has been provided. Although no experiments using mutants or transgenics were performed to analyse anorectal malformations, the normal developmental process described in the present study suggests that alterations in these patterns of development may be involved in the formation of anomalies in this posterior region of the embryo (Kimmel *et al.*, 2000). It is suggested therefore that in the development of the proctodeum there is integration of a number of processes and if the regulation of any of these processes is perturbed, anorectal malformations may result. As many of these processes are conserved, some of these may also apply to human development and the formation of anorectal malformations.

The correct morphological formation of the proctodeum and cloacal membrane as well as the rupture of the cloacal membrane, are important to ensure normal gut development to allow for excretion of substances. Alterations in morphogenesis, including that of the tailgut in mammals can hamper cloacal development and result in cloacal or anorectal malformations (Qi *et al.*, 2000a; Pyati *et al.*, 2006), such as anal and anorectal agenesis (van der Putte, 1986). Studies using SD mutant mice have shown that mesoderm may develop between the proctodeal ectoderm and hindgut endoderm, leading to anorectal malformations (Kluth *et al.* 1995).

Anorectal malformations can arise from the misexpression of certain genes, such as BMP-4 (Goldman *et al.*, 2006), which from the current study was found to be specifically expressed in the proctodeal region. The misexpression of genes can

include the overexpression and the underexpression of these genes and their proteins. For example, in mouse embryos that were treated with *all-trans* retinoic acid, anorectal malformations occurred (Bitoh *et al.*, 2001). A deficiency in ephrin-B2, a cell surface marker, in mice mutants was found to disrupt cell signalling leading to the failure of septation of the cloaca, fistula formation and anal atresia where the hindgut endoderm failed to form an opening with the outside of the body. Such anorectal malformations exactly mimic those, such as persistent cloaca seen in human development (Mo *et al.*, 2001; Dravis *et al.*, 2004).

Gene expression, such as BMP-4, is linked to apoptosis in embryogenesis. Although from the current study the involvement of the basement membrane and apoptosis is not clear in proctodeal development, the literature suggests that they both play an important role in the correct formation of the stomodeum and the proctodeum in other organisms. For example Qi *et al.* (2000a) found that excessive apoptosis in the tailgut region of rats may lead to a deficiency of the dorsal cloacal membrane and produce anorectal malformations. Thus, disruptions in these normal processes may lead to anorectal malformations.

A disruption in a number of factors involved in normal gut formation may contribute to the causation of cloacal or anorectal malformations, some of them which have been discussed in the current study. These factors may act alone or may be integrated to produce these malformations. In striving to understand the normal development of the proctodeal region, a greater comprehension of the malformations will be provided.

## 4.6 CONCLUSION

From this study a more comprehensive understanding of the development of the proctodeum and dissolution of the cloacal membrane in *Xenopus laevis* has been obtained. Morphological evidence has shown that the proctodeal depression becomes

apparent at stage 21 of development. The ectodermal and endodermal layers, in the proctodeal region then thin. Although the results obtained from immunolocalization of the basement membrane markers fibronectin and laminin were inconclusive, it appeared that a discontinuous basement membrane may be located between the proctodeal ectoderm and hindgut endoderm at stages 21 and 22 of development. This was seen to disappear by stage 23. This suggests that the basement membrane may play a role in early development of the proctodeum. By stage 24, the cloacal membrane had perforated, forming a channel from the hindgut to the exterior. Although the results obtained with the TUNEL method for apoptosis detection and immunolocalization of the pro-apoptotic protein Bax and anti-apoptotic protein Bcl-2 are tentative, there was preliminary evidence to suggest that during these early stages of development apoptosis may occur. BMP-4 expression often associated with apoptosis, decreased in the proctodeal region as development of the embryos continued from stage 21 to 26. The misexpression of this gene has been found in association with organisms with anorectal malformations.

A number of the features and processes described in proctodeal development are similar to stomodeal formation and appear to be conserved in various organisms. Therefore, future studies could be undertaken to solidify and elucidate the findings of the current study, enabling a greater understanding of the developmental processes and of malformations of this region, affording clinical applications.

# REFERENCES


1. Alberts, B., Johnson, A., Lewis, J., Raff, M., Roberts, K., and Walter, P. (2002). *Molecular Biology of the Cell.* Garland Science, USA.
2. Allan, J., and Kramer, B. (2002). *The Fundamentals of Human Embryology*. Witwatersrand University Press, South Africa.
3. Angerer, L.M., Oleksyn, D.W., Logan, C.Y., McClay, D.R., Dale, L., and Angerer, R.C. (2000). A BMP pathway regulates cell fate allocation along the sea urchin animal-vegetal embryonic axis. *Development* **127(5):** 1105-1114.
4. Arends, M.J., Morris, R.G., and Wyllie, A.H. (1990). Apoptosis: The Role of the Endonuclease. *American Journal of Pathology* **136(3):** 593-608.
5. Baker, A.J., Mooney, A., Hughes, J., Lombardi, D., Johnson, R.J., and Savill, J. (1994). Mesangial Cell Apoptosis: The Major Mechanisms for Resolution of Glomerular Hypercellularity in Experimental Mesangial Proliferative Nephritis. *The Journal of Clinical Investigation* **94(5):** 2105-2116.
6. Balinsky, B.I. (1965). *An Introduction to Embryology.* W.B. Saunders Company, USA.
7. Balinsky, B.I. (1975). *An Introduction to Embryology*. W.B. Saunders Company, USA.
8. Bitoh, Y., Shimotake, T., Kubota, Y., Kimura, O., and Iwai, N. (2001). Impaired Distribution of Retinoic Acid Receptors in the Hindgut-Tailgut Region of Murine Embryos With Anorectal Malformations. *Journal of Pediatric Surgery* **36(2):** 377-380.
9. Boise, L.H., González-García, M., Postema, C.E., Ding, L., Lindsten, T., Turka, L.A., Mao, Z., Nuñez, G., and Thompson, C.B. (1993). B*cl-x*, B*cl-2*-Related Gene That Functions as a Dominant Regulator of Apoptotic Cell Death. *Cell* **74(4):** 597-608.

10. Bossy-Wetzel, E., Newmeyer, D.D., and Green, D.R. (1998). Mitochondrial cytochrome *c* release in apoptosis occurs upstream of DEVD-specific caspase activation and independently of mitochondrial transmembrane depolarization. *The EMBO Journal* **17(1):** 37-49.
11. Branford, W.W., Essner, J.J., and Yost, H.J. (2000). Regulation of Gut and Heart Left-Right Asymmetry by Context-Dependent Interactions between *Xenopus* Lefty and BMP-4 Signalling. *Developmental Biology* **223(2):** 291-306.
12. Brown, D.G., Sun, X-M., and Cohen, G.M. (1993). Dexamethasone-induced Apoptosis Involves Cleavage of DNA to Large Fragments prior to Internucleosomal Fragmentation. *The Journal of Biological Chemistry* **268(5):** 3037-3039.
13. Bruch, S.W., Scott-Adzick, N., Goldstein, R.B., and Harrison, M.R. (1996). Challenging the Embryogenesis of Cloacal Exstrophy. *Journal of Pediatric Surgery* **31(6):** 768-770.
14. Callery, E.M. (2006). There's more than one frog in the pond: A survey of the Amphibia and their contributions to developmental biology. *Seminars in Cell and Developmental Biology* **17(1):** 80-92.
15. Chalmers, A.D., and Slack, J.M.W. (1998). Development of the Gut in *Xenopus laevis*. *Developmental Dynamics* **212(4):** 509-521.
16. Chalmers, A.D., and Slack, J.M.W. (2000). The *Xenopus* tadpole gut: fate maps and morphogenetic movements. *Development* **127(2):** 381-392.
17. Cohen, J.J. (1993). Apoptosis. *Immunology Today* **14(3):** 126-130.
18. Collart, C., Verschueren, K., Rana, A., Smith, J.C., and Huylebroek, D. (2005). The novel Smad-interacting protein Smicl regulates *Chordin* expression in the *Xenopus* embryo. *Development* **132(20):** 4575-4586.
19. Dale, L., and Jones, C.M. (1999). BMP signalling in early *Xenopus* development. *BioEssays* **21(9):** 751-760.

20. Dale, L., Howes, G., Price, B.M.J., and Smith, J.C. (1992). Bone morphogenetic protein-4: a ventralizing factor in early *Xenopus* development. *Development* **115(2):** 573-585.
21. Darzynkiewicz, Z., Juan, G., Li, X., Gorczyca, W., Murakami, T., and Traganos, F. (1997). Cytometry in Cell Necrobiology: Analysis of Apoptosis and Accidental Cell Death (Necrosis). *Cytometry* **27(1):** 1-20.
22. de Vries, P.A., and Friedland, G.W. (1974). The Staged and Sequential Development of the Anus and Rectum in Human Embryos and Fetuses. *Journal of Pediatric Surgery* **9(5):** 755-769.
23. Dickinson, A.J.G., and Sive, H. (2006). Development of the primary mouth in *Xenopus laevis*. *Developmental Biology* **295(2):** 700-713.
24. Drancourt, M., Jarlier, V., and Raoult, D. (2002). The Environmental Pathogen *Mycobacterium ulcerans* Grows in Amphibian Cells at Low Temperatures. *Applied and Environmental Microbiology* **68(12):** 6403-6404.
25. Dravis, C., Yokoyama, N., Chumley, M.J., Cowan, C.A., Silvany, R.E., Shay, J., Baker, L.A., and Henkemeyer, M. (2004). Bidirectional signalling mediated by ephrin-B2 and EphB2 controls urorectal development. *Developmental Biology* **271(2):** 272-290.
26. Erenpreisa, J., Freivalds T., Roach, H., and Alston, R. (1997). Apoptotic cell nuclei favour aggregation and fluorescence quenching of DNA dyes. *Histochemistry and Cell Biology* **108(1):** 67-75.
27. Fagotto, F., and Maxfield, F.R. (1994). Changes in yolk platelet pH during *Xenopus laevis* development correlate with yolk utilization: A quantitative confocal microscopy study. *Journal of Cell Science* **107(12):** 3325-3337.
28. Florian, J. (1933). The early development of man, with special reference to the development of the mesoderm and cloacal membrane. *Journal of Anatomy* **67(Pt 2):** 263-276.
29. Gavrieli, Y., Sherman, Y., and Ben-Sasson, S.A. (1992). Identification of Programmed Cell Death *In Situ* via Specific Labelling of Nuclear DNA Fragmentation. *The Journal of Cell Biology* **119(3):** 493-501.

30. Gilbert, S.F. (2003). *Developmental Biology.* Sinauer Associates, Inc., USA.
31. Giudice, G. (2001). Conserved cellular and molecular mechanisms in development. *Cell Biology International* **25(11):** 1081-1090.
32. Gold, R., Schmied, M., Rothe, H., Zischler, H., Breitschopf, H., Wekerle, H., and Lassmann, H. (1993). Detection of DNA Fragmentation in Apoptosis: Application of *In Situ* Nick Translation to Cell Culture Systems and Tissue Sections. *The Journal of Histochemistry and Cytochemistry* **41(7):** 1023-1030.
33. Goldman, D.C., Hackenmiller, R., Nakayama, T., Sopory, S., Wong, C., Kulessa, H., and Christian, J.L. (2006). Mutation of an upstream cleavage site in the BMP-4 prodomain leads to tissue-specific loss of activity. *Development* **133(10):** 1933-1942.
34. Goltzené, F., Skalski, M., Wolff, C.M., Meyer, D., Mager-Heckel, A-M., Darribère, T., and Remy, P. (2000). Heterotopic Expression of the XI-*Fli* Transcription Factor during *Xenopus* Embryogenesis: Modification of Cell Adhesion and Engagement in the Apoptotic Pathway. *Experimental Cell Research* **260(2):** 233-247.
35. Gont, L.K., Steinbeisser, H., Blumberg, B., and Robertis, E.M. (1993). Tail formation as a continuation of gastrulation: the multiple cell populations of the *Xenopus* tailbud derive from the late blastopore lip. *Development* **119(4):** 991-1004.
36. Gorczyca, W., Gong, J., and Darzynkiewicz, Z. (1993). Detection of DNA Strand Breaks in Individual Apoptotic Cells by the *in Situ* Terminal Deoxynucleotidyl Transferase and Nick Translation Assays. *Cancer Research* **53(8):** 1945-1951.
37. Graff, J.M. (1997). Embryonic Patterning: To BMP or not to BMP, That Is the Question. *Cell* **89(2):** 171-174.
38. Graff, J.M., Thies, R.S., Song, J.J., Celeste, A.J., and Melton, D.A. (1994). Studies with a Xenopus BMP Receptor Suggest That Ventral Mesoderm-Inducing Signals Override Dorsal Signals In Vivo. *Cell* **79(1):** 169-179.

39. Haffen, K., Kedinger, M., and Simon-Assmann, P. (1987). Mesenchyme-Dependent Differentiation of Epithelial Progenitor Cells in the Gut. *Journal of Pediatric Gastroenterology and Nutrition* **6(1):**14-23.
40. Hardin, J., and Armstrong, N. (1997). Short-Range Cell-Cell Signals Control Ectodermal Patterning in the Oral Region of the Sea Urchin Embryo. *Developmental Biology* **182(1):** 134-149.
41. Haworth, K.E., Healy, C., Morgan, P., and Sharpe, P.T. (2004). Regionalisation of early head ectoderm is regulated by endoderm and prepatterns the orofacial epithelium. *Development* **131(19):** 4797-4806.
42. Heasman, J. (1997). Patterning the *Xenopus* blastula. *Development* **124(21):** 4179-4191.
43. Hendren, W.H. (1998). Cloaca, The Most Severe Degree of Imperforate Anus. *Annals of Surgery* **228(3):** 331-346.
44. Hensey, C., and Gautier, J. (1998). Programmed Cell Death during *Xenopus* Development: A Spatio-temporal Analysis. *Developmental Biology* **203(1):**36-48.
45. Horb, M.E., and Slack, J.M.W. (2001). Endoderm Specification and Differentiation in *Xenopus* Embryos. *Developmental Biology* **236(2):** 330-343.
46. Hormia, M., Sahlberg, C., Thesleff, I., and Airenne, T. (1998). The Epithelium-Tooth Interface-A Basal Lamina Rich Laminin-5 and Lacking Other Known Laminin Isoforms. *Journal of Dental Research* **77(7):** 1479-1485.
47. Ishizuya-Oka, A., Ueda, S., Damjanovski, S., Li, Q., Liang, V. C-T., and Shi, Y-B. (1997). Anteroposterior Gradient of Epithelial Transformation during Amphibian Intestinal Remodelling: Immunohistochemical Detection of Intestinal Fatty Acid-Binding Protein. *Developmental Biology* **192(1):** 149-161.
48. Ishizuya-Oka, A., Hasebe, T., Shimizu, K., Suzuki, K., and Ueda, S. (2006). Shh/BMP-4 signalling pathway is essential for intestinal epithelial

development during *Xenopus* larval-to-adult remodelling. *Developmental Dynamics* **235(12):** 3240-3249.

49. Ito, Y., and Otsuki, Y. (1998). Localization of Apoptotic Cells in the Human Epidermis by an In Situ DNA Nick End-Labelling Method Using Confocal Reflectant Laser Microscopy. *The Journal of Histochemistry and Cytochemistry* **46(6):** 783-786.
50. Jacobson, M.D., Weil, M., and Raff, M.C. (1997). Programmed Cell Death in Animal Development. *Cell* **88(3):** 347-354.
51. Jain, M., and Weaver, D.D. (2004). Severe Lower limb Defects in Exstrophy of the Cloaca. *American Journal of Medical Genetics* **128A(3):** 320-324.
52. Karaulanov, E., Knöchel, W., and Niehrs, C. (2004). Transcriptional regulation of BMP-4 synexpression in transgenic *Xenopus*. *The EMBO Journal* **23(4):** 844-856.
53. Kerr, J.F.R., Harmon, B., and Searle, J. (1974). An electron-microscope study of cell deletion in the anuran tadpole tail during spontaneous metamorphosis with special reference to apoptosis of striated muscle fibres. *Journal of Cell Science* **14(3):** 571-585.
54. Khokha, M.K., Chung, C., Bustamante, E.L., Gaw, L.W.K., Trott, K.A., Yeh, J., Lim, N., Lin, J.C.Y., Taverner, N., Amaya, E., Papalopulu, N., Smith, J.C., Zorn, A.M., Harland, R.M., and Grammer, T.C. (2002). Techniques and Probes for the Study of *Xenopus tropicalis* Development. *Developmental Dynamics* **225(4):** 499-510.
55. Kimmel, S.G., Mo, R., Hui, C-C., and Kim, P.C.W. (2000). New Mouse Models of Congenital Anorectal Malformations. *Journal of Pediatric Surgery* **35(2):** 227-231.
56. Kluth, D., and Lambrecht, W. (1997). Current Concepts in the Embryology of Anorectal Malformations. *Seminars in Pediatric Surgery* **6(4):** 180-186.
57. Kluth, D., Hillen, M., and Lambrecht, W. (1995). The Principles of Normal and Abnormal Hindgut Development. *Journal of Pediatric Surgery* **30(8):** 1143-1147.

58. Koga, M., Kudoh, T., Hamada, Y., Watanabe, M., and Kageura, H. (2007). A new triple staining method for double *in situ* hybridization in combination with cell lineage tracing in whole-mount *Xenopus* embryos. *Development, Growth and Differentiation* **49(8):** 635-645.
59. Krajewska, M., Fenoglio-Preiser, C.M., Krajewski, S., Song, K., Macdonald, J.S., Stemmerman, G., and Reed, J.C. (1996a). Immunohistochemical Analysis of Bcl-2 Family Proteins in Adenocarcinomas of the Stomach. *American Journal of Pathology* **149(5):** 1449-1457.
60. Krajewska, M., Krajewski, S., Epstein, J.I., Shabaik, A., Sauvageot, J., Song, K., Kitada, S., and Reed, J.C. (1996b). Immunohistochemical Analysis of *Bcl-2*, *Bax*, *Bcl-X*, and *Mcl-1* Expression in Prostate Cancers. *American Journal of Pathology* **148(5):** 1567-1576.
61. Krajewski, S., Blomqvist, C., Franssila, K., Krajewska, M., Wasenius, V-M., Niskanen, E., Nordling, S., and Reed, J.C. (1995). Reduced Expression of Pro-apoptotic gene *Bax* Is Associated with Poor Response Rates to Combination Chemotherapy and Shorter Survival in Women with Metastatic Breast Adenocarcinoma. *Cancer Research* **55(19):** 4471-4478.
62. Kurata, T., Nakabayashi, J., Yamamoto, T.S., Mochii, M., and Ueno, N. (2001). Visualization of endogenous BMP signalling during *Xenopus* development. *Differentiation* **67(1-2):** 33-40.
63. Labat-Moleur, F., Guillermet, C., Lorimier, P., Robert, C., Lantuejoul, S., Brambilla, E., and Negoescu, A. (1998). TUNEL Apoptotic Cell Detection in Tissue Sections: Critical Evaluation and Improvement. *The Journal of Histochemistry and Cytochemistry* **46(3):** 327-334.
64. Lee, M.A., Heasman, J., and Whitman, M. (2001). Timing of endogenous activin-like signals and regional specification of the *Xenopus* embryo. *Development* **128(15):** 2939-2952.
65. Majno, G., and Joris, I. (1995). Apoptosis, Oncosis, and Necrosis: An Overview of Cell Death. *American Journal of Pathology* **146(1):** 3-15.

66. Mandhan, P., Quan, Q.B., Beasley, S., and Sullivan, M. (2006). *Sonic hedgehog*, *BMP-4*, and *Hox* genes in the development of anorectal malformations in Ethylenethiourea-exposed fetal rats. *Journal of Pediatric Surgery* **41(12):** 2041-2045.
67. Marshall, A.M. (1893). *Vertebrate Embryology.* Smith, Elder and Co., London.
68. Martínez-Barberá, J.P., Toresson, H., Rocha, S.D. and Krauss, S. (1997). Cloning and expression of three members of the zebrafish BMP family: *BMP-2a*, *BMP-2b* and *BMP-4*. *Gene* **198(1-2):** 53-59.
69. Migheli, A., Attanasio, A., and Schiffer, D. (1995). Ultrastructural detection of DNA strand breaks in apoptotic neural cells by *in situ* end-labelling techniques. *Journal of Pathology* **176(1):** 27-35.
70. Miller, S.A., Favale, A.M., and Knohl, S.J. (1993). Role for Differential Cell Proliferation in Perforation and Rupture of Chick Pharyngeal Closing Plates. *The Anatomical Record* **237(3):** 408-414.
71. Miyanaga, Y., Torregroza, I., and Evans, T. (2002). A Maternal Smad Protein Regulates Early Embryonic Apoptosis in *Xenopus laevis*. *Molecular and Cellular Biology* **22(5):** 1317-1328.
72. Mo, R., Kim, J.H., Zhang, J., Chiang, C., Hui, C-C., and Kim, P.C.W. (2001). Anorectal Malformation Caused by Defects in Sonic Hedgehog Signalling. *American Journal of Pathology* **159(2):** 765-774.
73. Moore, K.L. (1988). *The Developing Human: Clinically Oriented Embryology*. W.B. Saunders Company, USA.
74. Mundle, S., Iftikhar, A., Shetty, V., Dameron, S., Wright-Quinones, V., Marcus, B., Loew, J., Gregory, S., and Raza, A. (1994). Novel *In Situ* Double Labelling for Simultaneous Detection of Proliferations and Apoptosis. *The Journal of Histochemistry and Cytochemistry* **42(12):** 1533-1537.
75. Murray, P., and Edgar, D. (2000). Regulation of Programmed Cell Death by Basement Membranes in Embryonic Development. *The Journal of Cell Biology* **150(5):** 1215-1221.

76. Nebot-Cegarra, J., Fàbregas, P.J., and Sánchez-Pérez, I. (2005). Cellular proliferation in the urorectal septation complex of the human embryo at Carnegie stages 13-18: a nuclear area-based morphometric analysis. *Journal of Anatomy* **207(4):** 353-364.
77. Nieuwkoop, P.D., and Faber, J. (Eds). (1967). *Normal Table of Xenopus laevis (Daudin): A systematical and Chronological survey of the Development from the fertilized egg till the end of metamorphosis.* North-Holland Publishing Company, Amsterdam.
78. Ohta, k., Iwai, K., Kasahara, Y., Taniguchi, N., Krajewski, S., Reed, J.C., and Miyawaki, T. (1995). Immunoblot analysis of cellular expression of Bcl-2 family proteins, Bcl-2, Bax, Bcl-X and Mcl-1, in human peripheral blood and lymphoid tissues. *International Immunology* **7(11):** 1817-1825.
79. Paidas, C.N., Morreale, R.F., Holoski, K.M., Lund, R.E., and Hutchins, G.M. (1999). Septation and Differentiation of the Embryonic Human Cloaca. *Journal of Pediatric Surgery* **34(5):** 877-884.
80. Papan, C., Boulat, B., Velan, S.S., Fraser, S.E., and Jacobs, R.E. (2007). Two-dimensional and three-dimensional time-lapse microscopic magnetic resonance imaging of *Xenopus* gastrulation movements using intrinsic tissue-specific contrast. *Developmental Dynamics* **236(2):** 494-501.
81. Peña, A. (1997). Preface: Advances in Anorectal Malformations. *Seminars in Pediatric Surgery* **6(4):** 165-169.
82. Penington, E.C., and Hutson, J.M. (2002). The cloacal plate: the missing link in anorectal and urogenital development. *British Journal of Urology International* **89(7):** 726-732.
83. Perriton, C.L., Powles, N., Chiang, C., Maconochie, M.K., and Cohn, M.J. (2002). *Sonic hedgehog* Signalling from the Urethral Epithelium Controls External Genital Development. *Developmental Biology* **247(1):** 26-46.
84. Pollard, T.D., and Earnshaw, W.C. (2002). *Cell Biology.* Saunders, USA.

85. Pyati, U.J., Webb, A.E., and Kimelman, D. (2005). Transgenic zebrafish reveal stage-specific roles for BMP signalling in ventral and posterior mesoderm development. *Development* **132(10):** 2333-2343.
86. Pyati, U.J., Cooper, M.S., Davidson, A.J., Nechiporuk, A., and Kimelman, D. (2006). Sustained BMP signalling is essential for cloaca development in zebrafish. *Development* **133(11):** 2275-2284.
87. Qi, B.Q., Beasley, S.W., Williams, A.K., and Frizelle, F. (2000a). Apoptosis During Regression of the Tailgut and Septation of the Cloaca. *Journal of Pediatric Surgery* **35(11):** 1556-1561.
88. Qi, B.Q., Beasley, S.W., Williams, A.K., and Frizelle, F. (2000b). Clarification of the Process of Separation of the Cloaca Into Rectum and Urogenital Sinus in the Rat Embryo. *Journal of Pediatric Surgery* **35(12):** 1810-1816.
89. Qi, B.Q., Beasley, S.W., and Frizelle, F.A. (2002). Clarification of the Processes That Lead to Anorectal Malformations in the ETU-Induced rat Model of Imperforate Anus. *Journal of Pediatric Surgery* **37(9):** 1305-1312.
90. Reed, J.C. (1994). Bcl-2 and the regulation of Programmed Cell Death. *The Journal of Cell Biology* **124(1-2):** 1-6.
91. Rugh, R. (1951). *The Frog: Its Reproduction and Development*. McGraw-Hill Book Company, USA.
92. Sagerström, C.G., Grinblat, Y., and Sive, H. (1996). Anteroposterior patterning in the zebrafish, *Danio rerio*: an explant assay reveals inductive and suppressive cell interactions. *Development* **122(6):** 1873-1883.
93. Sasaki, Y., Iwai, N., Tsyda, T., and Kimura, O. (2004). Sonic Hedgehog and Bone Morphogenetic Protein-4 Expressions in the Hindgut Region of Murine Embryo With Anorectal Malformations. *Journal of Pediatric Surgery* **39(2):** 170-173.
94. Schlaifer, D., Krajewski, S., Galoin, S., Rigal-Huguet, F., Laurent, G., Massip, P., Pris, J., Delsol, G., Reed, J.C., and Brousset, P. (1996). Immunodetection of Apoptosis-Regulating Proteins in Lymphomas from

Patients with and without Human Immunodeficiency Virus Infection. *American Journal of Pathology* **149(1):** 177-185.

95. Schohl, A., and Fagotto, F. (2002). B-catenin, MAPK and Smad signalling during early *Xenopus* development. *Development* **129(1):** 37-52.
96. Schwartzman, R.A., and Cidlowski, J.A. (1993). Apoptosis: The Biochemistry and Molecular Biology of Programmed Cell Death. *Endocrine Reviews* **14(2):** 133-151.
97. Shapira, E., Marom, K., Yelin, R., Levy, A., and Fainsod, A. (1999). A role for the homeobox gene *Xvex-1* as part of the *BMP-4* ventral signalling pathway. *Mechanisms of Development* **86(1-2):** 99-111.
98. Siebert, J.R., Rutledge, J.C., and Kapur, R.P. (2005). Association of Cloacal Anomalies, Caudal Duplication, and Twinning. *Pediatric and Developmental Pathology* **8(3):** 339-354.
99. Slack, J.M.W. (1984). Regional biosynthetic markers in the early amphibian embryo. *Journal of Embryology Experimental Morphology* **80:** 289-319.
100. Tahara, Y., and Nakamura, O. (1961). Topography of the Presumptive Rudiments in the Endoderm of the Anuran Neurula. *Journal of Embryology and Experimental Morphology* **9(1):** 138-158.
101. Takahama, H., Sasaki, F., and Watanabe, K. (1988). Morphological Changes in the Oral (Buccopharyngeal) Membrane in Urodelan Embryos: Development of the Mouth Opening. *Journal of Morphology* **195(1):** 59-69.
102. Tam, P.P.L., Kanai-Azuma, M., and Kanai, Y. (2003). Early endoderm development in vertebrates: lineage differentiation and morphogenetic function. *Current Opinion in Genetics and Development* **13(4):** 393-400.
103. Tilly, J.L. (1994). Use of the Terminal Transferase DNA Labelling Reaction for the Biochemical and *in Situ* Analysis of Apoptosis. In: Celis, J.E. (Ed), *Cell Biology: A Laboratory Handbook*. Academic Press, USA.
104. Torrey, T.W. (1963). *Morphogenesis of the Vertebrates*. John Wiley and Sons, USA.

105. Tortora, G.J. (2005). *Principles of human Anatomy*. Bergen Community College, USA.

106. Touloukin, R.J. (1979). Anorectal Malformations. In: Bergsman, D. (Ed), *Birth Defects Compendium*. Macmillan Press, USA.

107. Trindade, M., Messenger, N., Papin, C., Grimmer, D., Fairclough, L., Tada, M., and Smith, J.C. (2003). Regulation of apoptosis in the *Xenopus* embryo by Bix-3. *Development* **130(19):** 4611-4622.

108. van der Putte, S.C.J. (1986). Normal and Abnormal Development of the Anorectum. *Journal of Pediatric Surgery* **21(5):** 434-440.

109. Vaux, D.L. (1993). Toward and understanding of the molecular mechanisms of physiological cell death. *Proceedings of the National Academy of Sciences of the United States of America* **90(3):** 786-789.

110. Wacker, S., Brodbeck, A., Lemaire, P., Niehrs, C., and Winklbauer. (1998). Patterns and control of cell motility in the *Xenopus* gastrula. *Development* **125(10):** 1931-1942.

111. Wacker, S., Grimm, K., Joos, T., and Winklbauer, R. (2000). Development and Control of Tissue Separation at Gastrulation in *Xenopus*. *Developmental Biology* **224(2):** 428-439.

112. Wardle, F.C., Wainstock, D.H., and Sive, H.L. (2002). Cement gland-specific activation of the *Xag-1* promoter is regulated by co-operation of putative Ets and ATF/CREB transcription factors. *Development* **129(19):** 4387-4397.

113. Watanabe, K., Sasaki, F., and Takahama, H. (1984). The Ultrastructure of Oral (Buccopharyngeal) Membrane Formation and Rupture in the Anuran Embryo. *The Anatomical Record* **210(3):** 513-524.

114. Waterman, R.E. (1977). Ultrastructure of Oral (Buccopharyngeal) Membrane Formation and Rupture in the Hamster Embryo. *Developmental Biology* **58(2):** 219-229.

115. Waterman, R.E. (1985). Formation and Perforation of Closing Plates in the Chick Embryo. *The Anatomical Record* **211(4):** 450-457.

116. Waterman, R.E., and Balian, G. (1980). Indirect immunofluorescent staining of fibronectin associated with the floor of the foregut during formation and rupture of the oral membrane in the chick embryo. *The Anatomical Record* **198(4):** 619-635.

117. Waterman, R.E., and Schoenwolf, G.C. (1980). The Ultrastructure of Oral (Buccopharyngeal) Membrane Formation and Rupture in the Chick Embryo. *The Anatomical Record* **197(4):** 441-470.

118. Wilson, P.A., Lagna, G., Suzuki, A., and Hemmati-Brivanlou, A. (1997). Concentration-dependent patterning of the *Xenopus* ectoderm by BMP-4 and its signal transducer Smad-1. *Development* **124(16):** 3177-3184.

119. Yao, L-C., Blitz, I.L., Peiffer, D.A., Phin, S., Wang, Y., Ogata, S., Cho, K.W.Y., Arora, K., and Warrior, R. (2006). Schnurri transcription factors from *Drosophila* and vertebrates can mediate BMP signalling through a phylogenetically conserved mechanism. *Development* **133(20):** 4025-2034.

120. Yokouchi, Y., Sakiyama, J-I., and Kuroiwa, A. (1995). Coordinated Expression of *Abd-B* Subfamily Genes of the *HoxA* Cluster in the Developing Digestive Tract of Chick Embryo. *Developmental Biology* **169(1):** 76-89.

121. Zhang, J., Houston, D.W., King, M.L., Payne, C., Wylie, C., and Heasman, J. (1998). The Role of Maternal VegT in Establishing the Primary Germ Layers in *Xenopus* Embryos. *Cell* **94(4):** 515-524.

# APPENDICES

## APPENDIX I: Buffers and Salt Solutions

Alkaline phosphatase (AP) buffer

| | |
|---|---|
| 100 mM | tris (pH 9.5) |
| 50 mM | magnesium chloride |
| 100 mM | sodium chloride |
| 2 mM | levamisol |
| 0.1% Tween-20 | |

Homogenizing buffer

Stock solution:

| | |
|---|---|
| 50 ml | glycerol |
| 0.54 g | magnesium acetate |
| 0.037 g | EDTA |
| 5 ml | triton-x-100 |

Make up to 500 ml with 50 mM tris/HCl (pH 7.5).

Autoclave.

Add 0.5 mM dithiothreitol.

Measure 10 ml of the stock solution and add 50 µl protease inhibitor cocktail (Sigma, P2714).

Hybridization buffer

| | |
|---|---|
| 50 ml | molecular biology grade formamide |
| 25 ml | 20X SSC (pH 7.0) |
| 2 ml | 50 mg/ml Torula RNA |
| 10 mg | heparin |
| 2 ml | 50X Denhardt's solution |
| 0.1 ml | Tween-20 |
| 0.1 g | CHAPS |
| 2 ml | 0.5 M EDTA (pH 7.5) |

Make up to 100 ml with sterile milliQ water.

(50X Denhardt's solution contains: 1% BSA, 1% Ficoll and 1% polyvinylpyrrolidone)

Maleic acid buffer (MAB)

| | |
|---|---|
| 150 mM | maleic acid |
| 100 mM | sodium chloride |
| 7.9 g/l | sodium hydroxide |
| 0.1% Tween-20 | |

Adjust pH to 7.5.

Modified Barth's saline solution (MBS)

Prepare two solutions: 0.1 M calcium chloride and 10X MBS.

- 0.1M calcium chloride:

  Dissolve 11.1 g calcium chloride in 1 l distilled water.

  Autoclave and store in aliquots at -20ºC or 4 ºC.

- 10X MBS salts:

| | |
|---|---|
| 880 mM | sodium chloride |
| 10 mM | potassium chloride |
| 10 mM | magnesium sulphate |
| 25 mM | sodium bicarbonate |

Prepare the final MBS solution by mixing 100 ml of 10X salt solution with 7 ml 0.1 M calcium chloride and adjust the volume up to 1 l with distilled water.

High salt Modified Barth's saline solution:

| | |
|---|---|
| 7 ml | 0.1 M calcium chloride |
| 100 ml | 10X MBS salts |
| 4 ml | 5 M sodium chloride |
| 888 ml | distilled water |

0.1X MBS:

Add 1 part MBS to 9 parts distilled water.

Modified Marc's ringer

| | |
|---|---|
| 0.1 M | sodium chloride |
| 20 mM | potassium chloride |
| 1 mM | magnesium sulphate |
| 2 mM | calcium chloride |
| 5 mM | HEPES (pH 7.8) |

MOPS buffer

10X MOPS buffer:

| | |
|---|---|
| 400 mM | MOPS (pH 7.5) |
| 500 mM | sodium chloride |
| 100 mM | magnesium chloride |

Make up in double distilled water.

1X MOPS Buffer:

Add 1 part 10X MOPS buffer to 9 parts distilled water.

Phosphate buffered saline (PBS)

To 1 l distilled water add:

| | |
|---|---|
| 8 g | sodium chloride |
| 1.8 g | disodium hydrogen phosphate |
| 0.2 g | potassium chloride |
| 0.2 g | potassium dihydrogen orthophosphate |

Adjust pH to 7.6.

Phosphate buffered saline (PBS) (Immunohistochemistry)

| | |
|---|---|
| 36.0 g | sodium chloride |
| 10.4 g | disodium hydrogen orthophosphate ($Na_2HPO_4.12H_20$) |
| 1.16 g | sodium dihydrogen orthophosphate ($NaH_2PO_4.2H_20$) |

Dissolve in 4 l distilled water.

Adjust pH to 7.1.

Phosphate buffered saline with Tween-20 (PBT)

Add 0.1% Tween-20 to PBS.

Sodium chloride/ sodium citrate buffer solution

20X SSC:

| | |
|---|---|
| 87.6 g | sodium chloride |
| 44.1 g | sodium citrate |

Dissolve in 500 ml distilled water and adjust to pH 7.4.

Autoclave.

2X SSC:

Add 50 ml 20X SSC to 450 ml distilled water.

0.5X SSC:

Add 1.25 ml 20X SSC to 48.75 ml distilled water.

0.2X SSC:

Add 5 ml 20X SSC to 495 ml distilled water.

10X Tris/acetate/ethylenediaminetetraacetic acid (EDTA) (TAE) buffer (pH 8.18-8.29)

| | |
|---|---|
| 4.84 g | tris |
| 10.9 g | glacial acetic acid |
| 2.92 g | EDTA |

Dissolve in 1 l distilled water.

Tris buffered saline (Dot blot)

| | |
|---|---|
| 6.06 g | tris |
| 8.77 g | sodium chloride |

Add to 1 l distilled water.

Adjust pH to 7.6.

Tris with Tween-20

Add 0.05% (100 µl) Tween-20 to 200 ml tris buffered saline (pH 7.6).

Tris-EDTA buffer (pH 9.0): 10 mM tris base, 1 mM EDTA, 0.05% Tween-20

| | |
|---|---|
| 1.21 g | tris |
| 0.37 g | EDTA |

Dissolve in 1 l distilled water.

Adjust pH to 9.0

Add 0.5 ml Tween-20 and mix well.

Tris/HCl: 0.05 M tris buffer (pH 7.6)

Mix 100 ml 1 M tris with 76.8 ml 1 N HCl.

Adjust to pH 7.6.

Make up to 2 l with distilled water.

Tris/saline: 0.95% sodium chloride and 0.05 M tris/HCl (pH 7.6)

Dissolve 42.75 g sodium chloride in 4.5 l distilled water.

Add 500 ml tris/HCl.

# APPENDIX II: Fixatives

Bouin's solution

| | |
|---|---|
| 75 ml | saturated aqueous picric acid solution (0.91 g picric acid in 75 ml distilled water) |
| 25 ml | 40% formaldehyde |
| 5 ml | glacial acetic acid |

Carnoy's fixative

| | |
|---|---|
| 60 ml | absolute methanol |
| 30 ml | chloroform |
| 10 ml | glacial acetic acid |

10% Neutral buffered formalin

| | |
|---|---|
| 100 ml | formalin |
| 6.5 g | disodium hydrogen phosphate |
| 3.5 g | sodium dihydrogen phosphate |
| 900 ml | distilled water |

4% Paraformaldehyde

Make up PBS:

| | |
|---|---|
| 8.5 g | sodium chloride |
| 1.07 g | disodium hydrogen phosphate |
| 0.39 g | sodium dihydrogen orthophosphate (anhydrous) |

Add 4 g paraformaldehyde to 100 ml PBS.

Heat to 60ºC.

Add 4% sodium hydroxide drop by drop until clear.

Adjust pH to 7.4.

# APPENDIX III: Staining Solutions

Gill's haematoxylin (Gill *et al.*, 1974) (Gordon's method of preparation)

| | |
|---|---|
| 2.0 g | haematoxylin |
| 0.2 g | sodium iodate |
| 17.6 g | aluminium sulphate |
| 750 ml | distilled water |
| 250 ml | ethylene glycol |
| 20 ml | glacial acetic acid |

Mix the distilled water and ethylene glycol.

Add the haematoxylin and mix until it has dissolved.

Add the sodium iodate and then the aluminium sulphate and mix until dissolved.

Add the glacial acetic acid and stir for 1 hour.

Filter before use.

# APPENDIX IV: Other Solutions

Bloto (Blocking solution for dot blot)

| | |
|---|---|
| 100 ml | tris (pH 7.6) |
| 5 g | milk powder |
| 50 µl | 0.05% Tween-20 |

Blocking solution

Add 1 part Boehringer Mannheim Blocking reagent stock solution, 1 part lamb serum and 8 parts MAB.

Boehringer Mannheim Blocking reagent stock solution:

Dissolve the Boehringer Mannheim Blocking reagent (Roche, 1 096 176) in MAB to make a 10% stock solution.

3.3'-Diaminobenzidine (DAB) (Fibronectin and laminin immunohistochemistry)

Weigh 1 mg DAB into a bijou bottle.

At the start of the second day of the run put a measuring cylinder containing 29 ml distilled water into the fridge at 4ºC.

Just before use add 2 ml tris/HCl (pH 7.6) to DAB in bijou bottle.

Then add 1 ml 30% Perhydrol to the now cold distilled water to make a 1% solution-mix well.

Add 20 µl of the 1% Perhydrol to the DAB solution, mix on whirlimix.

3.3'-Diaminobenzidine (DAB) (Bax and Bcl-2 immunohistochemistry)

Add 1 part DAB/ metal concentrate (10X concentration) to 9 parts peroxide buffer.

Diluent for anti-sera

| | |
|---|---|
| 100 ml | tris/saline |
| 0.25 g | sodium azide |
| 5 mg | BSA |
| 40 mg | EDTA |
| 1 ml | swine serum |

Hydrogen peroxide solution

| | |
|---|---|
| 2 ml | 30% hydrogen peroxide solution |
| 2 ml | formamide |
| 36 ml | 2X SSC |

0.1 M Triethanolamine (pH 7.8)

Dissolve 9.29 g triethanolamine to 480 ml milliQ water.

Adjust the ph to 7.8, then make up the solution to 500 ml with milliQ water.

Filter sterilize.

# APPENDIX V: Technical Methods

3-Aminopropyltriethoxysilane treated slides (Silane-coated slides)

Wash glass slides in detergent for 30 minutes.

Wash glass slides in running tap water for 30 minutes.

Wash glass slides in distilled water for 2 x 5 minutes.

Wash glass slides in 95% alcohol for 2 x 5 minutes.

Air dry for 10 minutes.

Immerse in 2% silane in acetone for 30 minutes.

Wash in acetone, 1-2 dips.

Wash in distilled water.

Dry overnight at 42ºC.